Hybrid Digital Control of Piezoelectric Actuators

Mohsen Bazghaleh

School of Mechanical Engineering
The University of Adelaide
South Australia 5005
Australia

A thesis submitted in fulfilment of the requirements for the degree of Ph.D. in Engineering on the 28th of October 2013

Abstract

Nanopositioning, as a core aspect of nanotechnology, concerns the control of motion at nanometre scale and is a key tool that allows the manipulation of materials at the atomic and molecular scale. As such it underpins advances in diverse industries including biotechnology, semiconductors and communications.

The most commonly used nanopositioner is the piezoelectric actuator. Aside from being compact in size, piezoelectric actuators are capable of nanometre resolution in displacement, have high stiffness, provide excellent operating bandwidth and high force output. Consequently they have been widely used in many applications ranging from scanning tunnelling microscopes (STM) to vibration cancellation in disk drives. However, piezoelectric actuators are nonlinear in nature and suffer from hysteresis, creep and rate-dependencies that reduce the positioning accuracy.

A variety of approaches have been used to tackle the hysteresis of piezoelectric actuators including sensor-based feedback control, feedforward control using an inverse-model and charge drives. All have performance limitations arising from factors such as parameter uncertainty, bandwidth and sensor-induced noise.

This thesis investigates the effectiveness of a synergistic approach to the creation of hybrid digital algorithms that tackle challenges arising in the control of non-linear devices such as piezoelectric actuators. Firstly, a novel digital charge amplifier (DCA) is presented. The DCA overcomes inherent limitations found in analog charge amplifiers developed in previous research.

In order to extend the DCA operational bandwidth, a complementary filter was combined with the DCA along with a non-linear black-box model derived using system identification techniques. To maximize the model accuracy a novel method is utilized that reduces error accumulation in the model. This method is generally applicable to many dynamic models. A non-linear model is also used with a data fusion algorithm to ensure the DCA does not exhibit drift, an issue common to most of charge amplifiers.

The proposed hybrid digital system is evaluated and it is shown that hysteresis is significantly decreased, while operational bandwidth is extended with no displacement drift. Experimental results are presented throughout to fully validate the proposed system.

Declarations

I certify that this work contains no material which has been accepted for the award of any other degree or diploma in my name, in any university or other tertiary institution and, to the best of my knowledge and belief, contains no material previously published or written by another person, except where due reference has been made in the text. In addition, I certify that no part of this work will, in the future, be used in a submission in my name, for any other degree or diploma in any university or other tertiary institution without the prior approval of the University of Adelaide and where applicable, any partner institution responsible for the joint-award of this degree.

I give consent to this copy of my thesis when deposited in the University Library, being made available for loan and photocopying, subject to the provisions of the Copyright Act 1968.

The author acknowledges that copyright of published works contained within this thesis resides with the copyright holder(s) of those works.

I also give permission for the digital version of my thesis to be made available on the web, via the University's digital research repository, the Library Search and also through web search engines, unless permission has been granted by the University to restrict access for a period of time.

Mohsen Bazghaleh Date

Acknowledgements

I would like to take this opportunity to thank a number of people whose support and input was crucial in the completion of my research. First and foremost, I would like to express my utmost gratitude to my principal supervisor, Dr Steven Grainger, for his infinite patience, constant support, encouragement and advice throughout my Ph.D. degree. This thesis would not have been completed without his support. Thanks should also go to my co-supervisors, Associate Professor Ben Cazzolato and Dr Tien-Fu Lu.

I also would like to thank my colleagues, Jayesh Minase and Dr Morteza Mohammadzaheri for their collaboration in my research. I greatly appreciate their help with proofreading, and suggestions for improvements from Karen Adams, Peter Ward and Alison-Jane Hunter.

Finally, my sincere thanks go to my parents Mohammad and Mitra for their patience and never-ending support throughout my entire time at university. Without their support and encouragement, the writing of this thesis would have been a much more difficult process.

Contents

Notation

$+x$	Positive electrode in the x direction
$-x$	Negative electrode in the x direction
$+y$	Positive electrode in the y direction
$-y$	Negative electrode in the y direction
$\mathbf{b}$	Bias in semi-linear ANN
b	Damping of a piezoelectric actuator
C	Centre of a cluster
C_{L}	Capacitance of a load capacitance
C_{p}	Capacitance of a piezoelectric actuator
C_{s}	Sensing capacitor
C_{series}	Capacitor in series with a piezoelectric actuator
D	Density function
D	Electrical displacement (charge per unit area)
d	Piezoelectric material constants (Chapter 2)
	Displacement of a piezoelectric actuator (other chapters)
$\hat{d}_{\mathrm{ANN}}$	Output displacement of the ANN model
d_{a}	Actual displacement
d_{d}	Desired displacement
$\hat{d}_{\mathrm{GDCDE}}$	Output displacement of the GDCDE unit

d_{r}	Reference displacement
E	Electric field
e	Error
e_{Is}	Error of an electric current
e_{m}	Error at the output of the NARX model
$e_{\mathrm{q\_opt}}$	Error in the optimal output charge
F	Artificial neural network
f	Output of fuzzy rules and FISs
f	Function
f_{critical}	Break (critical) frequency of a system
F_{ext}	Force imposed from an external mechanical source
F_{t}	Transduced force from an electrical domain
$H(s)$	Continuous transfer function between $V_{\mathrm{o}}(t)$ *and* $V_{\mathrm{s}}(t)$
$H(z)$	Discrete transfer function between $V_{\mathrm{o}}(t)$ and $V_{\mathrm{s}}(t)$
I_{L}	Electric current of a load
I_n	Electric Current source
I_{p}	Electric current of a piezoelectric actuator
I_{s}	Electric current of a sensing resistor/capacitor
k	Proportional gain
K	Gain (Charge to displacement)
K_{c}	Closed loop gain
k_{p}	Stiffness of a piezoelectric actuator
m	Mass of a piezoelectric actuator (Chapter 2)
	The number of rules of a FIS (Others)
$MSE_{\mathrm{e\_opt}}$	Mean square error (MSE) of $e_{\mathrm{q\_opt}}$

N	Number of previous displacements (Chapter 4)
	Activation function (Chapter 6)
n	Number of inputs to a FIS (Chapter 4)
	Number of data elements in each column of raw data (Chapter 6)
n_f	Number of terms of discrete sum function
p	Consequent parameter of fuzzy inference system
q	Consequent parameter of fuzzy inference system
q_{actual}	Actual charge across piezoelectric actuator
q_{DCA}	Charge calculated by DCA unit
$q_{desired}$	Desired charge
q_{in}	Input charge
q_L	Charge across a load
$q_{measured}$	Measured charge across a piezoelectric actuator
q_{model}	Charge calculated by the NARX model
$q_{optimal}$	Optimal output charge
q_p	Charge across a piezoelectric actuator
r	Consequent parameter of fuzzy inference system
r_a	Range of influence
r_b	Squash factor
r_d	Displacement (Output) order
r_{de}	Discrete delay time
$R_{inputADC}$	ADC input resistance
R_L	DC impedance of a load
R_p	Protection circuit resistor
R_s	Sensing resistor

R_T	Total resistance
r_u	Input order
r_V	Piezoelectric voltage (input) order
r_y	Output order
S	Integration area
S	Strain of a piezoelectric actuator
s	Sampling (index)
s	Compliance matrix
$\mathbf{T}$	weight of connections of the ANN
T	Stress
t	Time
t_d	Delay time (Dead time)
t_f	Final time of operation
T_p	Electromechanical transformer ratio
T_s	Sampling time
u	Input to the model
V	Applied voltage
v	piezoelectric actuator velocity
V_{bias}	Bias voltage at the input of an ADC
V_i / V_{in}/ v_{in}	Input voltage
v_{mrc}	Voltage across the Maxwell elasto-slip element
V_o	Output of the voltage amplifier
V_p	Voltage across a piezoelectric actuator
V_{Pext}	Last extremum value of applied voltage
$\mathbf{V_{ps}}$	Vector of the present and a number of previous piezoelectric-

	voltage values
V_{ref}	Reference voltage
V_s	Sensing voltage across the sensing resistor/Capacitor
V_{si}	Strain-induced voltage
v_t	Back-emf from the mechanical side of a piezoelectric actuator
W	Weight of connections of the ANN
w	Weight of a rule in a FIS
w_a	DCA weighting coefficients
W_{ANN}	ANN weighting coefficients
w_b	NARX model weighting coefficients
W_{GDCDE}	GDCDE weighting coefficients
x	A datum in clustering
x	Input to the activation function N
y	Output of the model

Symbols

α	Switching value of Preisach model
β	Switching value of Preisach model
$\gamma_{\alpha\beta}$	Elementary hysteresis operator
Δ	Nonlinear impedance
ϵ	Permittivity
μ (.)	Membership grade in FISs
μ (.,.)	Weighting function of the Preisach model
μ_n	Mean
σ_n	Standard deviation
ω_c	Cut-off frequency

1 Introduction

Nanotechnology is the multidisciplinary science of manufacturing and manipulation of objects down to nanometre size. Nanopositioning is a core aspect of nanotechnology and concerns the control of motion at nanometre scale and is a key tool that allows the manipulation of materials at the atomic and molecular scales. As such, it underpins advances in diverse industries including biotechnology, semiconductors and communications. Nanopositioning systems require precise actuation on the nanometre scale and they are generally driven using solid state actuators manufactured using smart materials.

The most commonly used nanopositioner is the piezoelectric actuator. Aside from being compact in size, they are capable of nanometre resolution in displacement, have high stiffness, provide excellent operating bandwidth and high force output (Devasia *et al.*, 2007). Consequently they have been widely used in many applications ranging from scanning tunnelling microscopes (STM) (Wiesendanger, 1994) to vibration cancellation in disk drives (Ma and Ang, 2000).

However, piezoelectric actuators suffer from hysteresis and creep which reduce the positioning accuracy and are the most important challenges in the use of piezoelectric actuators (Leang and Devasia, 2002). A number of

previous control methods have attempted to tackle these issues; however the problems are still not completely solved.

1.1 Aims and objectives

The aim of this research is to investigate the role of hybrid digital algorithms in tackling challenges arising in the control of non-linear systems. In this research, hysteresis, which is the main source of piezoelectric actuator non-linearity, was chosen in order to evaluate the performance of the proposed hybrid digital approach. The proposed control systems are tested and evaluated on a piezoelectric stack actuator AE0505D44H40 from NEC and piezoelectric tube actuator PI –PT130.24 from PI.

Thus the objectives of this research are the:

- Extensive investigation of digital approaches to implement charge amplifiers.
- Creation of innovative, holistic models, appropriate to the linearization, compensation and control of piezoelectric actuators.
- Investigation of hybrid methods to improve the accuracy of models.
- Investigation of multiple conceptual technologies, such as Artificial Neural Networks (ANNs), fuzzy logic and complementary filters to improve the tracking performance and extend the operational bandwidth of actuators.

1.2 Publications arising from this thesis

The research outcomes of this thesis have led to the generation of refereed publications, including journal papers and refereed conference papers which are listed in the following:

Refereed Journal Papers:

1. Bazghaleh**,** M., Grainger, S., Mohammadzaheri, M., Cazzolato, B. and Lu, T.-F., 2013. A digital charge amplifier for hysteresis elimination in piezoelectric actuators. *Smart Materials and Structures* 22, 075016.

2. Bazghaleh**,** M., Grainger, S., Mohammadzaheri, M., Cazzolato, B. and Lu, T.-F., 2013. A novel digital charge-based displacement estimator for sensorless control of a grounded-load piezoelectric tube actuator. *Sensors and Actuators A: Physical* 198, 91-98.

3. Bazghaleh**,** M., Mohammadzaheri, M., Grainger, S., Cazzolato, B. and Lu, T.-F., 2013. A new hybrid method for sensorless control of piezoelectric actuators. *Sensors and Actuators A: Physical* 194, 25-30.

4. Mohammadzaheri, M., Grainger, S. and Bazghaleh**,** M., 2012. A comparative study on the use of black box modelling for piezoelectric actuators. *International Journal of Advanced Manufacturing Technology* 63, 1247-55.

5. Mohammadzaheri, M., Grainger, S. and Bazghaleh**,** M., 2012. Fuzzy Modeling of a Piezoelectric Actuator. *International Journal of Precision Engineering and Manufacturing* 13, 663-670.

Under-review Journal Papers:

1. Bazghaleh**,** M., Grainger, S., Cazzolato, B. and Lu, T.-F., 2013. Implementation and analysis of an innovative digital charge amplifier for hysteresis reduction in piezoelectric stack actuators. *Review of Scientific Instruments.* Under-review.

Refereed Conference Papers:

1. Bazghaleh**,** M., Grainger, S., Cazzolato, B. and Lu, T.-F., 2012. Using frequency-weighted data fusion to improve the performance of a digital charge amplifier. *In: IEEE International Conference on Robotics and Automation (ICRA).* St. Paul, MN, USA.

2. Mohammadzaheri, M., Grainger, S., Bazghaleh**,** M. and Yaghmaee, P., 2012. Intelligent modeling of a piezoelectric tube actuator. *In: International Symposium on Innovations in Intelligent Systems and Applications*. Trabzon, Turkey.

3. Bazghaleh**,** M., Grainger, S., Cazzolato, B. and Lu, T.-F., 2011. Model-based drift correction in digital charge amplifier. *In: 15th International Conference on Mechatronic Technology*. Melbourne, Australia.

4. Bazghaleh**,** M., Grainger, S., Cazzolato, B. and Lu, T.-F., 2010. An innovative digital charge amplifier to reduce hysteresis in piezoelectric actuators. *In: Australasian Conference on Robotics and Automation*. Brisbane, Australia.

1.3 Preview of the thesis

This thesis comprises, in part, manuscripts that have been published or submitted for publication in international peer-reviewed journals in accordance with the 'Academic Program Rules 2013' approved by the Research, Education and Development Committee of the University of Adelaide. In addition three conference papers, which are also relevant to the present work, are included in the appendix. This section provides brief descriptions of each publication and the links between publications in order to show how the objectives of this thesis are achieved.

Chapter 2 covers previous literature regarding the displacement control of piezoelectric actuators including feedback voltage drive, feedforward voltage drive and charge drive. This chapter shows that while there has been much research into the control of piezoelectric actuators, there is an opportunity to explore digitally implemented charge amplifiers within an integrated hybrid system. To establish the field of knowledge, this chapter also includes some general background on piezoelectric actuators and their behaviour.

Chapter 3 presents a novel digital charge amplifier (DCA). It is discussed how the DCA can reduce hysteresis and improve the linearity of piezoelectric actuators. This easily implemented, digital charge drive approach opens up the possibility of integration with other control methods such as model-based methods to improve the performance of the displacement controller which are investigated in the subsequent chapters.

Chapter 4 consists of two journal papers. The first paper is focused on black-box modelling of a piezoelectric stack actuator. Appropriate selection

of the inputs to the model is an important task in black-box modelling. In this paper, current and previous values of voltage, previous values of the displacement and for the first time extremum values of input voltage and/or displacement in each cycle of operation are used as an input to the model. In addition, in order to understand the role of each input in the model and to choose the most appropriate inputs, fuzzy subtractive clustering and neuro-fuzzy networks are used.

The second paper proposes a novel hybrid method to increase the accuracy of the model. This is achieved through the use of a method that employs the velocity signal, which is related to the current passing the piezoelectric actuator, to reduce the effect of error accumulation on the output displacement of the model. This method is then theoretically and experimentally verified.

In Chapter 5 a model-based drift correction technique is proposed to remove the drift and improve the tracking performance of the DCA. It uses data fusion to integrate the reliability and short term accuracy of the DCA, with the long term accuracy of the non-linear model, to realise the benefits of both techniques. Experimental results clearly show the elimination of drift and improvements in tracking performance.

In order to extend the DCA operational bandwidth, a novel hybrid digital method is proposed in Chapter 6. In this method a non-linear model was designed and trained to estimate displacement based on the piezoelectric voltage at low frequencies. The model and charge-based displacement estimators were used together through a complementary filter to increase the bandwidth of displacement estimation and control. In addition, the system is

designed to be capable of driving grounded-loads such as piezoelectric tube actuators.

Finally, conclusions and future work is presented in Chapter 7.

References

Devasia, S., Eleftheriou, E. and Moheimani, S.O.R., 2007. A survey of control issues in nanopositioning. *IEEE Transactions on Control Systems Technology* 15(5), 802–823.

Leang, K.K. and Devasia, S.,2002. Hysteresis, creep and vibration compensation for piezoactuators: Feedback and feedforward control. *In: Proceedings of 2nd IFAC Conference on Mechatronic Systems.* pp. 283–289.

Ma, J. and Ang, M., 2000. High-bandwidth macro/microactuation for hard-disk drive. *In: Proceedings of the SPIE* 4194, pp. 94-102.

Wiesendanger, R., 1994. Scanning Probe Microscopy and Spectroscopy: Methods and Applications. *Cambridge: Cambridge University Press*.

2 Background and Literature Review

The purpose of this chapter is to provide a general background on piezoelectric actuators and to review all relevant literature relating to controlling piezoelectric actuators, mostly focussing on charge drives.

This chapter is structured around four sections. Section 2.1 discusses how piezoelectric actuators work. In Section 2.2, the non-linearities associated with piezoelectric actuators are explained. Control of piezoelectric actuator displacement, including displacement feedback voltage drive, feedforward voltage drive and charge drive, is described in Section 2.3. Section 2.4 presents the conclusions.

2.1 Piezoelectric actuators

The Curie brothers discovered the piezoelectric effect in 1880. They realised that compressing a piezoelectric material results in an electric charge. After further investigation, they also found the inverse piezoelectric effect, where an applied electric charge results in deformation of the material. They eventually built a new type of actuator called ‘the piezoelectric actuator’ (Ballato, 1996).

Figure 2.1 shows a schematic of a single layer piezoelectric actuator. The lead zirconate titanate (PZT) ceramic, which is a popular piezoelectric material, is in the centre, with electrodes above and below. The PZT will be deformed when an electric field is applied. Single layer piezoelectric actuators are sometimes called "moving capacitors" because, from the electric point of view, they are similar to a capacitor with the exception that they move.

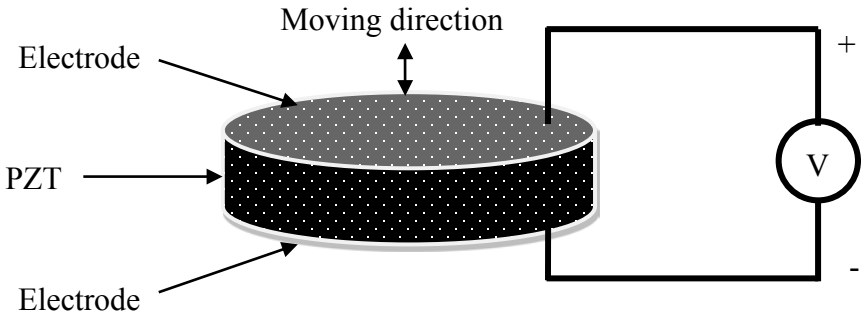

Figure 2.1: Schematic of a single layer piezoelectric actuator

In order to increase actuating forces and displacements, a number of single layer piezoelectric materials are often assembled in series to build piezoelectric stack actuators.

Another type of piezoelectric actuator is the piezoelectric tube actuator which is most widely used in Scanning Probe Microscopes (SPMs) to manipulate matter at the nanometre scale (Moheimani, 2008). In traditional SPMs, tripod positioners formed from three piezoelectric stack actuators were employed for movement in the x, y and z directions. Binnig and Smith (1986) proposed the use of piezoelectric tube actuators instead. Compared to tripod positioners, piezoelectric tube actuators offer better accuracy, higher bandwidth and an easier manufacturing process (Devasia *et al.*, 2007), while

their smaller size simplifies vibration isolation (Chen, 1992). Piezoelectric tubes are the foremost actuators in atomic force microscopy (AFM) (Abramovitch *et al.*, 2007, Kuiper and Schitter, 2010) and are likely to remain the most widely used positioning actuators in other micro-scale and nano-scale positioning tasks for several years (Moheimani, 2008), such as displacement of fibre optics (Leung *et al.*, 2008) and ultrasonic applications (Hui *et al.*, 2010).

Figure 2.2 shows a schematic of a piezoelectric tube actuator. Typically the tube has one grounded inner electrode and four equally distributed outer electrodes. The bottom of the tube is fixed and the top moves in the x, y and z directions.

An applied voltage between an external and the internal electrode will bend the tube and the sign of the applied voltage determines the direction in which it bends. This means that by applying a positive and negative voltage with equal magnitudes on the $-x$ and $+x$ electrodes, the tube will bend in the x direction. Similarly, it can move in the y direction. To actuate the tube in the z direction, equal voltages should be applied to all four external electrodes.

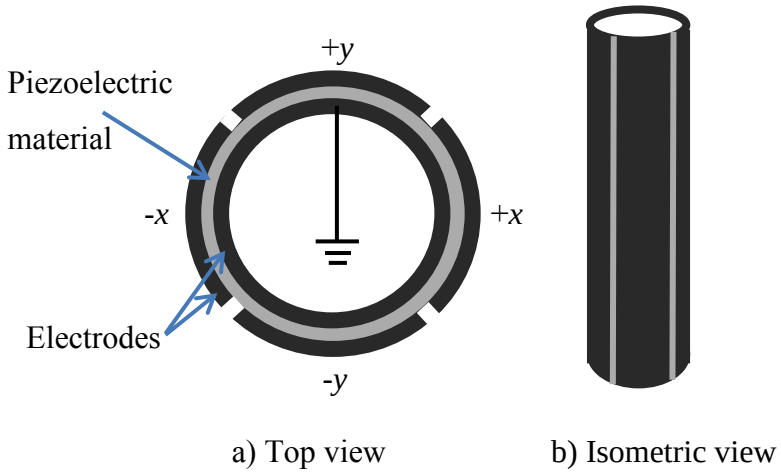

Figure 2.2: Piezoelectric tube scanner

2.2 Non-linearities in piezoelectric actuators

The relationship between piezoelectric actuator displacement and voltage suffers from hysteresis and creep, which are nonlinear in nature and reduce positioning accuracy (Leang and Devasia, 2002). These non-linearities are explained by the misalignment of molecular dipoles, which constitute piezoelectric materials, and internal power dissipation within the piezoelectric actuators (Vautier and Moheimani, 2005).

Piezoelectric actuators exhibit hysteresis when driven by voltage amplifiers. Hysteresis depends on a combination of both the currently applied voltage as well as the previously applied voltage (Kuhnen and Janocha, 1998). In practice, it means that, for similar values of applied piezoelectric voltage, the piezoelectric actuator has a variety of displacement values, and this cannot be described with linear models. Hysteresis should not be confused with phase lag which is a linear effect, while hysteresis is a nonlinear effect.

The hysteresis loop has sharp reversal peaks at the extrema, while the phase lag has the shape of an ellipse with more rounded shape at the extrema (Moheimani and Fleming, 2006).

Figure 2.3 illustrates a hysteresis loop when the piezoelectric stack actuator AE0505D44H40 from NEC is driven by a voltage amplifier. For the displacement range of 11.54μm, the maximum hysteresis is 1598 nm for a driving frequency of 10 Hz. Therefore the maximum hysteresis is about 14% of the displacement range.

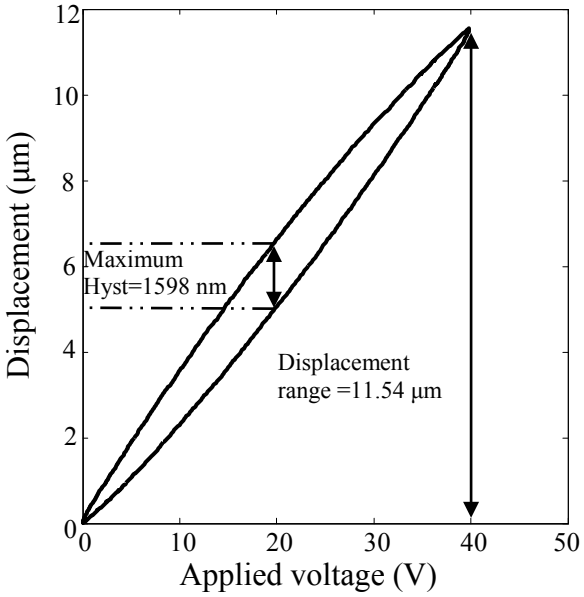

Figure 2.3: Hysteresis loop between applied voltage and displacement

The overall voltage to displacement relationship of piezoelectric actuators is rate-dependent. In the literature, this effect is explained in two different ways. In some articles (Yanding *et al.*, 2013, Smith *et al.*, 2000, Vautier and Moheimani, 2005, Devasia *et al.*, 2007) the hysteresis effect is assumed to be rate-dependent, while other authors (Croft and Devasia, 1998, Wu and

Zou, 2007, Adriaens, 2000) have assumed that hysteresis is rate-independent and that the rate-dependent behaviour is because of the linear dynamics of piezoelectric actuators. The second explanation is more convenient for modeling purposes, as it allows the linearity and non-linearity of piezoelectric actuators to be treated separately.

Another form of non-linearity in piezoelectric actuators is called creep. It is the result of the remnant polarization which continues to change after the applied signal reaches its final value and typically is an issue at low frequencies (Meeker, 1996).

Figure 2.4 shows the AE0505D44H40 piezoelectric actuator displacement response to a 40V input step signal at time 0s. It can be seen that it takes 4.5 seconds to reach the final value (11.5 μm). The displacement continues to change after the input voltage reaches its final value (in this case 40V).

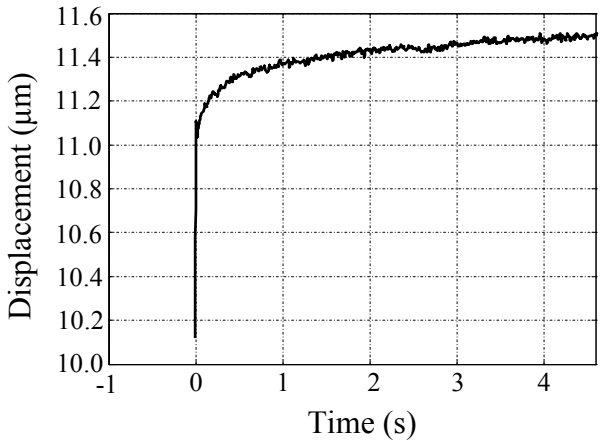

Figure 2.4: Creep in a piezoelectric actuator

The total error in the displacement of piezoelectric actuators is the result of both hysteresis and creep effects. Hysteresis and creep together can cause as

much as 40% error in the position of piezoelectric actuators (Barrett and Quate, 1991).

2.3 Control of displacement

Because hysteresis and creep affect the positioning accuracy of the piezoelectric actuator, to achieve high accuracy the piezoelectric non-linearities have to be compensated for. This section reviews different approaches to controlling the displacement of piezoelectric actuators with this compensation.

2.3.1 Displacement feedback voltage drive (sensor-based control)

In sensor-based control, the displacement of a piezoelectric actuator is measured (by a variety of sensors such as strain gauges, capacitive sensors, optical sensors and eddy current sensors) and a feedback controller is used to equalize the desired displacement with the actual displacement measured by the sensor (Figure 2.5).

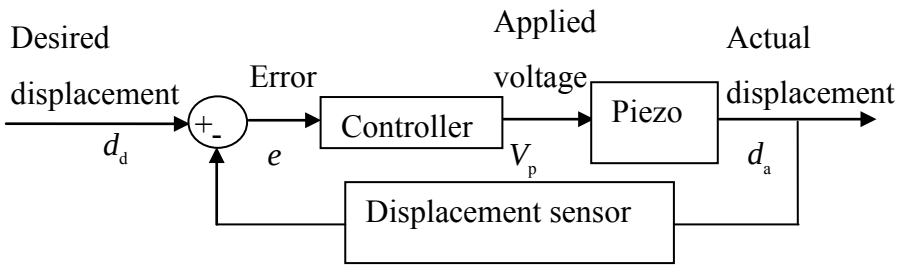

Figure 2.5: Displacement feedback control

Proportional-integral-derivative (PID) controllers are very common for this purpose. Although they provide accurate positioning, especially at low frequency, stability is an important issue in feedback controllers and at high

frequencies, because of the resonance frequency of the actuator, the system may become unstable if the feedback gains are too high. Adaptive control (Shieh *et al.*, 2004), (Tan and Baras, 2005) and robust control (Pare and How, 1998, Jonsson, 1998) are two common methods which have been utilized to tackle this issue. Other issues with feedback controllers are the physical size of sensors, sensor-induced noise, high cost, tracking lag and limited bandwidth (Fleming and Leang, 2008).

2.3.2 Feedforward voltage drive (model-based control methods)

Feed-forward control can be used to compensate for the non-linearities of a piezoelectric actuator using an inverse mathematical model of the system dynamics (Wang *et al.*, 2011, Zhao and Jayasuriya, 1995, Krejci and Kuhnen, 2001). Two approaches are common to find the inverse model. In the first approach, the non-linearities of a piezoelectric actuator are modelled, e.g., the Preisach model (Ge and Jouaneh, 1995) or the Maxwell resistive model (Goldfarb and Celanovic, 1997b), and then the model is inverted. In the second approach, the inverse model (as an example, using Preisach techniques) is directly calculated and utilized to drive the piezoelectric actuator (Croft *et al.*, 2001). Generally the second approach requires less effort because there is no need to find the original model. In such feedforward methods, the inverse model is cascaded with the piezoelectric actuator.

Compared to the feedback displacement control method, this method has reduced hardware complexity since displacement sensors are not required. However, the parameter sensitivity and modelling complexity are the main

challenges in designing feedforward controllers. The next section provides an overview of piezoelectric modelling.

2.3.2.1 Modelling piezoelectric actuators

A well-known model of piezoelectric actuators is that described by the standards committee of the IEEE (Meeker, 1996), which presents linear equations to describe piezoelectric behaviour. These equations are represented in matrix notion as follows:

$$S_p = s^E_{pq} T_q + d_{kp} E_k \tag{2.1}$$

$$D_k = d_{kp} T_p + \epsilon^T_{ki} E_i \tag{2.2}$$

where S is the strain, s is the compliance matrix, T is the stress, d are the piezoelectric material constants, E is the electric field, D is the electrical displacement (charge per unit area) and ϵ is the permittivity. The subscripts p, q = 1,2,3,4,5,6 and k and i=1,2,3 represent different directions within the material coordinate system as shown in Figure 2.6.

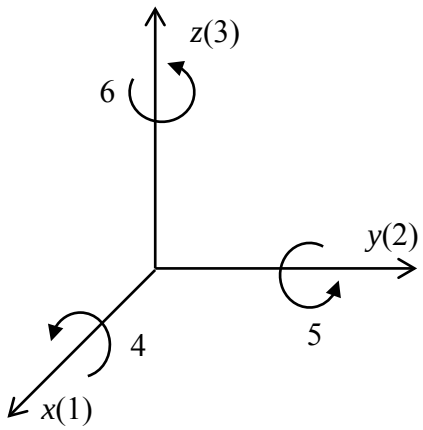

#	Axis
1	x
2	y
3	z
4	Shear around *x*
5	Shear around *y*
6	Shear around *z*

Figure 2.6: Directions within the material coordinate system

Equation (2.1) describes the inverse piezoelectric effect and Equation (2.2) describes the direct piezoelectric effect as described in Section 2.1. These equations represent both the strain and the electric displacement as being linearly dependent of the stress and the electric field. These linear equations, however, have proved inadequate in many instances due to the significant nonlinearities such as hysteresis and creep in piezoelectric actuators. If these non-linearities are not considered in modelling, a large displacement error is generated. The Maxwell resistive capacitor (MRC) model (Goldfarb and Celanovic, 1997a) and the Preisach model (Ge and Jouaneh, 1995) are two important nonlinear mathematical modelling methods.

An electromechanical model, which is shown in Figure 2.7, is proposed by Goldfarb and Celanovic (1997a and 1997b). It describes both the mechanical and electrical aspects of piezoelectric actuators, and the relationship between them.

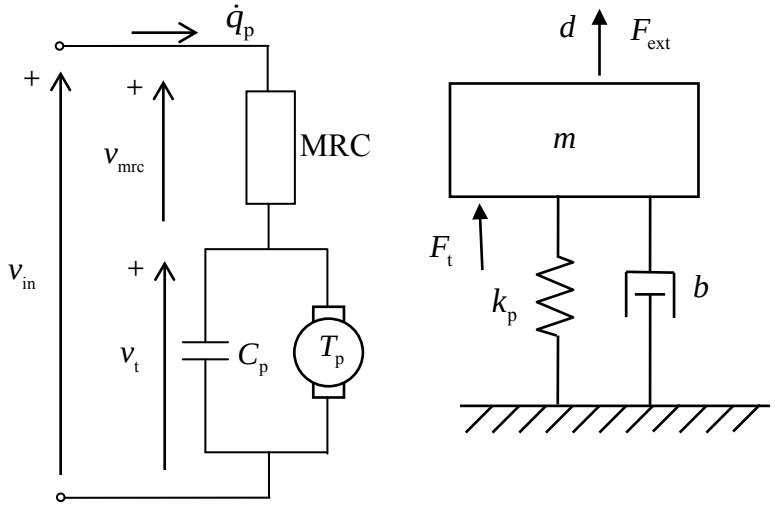

Figure 2.7: The electromechanical model of a piezoelectric actuator

According to Figure 2.7, the behaviour of the piezoelectric actuator is described by:

$$q_{\mathrm{p}} = T_{\mathrm{p}} d + C_{\mathrm{p}} v_{\mathrm{t}} \tag{2.3}$$

$$v_{\mathrm{in}} = v_{\mathrm{mrc}} + v_{\mathrm{t}} \tag{2.4}$$

$$v_{\mathrm{mrc}} = \mathrm{MRC}(q_{\mathrm{p}}) \tag{2.5}$$

$$F_t = T_{\mathrm{p}} v_{\mathrm{t}} \tag{2.6}$$

$$m\ddot{d} + b\dot{d} + k_{\mathrm{p}} d = F_t + F_{\mathrm{ext}} \tag{2.7}$$

where q_{p} is the overall charge across the piezoelectric actuator, T_{p} is the electromechanical transformer ratio, d is the displacement of the actuator, C_{p} is the linear capacitor, v_{t} is the back-emf from the mechanical side, v_{in} is the applied voltage, Maxwell Resistive Capacitor (MRC) models the non-linearity behaviour of the piezoelectric actuator, v_{mrc} is the voltage across the MRC unit, F_{t} is the transduced force from the electrical domain, m, b, and k_{p} are the mass, damping, and stiffness of the actuator, and F_{ext} is the force imposed from the external mechanical source.

The behaviour of molecular dipoles, from which the piezoelectric materials are formed, is the main reason for the non-linear behaviour of piezoelectric actuators. When a sufficient electric field is applied to a piezoelectric actuator, the direction of each dipole will be changed to align with the electric field. The movement of each dipole depends on the initial orientation and the strength of the electric field. The non-linear behaviour is due to the change in the directions of all the dipoles in the piezoelectric actuator.

The MRC method is a linear parametric method of modelling the non-linear hysteresis behaviour of a piezoelectric actuator. In this method, each dipole is modeled by an elasto-slide element. Each elasto-slide element, which consists of an ideal spring coupled to a massless block, has a hysteretic behaviour and the summation of all the elasto-slide elements models the hysteresis behaviour of piezoelectric actuators. Therefore this model is a piece-wise approximation of the hysteresis and is based on physical principles (Goldfarb and Celanovic, 1997b).

In the MRC model, because the hysteresis is modeled by a combination of elements, the number of parameters is relatively large. Therefore, such a model is not very suitable for controller design purposes.

In 1995, the Preisach phenomenological model, originally devised by the German physicist in 1935 to describe hysteresis phenomena in magnetic systems (Preisach, 1935), was used to model piezoelectric actuators (Ge and Jouaneh, 1995) and is now widely accepted (Boukari *et al.*, 2011, Liaw and Shirinzadeh, 2011, Zhang *et al.*, 2009).

The relation between the displacement of the piezoelectric actuator, $d(t)$, and the voltage across the piezoelectric actuator, $V_{\mathrm{p}}(t)$, is expressed by:

$$d(t) = \iint_{\alpha \geq \beta} \mu(\alpha, \beta)\gamma_{\alpha\beta}[V_{\mathrm{p}}(t)]\, d\alpha\, d\beta \tag{2.8}$$

where $\mu(\alpha, \beta)$ is a weighting function of the Preisach model and $\gamma_{\alpha\beta}$ are the elementary hysteresis operators with switching values α and β shown in Figure 2.8.

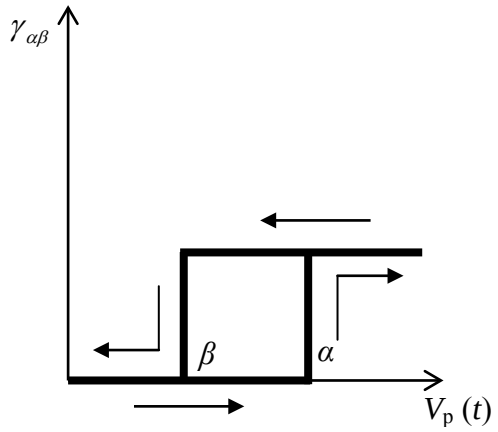

Figure 2.8: Hysteresis operator $\gamma_{\alpha\beta}[V_p(t)]$

Because the hysteresis operators $\gamma_{\alpha\beta}$ are two position relays, the double integration in Equation (2.8) can be represented as a summation of weighted relays connected in parallel as shown in Figure 2.9.

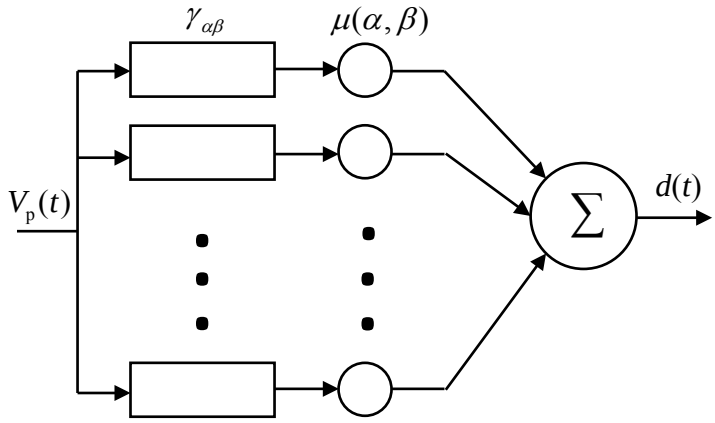

Figure 2.9: The block diagram of Preisach model

The Preisach model fails to model asymmetric hysteresis loops and this has been addressed in a variation, the Prandtl-Ishlinskii model (Zareinejad *et al.*, 2010). Other extended and modified versions of Preisach model have been

published (Li and Tan, 2004, Song and Li, 1999, Dupre *et al.*, 2001, Ge and Jouaneh, 1997, Han and Zhu, 2009, Yu *et al.*, 2002).

Recently a variety of black box models has been used in the modelling of piezoelectric actuators. They include Multi-Layer Perceptrons (MLPs) (Dong *et al.*, 2008, Yang *et al.*, 2008, Zhang *et al.*, 2010), Radial Basis Function Networks (RBFNs) (Dang and Tan, 2007), Recurrent Fuzzy Neural Networks (RFNNs) (Lin *et al.*, 2006b), wavelet neural networks (Lin *et al.*, 2006a), Nonlinear Auto-Regressive Moving Average models with eXogenous inputs (NARMAX models) (Deng and Tan, 2009) and non-standard Artificial Neural Networks (ANNs) (Hwang *et al.*, 2001).

Contemporary, universal approximators are available with proven ability in system modeling; hence, the modeling technique is not a critical issue. In this thesis, Nonlinear Auto-Regressive models with eXogenous inputs (NARX models), commonly used for classical system identification (Nelles, 2001), are utilized.

According to the NARX structure, for a single input-single output system such as a one-dimensional piezoelectric actuator (Nelles, 2001),

$$\begin{aligned} y(t) = f\,(&u(t-t_d),\, u(t-t_d-T_s),\ldots,\, u(t-t_d-r_u T_s), y(t-T_s),\\ &y(t-2T_s),\ldots,\, y(t-r_y T_s)\,), \end{aligned} \tag{2.9}$$

where u is input to the model (applied voltage), y is output of the model (displacement), T_s is sampling time, t_d is delay time, and r_u and r_y are input and output orders respectively. f can be approximated by any nonlinear function. More explanation is provided in Chapter 4.

The disadvantage of NARX models is that the current output error depends on previous output errors and hence the estimation error may accumulate.

Error accumulation is a serious problem for a NARX model and in an extreme situation the model can become unstable (Nelles, 2000). More detail about this issue is discussed in Chapter 3.

2.3.3 Charge drive

Comstock (1981) showed that if a piezoelectric actuator is driven by charge instead of voltage, the hysteresis loop is reduced significantly. Figure 2.10 shows a simplified electromechanical model (Goldfarb and Celanovic, 1997a and Moheimani and Vautier, 2005) of a piezoelectric actuator which is used to explain why the hysteresis loop is reduced by charge driven methods. The model consists of a voltage source, V_{si}, which is the strain-induced voltage, a piezoelectric capacitance C_p, a nonlinear impedance Δ which models the hysteresis and a parallel resistor R_L which models the charge leakage. As described in Goldfarb and Celanovic (1997a) the displacement of the piezoelectric actuator is proportional to the charge across the capacitor q_p.

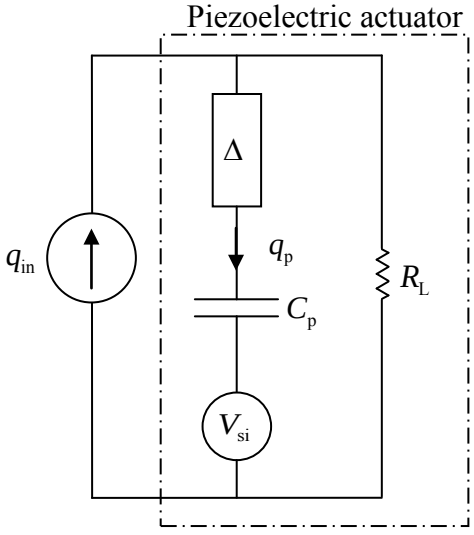

Figure 2.10: Lumped parameter model of a piezoelectric actuator

Using the model in Figure 2.10 as a starting point, initially the effect of R_L is ignored to simplify the discussion. Because of the nonlinear impedance Δ, when the piezoelectric actuator is driven by a voltage source, the applied voltage is not linearly related to the voltage or the charge across the capacitor q_p. Thus the effect of hysteresis can clearly be noted between the applied voltage and the output displacement.

In contrast, if the voltage amplifier is replaced by a charge amplifier, the charge q_p across the capacitor C_p is equal to the applied charge q_{in} and, because the nonlinear impedance Δ does not have any effect on the charge q_p, the hysteresis is removed and the output displacement is linear with the applied charge q_{in}. However the DC impedance of the load, R_L, causes parasitic charge leakage which limits the application of the charge amplifier at low frequencies. To determine this, the model may be simplified by neglecting the effects of the nonlinear impedance and V_{si} (Clayton *et al.*, 2008). Hence the simplified model will only have the capacitor C_p in parallel with R_L. Therefore the transfer function between q_{in} and q_p is given by:

$$\frac{q_p(s)}{q_{in}(s)} = \frac{R_L C_p s}{R_L C_p s + 1}. \tag{2.10}$$

Equation (2.10) is a high-pass filter with a cut-off frequency $f_c = \frac{1}{2\pi R_L C_p}$.

It means that at low frequencies $q_p(s)$ is not equal to $q_{in}(s)$. Therefore the charge amplifier has poor low frequency performance because of the parasitic charge leakage of the piezoelectric actuator (Spiller *et al.*, 2011).

2.3.3.1 The implementation of charge amplifiers

Despite the low frequency limitations, many approaches have been used to implement charge amplifiers since they were first used in 1981 by Comstock. The aim of this section is to review the literature on the implementation of charge amplifiers. Charge amplifiers are broadly classified as either capacitor insertion, time controlled current amplifiers and sense capacitor.

2.3.3.2 Capacitor insertion

The capacitor insertion method proposed by (Kaizuka and Siu, 1988) is one of the simplest ways to reduce hysteresis. In this method, a capacitor is inserted in series with a piezoelectric actuator and a voltage source drives the series combination. It has been shown that the charge across the piezoelectric actuator is proportional to the voltage source and, because the charge is also proportional to the displacement (Newcomb and Flinn, 1982, Fleming and Moheimani, 2005), the displacement source is proportional to the voltage.

To explain this method more completely, the piezoelectric actuator is considered a non-linear capacitor (Goldfarb and Celanovic, 1997a), meaning that the capacitance of the piezoelectric actuator is changing over time. A change in the capacitance will cause a change in the charge across the piezoelectric actuator and this change is the main reason for the hysteresis loop. The sensitivity factor $\frac{dq_{\mathrm{p}}}{dC_{\mathrm{p}}}$ quantifies this effect. Where q_{p} is the charge across a piezoelectric actuator and C_{p} is the capacitance of the actuator. A reduction in the sensitivity factor means that the charge on the piezoelectric actuator is less sensitive to the change of the capacitance of the piezoelectric actuator with a consequent reduction in the hysteresis loop.

As shown in Minase *et al.* (2010), when the piezoelectric actuator is driven by a voltage amplifier the sensitivity factor is

$$\frac{dq_{\mathrm{p}}}{dC_{\mathrm{p}}} = V_{\mathrm{p}}, \tag{2.11}$$

where V_{p} is the voltage across the actuator. While, when it is driven by the capacitor insertion method, it is

$$\frac{dq_{\mathrm{p}}}{dC_{\mathrm{p}}} = \left(\frac{C_{\mathrm{series}}}{C_{\mathrm{series}} + C_{\mathrm{p}}} \right) V_{\mathrm{p}}, \tag{2.12}$$

where C_{series} is the inserted capacitor. It can clearly be seen that when the capacitor insertion method is used the sensitivity factor is reduced by a factor

$$a = \frac{C_{\mathrm{series}}}{C_{\mathrm{series}} + C_{\mathrm{p}}}. \tag{2.13}$$

Therefore this reduction in the sensitivity factor causes a reduction in the hysteresis loop. In other words, the series capacitor operates as a charge regulator across the piezoelectric actuator.

However, in the capacitor insertion method the applied voltage is divided between the piezoelectric actuator and the inserted capacitor. As a result, less voltage will be applied across the piezoelectric actuator, reducing the maximum displacement range for a given voltage. In other words, to get the same displacement range a higher voltage source is required.

2.3.3.3 Time controlled current amplifier

A current amplifier can be used for charge control because the charge on the piezoelectric actuator is equal to the integral of the applied electric current. This method has been described by a number of authors (Newcomb and Flinn, 1982, Dorlemann *et al.*, 2002, Fleming and Moheimani, 2003, Ru *et al.*, 2008, Spiller *et al.*, 2011). Figure 2.11 provides a simplified diagram of a basic current amplifier. The closed-loop with high gain, k, equalizes the reference signal V_{ref} with the sensing voltage V_{s}. Therefore, the load current, I_{L}, is given by

$$I_{\text{L}} = \frac{V_{\text{ref}}}{R_{\text{s}}}, \tag{2.14}$$

where R_{s} is a sensing resistor. In other words, this is a current amplifier with gain $\frac{1}{R_{\text{s}}}$.

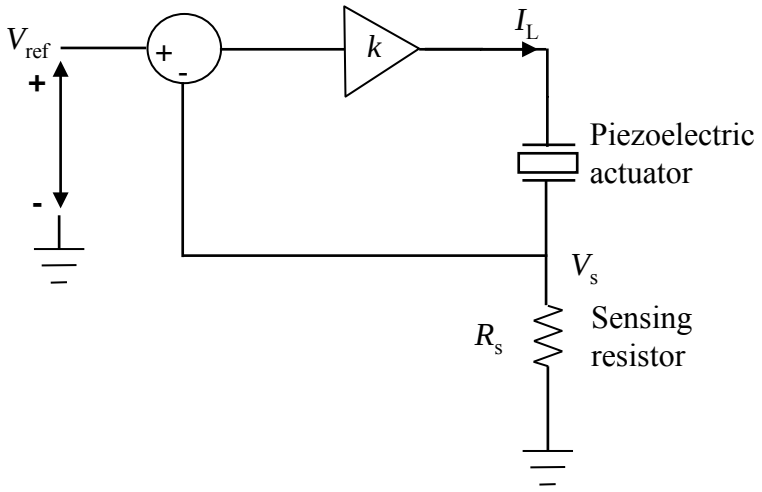

Figure 2.11: Basic current amplifier

Newcomb and Flinn (1982) implemented a charge regulator based on a current amplifier. They used two constant current sources to regulate the current on the piezoelectric actuator as shown in Figure 2.12. The current source I_1 provides a positive current on the piezoelectric actuator, which causes extension of the piezoelectric actuator, while I_2 applies a negative current which causes contraction. The voltage V_{in} controls the switch for applying either a positive or negative current. The amount of charge on the piezoelectric actuator can be regulated by controlling the time interval of the positive and negative V_{in}.

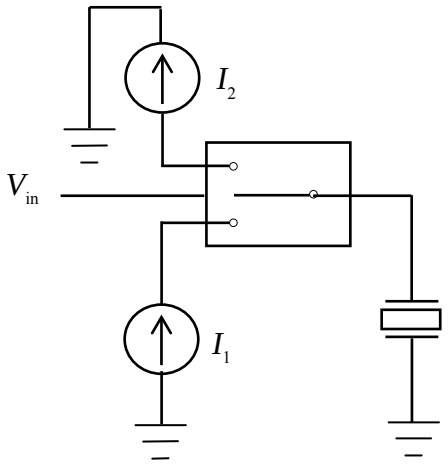

Figure 2.12: Simplified diagram of current source piezo regulation (Newcomb and Flinn, 1982)

Furutani and Iida (2006) improved the Newcomb and Flinn (1982) method by using current pulse modulation to control the charge on the piezoelectric actuator as shown in Figure 2.13. It consists of current sources, current sinks and controlling switches. The switches control the current going to the piezoelectric actuator. At any one time only one switch is on. Current sources are used to increase the piezoelectric actuator charge whereas sinks decrease the charge. To generate rapid displacements, large sources are used

and for small and accurate displacements, small current sources or sinks are used (Furutani and Iida, 2006). Compared to Newcomb and Flinn (1982), this method is more costly because more current sources are needed.

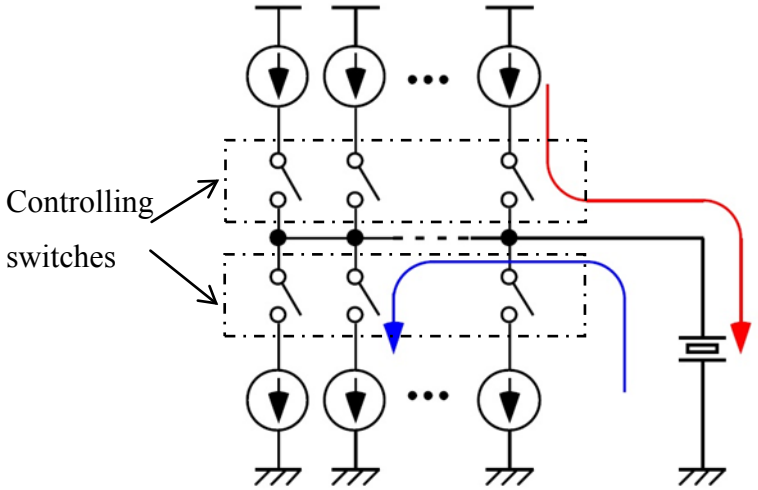

Figure 2.13: Schematic of current pulse driving method (Furutani and Iida, 2006)

Ru (2008) also modified the basic current amplifier, utilizing a switch with two sensing resistors. For quick positioning and fast response, a smaller sensing resistor is selected by the switch, allowing more charge to the piezoelectric actuator, while for precise positioning a larger resistor is selected.

None of these methods address the problem of voltage drift caused by dielectric leakage of the piezoelectric actuator and current leakage of the current source. They can therefore only work for a limited time.

2.3.3.4 Sense capacitor

Figure 2.14 shows a diagram of an ideal charge amplifier with a sensing capacitor with capacitance C_s. A high gain feedback loop is used to equalize the voltage across the sensing capacitor V_s with the reference voltage V_{ref}.

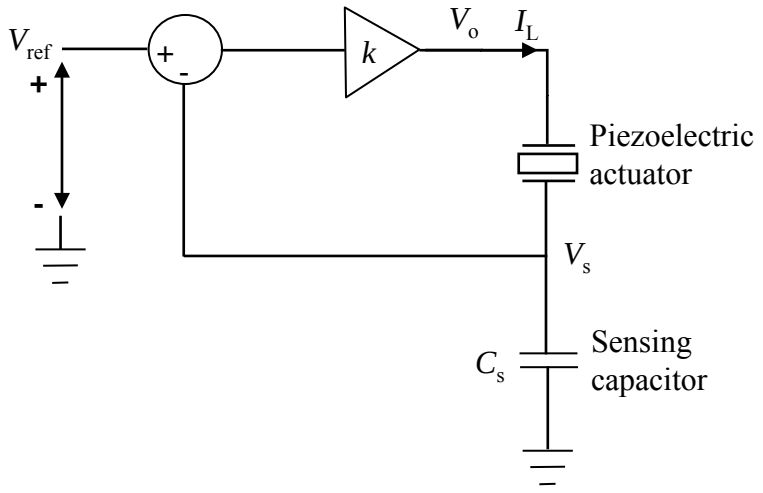

Figure 2.14: Ideal charge amplifier

In the Laplace domain, the load current $I_L(s)$ is equal to $V_{ref}(s)C_s s$. Because $I_L(s)$ is also equal to $q_L(s)s$, then

$$q_L(s) = C_s V_{ref}(s), \tag{2.15}$$

where q_L is the charge across the piezoelectric actuator. In other words, this is a charge amplifier with gain C_s.

In practice, because the sensing capacitor is not ideal, and due to dielectric leakage of the piezoelectric actuator, the current I_L will contain a DC component. As the sensing capacitor C_s integrates the current I_L, the voltage and the charge across the sensing capacitor will drift. The output voltage, V_o , will therefore drift and finally saturate at the maximum output voltage after a period of time.

The main complexity in designing this type of charge amplifier is to solve this drift problem. The two common methods to practically implement charge amplifiers while removing drift will be described in the following.

The first method proposed by Comstock (1981) is shown in Figure 2.15. It consists of an ideal charge amplifier and an initialization circuit which is periodically activated by a timer. The initialization circuit uses three switches to discharge the actuator and return the DC voltage across the actuator to zero in order to avoid saturation.

As can be seen from Figure 2.15 when switch 1 is closed, the sensing capacitor will be short circuited and the voltage across it will be set to zero. This discharges the sensing capacitor and avoids saturation.

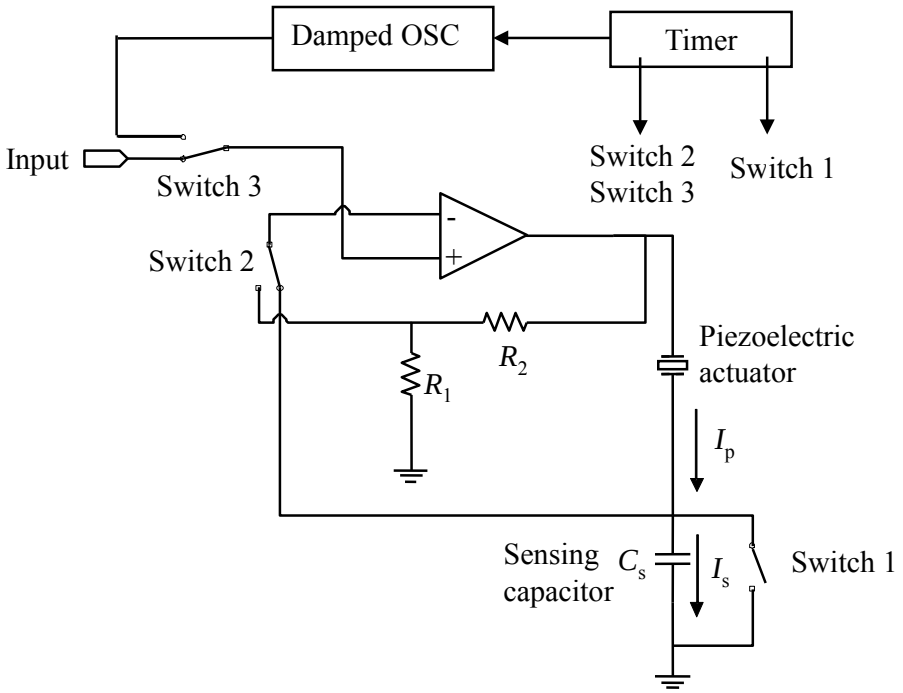

Figure 2.15: Charge controlled piezoelectric actuator (Comstock, 1981)

In the circuit shown in Figure 2.15, the timer drives switch 2 which connects the op-amp output to the inverting input through feedback resistor R_2. Because R_1 is connected to ground, the amplifier gain will be set to *Gain* = $1+\frac{R_2}{R_1}$ during the initialization. Switch 3 is used to divert the op-amp input

from the normal input to the damped oscillator input. This switch is closed during the initialization. The damped oscillator produces a down-ramped oscillation at low frequency, consisting of a low frequency sine wave modulated with a down ramp signal. The applied voltage oscillates around the mid-range displacement of the actuator. In this manner, eventually the system will settle at mid-range, point A in Figure 2.16, and the system will switch to normal mode. This point is equivalent to zero displacement and zero charge, which is the starting point at which time it can be switched to normal mode (Comstock, 1981).

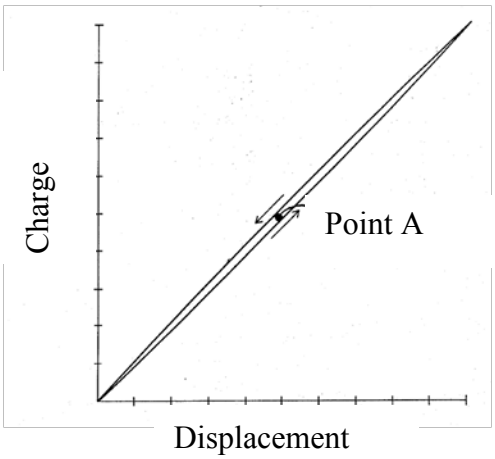

Figure 2.16: Hysteresis of charge controlled piezo (Comstock, 1981)

Main *et al.* (1995) also used the Comstock (1981) method with an additional current buffer at the output of the amplifier to improve the amplifier bandwidth. In both methods, the sudden discharge of the sensing capacitor through switch 1 causes output signal distortion at low frequencies and also undesirable high frequency disturbance (Fleming and Moheimani, 2003).

The second method to avoid drift is to employ a DC feedback path, as shown in Figure 2.17. As with the ideal charge amplifier, the feedback loop is utilized to equalize the voltage across the sensing capacitor with the reference voltage V_{ref}. The DC feedback path consists of resistors R_1 and R_2 which model the current leakage of the input terminal of the op-amp and current leakage of the sensing capacitor and piezoelectric actuator. In practice, the values of these resistors are not known. Therefore these resistors are replaced with additional resistance in order to manage the sensing voltage drift (Fleming and Moheimani, 2005).

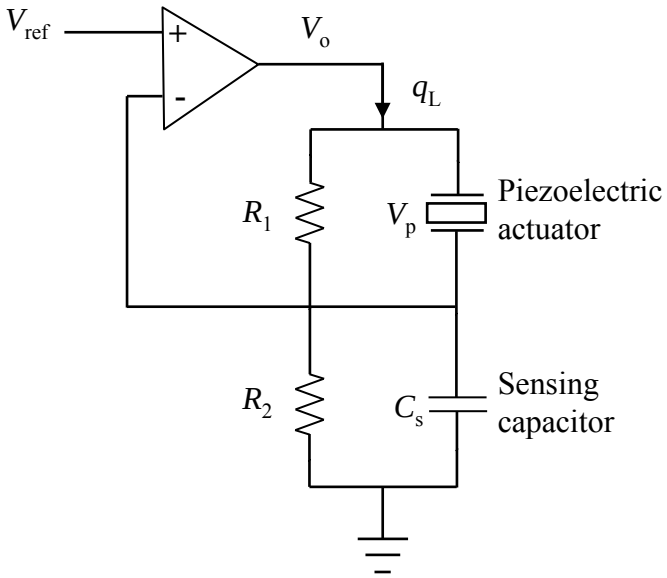

Figure 2.17: Circuit diagram of a charge amplifier with DC feedback path

Because of the DC feedback path, the charge amplifier has a different transfer function from the ideal charge amplifier. The transfer function between the load charge and the reference voltage is

$$\frac{q_{\mathrm{L}}(s)}{V_{\mathrm{ref}}(s)}=C_{\mathrm{s}}\frac{s}{s+\dfrac{1}{R_1C_{\mathrm{p}}}}, \tag{2.16}$$

where $q_{\mathrm{L}}(s)$ is the load charge, C_{s} is the sensing capacitor and C_{p} is the linear capacitance of the piezoelectric actuator. Equation (2.16) is a high pass filter with cut off frequency

$$\omega_{\mathrm{c}}=\frac{1}{R_1C_{\mathrm{p}}} \tag{2.17}$$

At frequencies well below ω_{c}, the impedance of resistors R_1 and R_2 are much smaller than the impedances C_{p} and C_{s}. Therefore, C_{p} and C_{s} are negligible. Hence

$$V_{\mathrm{p}}(s)=\frac{R_1}{R_2}V_{\mathrm{ref}}(s) \tag{2.18}$$

which is a voltage amplifier with gain $\frac{R_1}{R_2}$. Therefore at low frequencies because of the DC feedback path, the system is a voltage amplifier which cannot compensate the hysteresis loop of the piezoelectric actuator and hence there is a nonlinear relation between the reference signal and the displacement.

Many improvements have been made to the low frequency performance of the charge amplifier with DC feedback path. Fleming and Moheimani (2004) developed a hybrid DC-accurate charge amplifier for linear piezoelectric positioning. They added a voltage feedback loop to improve the low frequency response. However, compared to the charge amplifier

with DC feedback path the new voltage feedback limits the operational bandwidth. Their system works as a voltage amplifier at low frequencies and therefore it is still a non-linear system at low frequencies.

Yi and Veillette (2005) introduced a charge control system, utilizing an inverting amplifier in a feedback loop to drive a piezoelectric actuator. A lead compensator is also used to ensure the stability of the feedback loop. Moreover, a DC feedback path is utilized to eliminate the drift. However, the minimum frequency which the system can deal with as a charge controller is limited by the DC feedback path. This system is also unable to drive a grounded-load.

Fleming and Moheimani (2005) modified the charge amplifier with DC feedback path to be suitable for driving a grounded-load such as a piezoelectric tube actuator. As with Yi and Veillette (2005), they alleviated the drift problem by using a DC feedback path which limits the minimum frequency of the charge control operation. Given that a piezoelectric actuator is driven by an ideal charge amplifier, because of the voltage drop across the sensing capacitor, the maximum displacement achievable will be reduced.

2.4 Conclusion

The literature suggests that the main issue with designing a charge amplifier is drift, which can cause saturation of the load. While a number of authors have neglected the drift problem others have utilized additional analog circuitry to avoid it. In spite of this, additional analog circuitry often prevents the wide acceptance of charge drive methods (Kaizuka and Siu, 1988) and increases their implementation complexity and cost. Furthermore, this additional circuitry added to charge drive methods tackle the limitations

of operation, results in limitation of the lowest frequency of operation. As a consequence, charge amplifiers have not been widely applied.

As proposed charge methods adopted to date were implemented using analog circuitry. An opportunity exists to investigate the potential of a digital charge amplifier. A significant advantage of digital-based systems is their low-cost. Furthermore, digital systems should eliminate problems of drift due to ageing and temperature effects, as well as problems of reproducibility due to component variations arising from manufacturing tolerances that plague analog processing techniques. Most importantly, digital systems will make it possible to incorporate charge control with other displacement control methods, such as model-based control. Thus there is an opportunity to explore a digitally implemented charge amplifier within a hybrid system that can integrate charge control with other displacement controls such as model-based controls to achieve new levels of performance.

References

Abramovitch, D.Y., Andersson, S.B., Pao, L.Y. and Schitter, G., 2007. A tutorial on the mechanisms, dynamics and control of Atomic Force Microscopes. *In: American Control Conference.* pp. 3488–3502.

Adriaens, H.J.M.T.A., Koning, W.L.D. and Banning R., 2000. Modeling piezoelectric actuators. *IEEE/ASME Transactions on Mechatronics.* 5(4), 331–41.

Ballato, A., 1996. Piezoelectricity: History and new thrusts. *In: Proceedings of the IEEE Ultrasonics Symposium* 1, pp. 575-583.

Barrett, R.C. and Quate, C.F., 1991. Optical scan-correction system applied to atomic force microscopy. *Review of Scientific Instruments* 62(6)**,** 1393-1399.

Boukari, A. F., Carmona, J. C., Moraru, G., Malburet, F., Chaaba, A. and Douimi, M., 2011. Piezo-actuators modeling for smart applications. *Mechatronics* 21(1), 339-349.

Chen, C.J., 1992. Electromechanical deflections of piezoelectric tubes with quartered electrodes**.** *Applied Physics Letters* 60(1), 132–134.

Chen, W.T. and Tsao, S.H., 1977. Ink jet head. *IBM Technical Disclosure Bulletin* 20(2), 504–505.

Clayton, G.M., Tien, S., Fleming, A.J., Moheimani, S.O.R. and Devasia, S., 2008. Inverse-feedforward of charge-controlled piezopositioners. *Mechatronics* 18(5)**,** 273-281.

Comstock, R.H., 1981. Charge control of piezoelectric actuators to reduce hysteresis effects. *U.S. Patent* No. 4,263,527.

Croft, D. and Devasia, S., 1998. Hysteresis and vibration compensation for piezoactuators. *Journal of Guidance, Control, and Dynamics* 21(5)**,** 710-717.

Croft, D., Shed, G. and Devasia, S., 2001. Creep, hysteresis, and vibration compensation for piezoactuators: Atomic force microscopy application. *Transactions of the ASME. Journal of Dynamic Systems, Measurement and Control* 123**,** 35-4343.

Dang, X. J. and Tan, Y. H., 2007. RBF neural networks hysteresis modelling for piezoceramic actuator using hybrid model. *Mechanical Systems and Signal Processing* 21(1), 430-440.

Deng, L. and Tan, Y. H., 2009. Modeling hysteresis in piezoelectric actuators using NARMAX models. *Sensors and Actuators A: Physical* 149(1), 106-112.

Devasia, S., Eleftheriou, E. and Moheimani, S.O.R., 2007. A survey of control issues in nanopositioning. *IEEE Transactions on Control Systems Technology* 15(5), 802–823.

Dong, R., Tan, Y. H., Chen, H. and Xie, Y. Q., 2008. A neural networks based model for rate-dependent hysteresis for piezoceramic actuators. *Sensors and Actuators A: Physical* 143(2), 370-376.

Dorlemann, C., Muss, P., Schugt, M. and Uhlenbrock, R., 2002. New high speed current controlled amplifier for PZT multilayer stack actuators. *In: 8th International Conference on New Actuators.* Bremen, Germany, pp. 11-12.

Dupre, L., Van Keer, R. and Melkebeek, J., 2001. Generalized scalar preisach model for grain oriented materials excited along arbitrary directions. *Journal of Applied Physics* 89(11), 7245-7247.

Fleming, A.J. and Leang, K.K., 2008. Evaluation of charge drives for scanning probe microscope positioning stages. *In: American Control Conference*. pp. 2028–2033.

Fleming, A.J. and Moheimani, S.O.R., 2003. Improved current and charge amplifiers for driving piezoelectric loads. *In: Proceedings of the SPIE 5052.* pp. 242-252.

Fleming, A.J. and Moheimani, S.O.R., 2005. A grounded-load charge amplifier for reducing hysteresis in piezoelectric tube scanners. *Review of Scientific Instruments* 76(7), 73707.

Furutani, K. and Iida, K., 2006. A driving method of piezoelectric actuator by using current pulses. *Measurement Science and Technology* 17(2)**,** 2387.

Ge, P. and Jouaneh, M., 1995. Modeling Hysteresis in piezoceramic actuators. *Precision Engineering* 17(3), 211-221.

Ge, P. and Jouaneh, M., 1997. Generalized Preisach Model for hysteresis nonlinearity of piezoceramic actuators. *Precision Engineering* 20(2), 99-111.

Goldfarb, M. and Celanovic, N., 1997a. A lumped parameter electromechanical model for describing the nonlinear behavior of piezoelectric actuators. *Journal of Dynamic Systems, Measurement, and Control* 119, 478–485.

Goldfarb, M. and Celanovic, N., 1997b. Modeling piezoelectric stack actuators for control of micromanipulation. *IEEE Control Systems Magazine* 17, 69–79.

Han, Y. and Zhu, J., 2009. Implementation procedure for the generalized moving preisach model based on a first order reversal curve diagram. *Rare Metals* 28(4), 355-360.

Hui, Z., Shu-yi, Z. and Li, F., 2010. Simplified formulae to investigate flexural vibration characteristics of piezoelectric tubes in ultrasonic micro-actuators. *Ultrasonics* 50(3), 397–402.

Hwang, C. L., Jan, C. and Chen, Y. H., 2001. Piezomechanics using intelligent variable-structure control. *IEEE Transactions on Industrial Electronics* 48(1), 47-59.

Jonsson, U., 1998. Stability of uncertain systems with hysteresis nonlinearities. *International Journal of Robust and Nonlinear Control* 8**,** 279-293.

Kaizuka, H. and Siu, B., 1988. A simple way to reduce hysteresis and creep when using piezoelectric actuators. *Japanese Journal of Applied Physics* 27(5), 773–776.

Krejci, P. and Kuhnen, K., 2001. Inverse control of systems with hysteresis and creep. *In: IEE Proceedings-Control Theory and Applications*. pp. 185-192.

Kuhnen, K. and Janocha, H., 1998. Compensation of the creep and hysteresis effects of piezoelectric actuators with inverse systems. *In: The 6th International Conference on New Actuators.* pp. 426–429.

Kuiper, S. and Schitter, G., 2010. Active damping of a piezoelectric tube scanner using self-sensing piezo actuation. *Mechatronics* 20(6), 656–665.

Leang, K.K. and Devasia, S., 2002. Hysteresis, creep, and vibration compensation for piezoactuators: Feedback and feedforward control paper. *In: The 2nd IFAC Conference on Mechatronic Systems* Berkeley, CA, pp. 283–289.

Leung, M., Yue, J., Razak, K.A., Haemmerle, E., Hodgson, M. and Gao, W., 2008. Development of a 1 × 2 piezoelectric optical fiber switch – art. No. 683603. *Proceedings of* the *Society of Photo-Optical Instrumentation Engineers* 6836, 83603.

Li, C. and Tan, Y., 2004. A neural networks model for hysteresis nonlinearity. *Sensors and Actuators A: Physical* 112(1), 49-54.

Liaw, H. C. and Shirinzadeh, B., 2011. Robust adaptive constrained motion tracking control of piezo-actuated flexure-based mechanisms for micro/nano manipulation. *IEEE Transactions on Industrial Electronics* 58(4), 1406-1415.

Lin, F. J., Shieh, H. J. and Huang, P. K., 2006a. Adaptive wavelet neural network control with hysteresis estimation for piezo-positioning mechanism. *IEEE Transactions on Neural Networks* 17(2), 432-444.

Lin, F. J., Shieh, H. J., Huang, P. K. and Teng, L. T., 2006b. Adaptive control with hysteresis estimation and compensation using RFNN for piezo-actuator. *IEEE Transactions on Ultrasonics Ferroelectrics and Frequency Control* 53(9), 1649-1661.

Main, J.A., Garcia, E. and Newton, D.V., 1995. Precision position control of piezoelectric actuators using charge feedback. *In: Proceedings of the SPIE - The International Society for Optical Engineering.* pp. 243-254.

Meeker, T. R., 1996. Publication and proposed revision of ANSI/IEEE standard 176-1987. ANSI/IEEE Standard on Piezoelectricity. *IEEE Transactions on Ultrasonics Ferroelectrics and Frequency Control* 43(5), 717-718.

Minase, J., Lu, T.F., Cazzolato, B. and Grainger, S.,2010. A review, supported by experimental results, of voltage, charge and capacitor insertion method for driving piezoelectric actuators. *Precision Engineering: Journal of International Society for Precision Engineering and Nanotechnology* 34(4), 692–700.

Moheimani, S.O.R., 2008. Invited review article: Accurate and fast nanopositioning with piezoelectric tube scanners: Emerging trends and future challenges. *Review of Scientific Instruments* 79(7), 071101.

Moheimani, S.O.R. and Fleming, A.J., 2006. Piezoelectric transducers for vibration control and damping. *Advances in Industrial Control.* London: Springer.

Moheimani, S.O.R. and Vautier, B.J.G., 2005. Resonant control of structural vibration using charge-driven piezoelectric actuators. *IEEE Transactions on Control Systems Technology* 13(6), 1021-1035.

Nelles, O., 2000. Nonlinear System Identification: From classical approaches to neural networks and fuzzy models, *Springer*.

Nelles, O., 2001. Nonlinear system identification. *Springer-Verlag*. Berlin, Heidelberg.

Newcomb, C.V. and Flinn, I., 1982. Improving the linearity of piezoelectric ceramic actuators. *Electronics Letters* 18(11), 442–444.

Pare, T.E. and How, J.P., 1998. Robust H-infinity controller design for systems with hysteresis nonlinearities. *In: Proceedings of the 37th IEEE Conference on Decision and Control.* pp. 4057-4062.

Preisach, F., 1935. Uber die magnetische nachwirkung. *Zeitschrift für Physik* 94(5-6), 277-302

Ru, C.H., Chen, L.G., Shao, B., Rong, W.B. and Sun, L.N., 2008. A new amplifier for improving piezoelectric actuator linearity based on current switching in precision positioning. *Measurement Science and Technology* 19(1), 015203.

Shieh, H.J., Lin, F. J., Huang, P.K. and Teng, L.T., 2004. Adaptive tracking control solely using displacement feedback for a piezo-positioning mechanism. *IEE Proceedings-Control Theory and Applications* 151(5), 653–660.

Smith, R.C., Ounaies, Z. and Wieman, R., 2000. A model for rate-dependent hysteresis in piezoceramic materials operating at low frequencies. *In: Institute for Computer Applications in Science and Engineering (ICASE).*

Song, D. W. and Li, C. J., 1999. Modeling of piezo actuator's nonlinear and frequency dependent dynamics. *Mechatronics* 9(4), 391-410.

Špiller, M., and Hurák, Z., 2011. Hybrid charge control for stick–slip piezoelectric actuators. *Mechatronics* 21(1), 100-108.

Tan, X., and Baras, J.S., 2005. Adaptive identification and control of hysteresis in smart materials. *IEEE Transactions on Automatic Control* 50(6), 827-839.

Vautier, B.J.G. and Moheimani, S.O.R, 2005. Charge driven piezoelectric actuators for structural vibration control: Issues and implementation. *Smart Materials and Structures* 14**,** 575-586.

Wang, D. H., Zhu, W. and Yang, Q., 2011. Linearization of stack piezoelectric ceramic actuators based on Bouc-wen model. *Journal of Intelligent Material Systems and Structures* 22**,** 401-413.

Wu, Y. and Zou, Q.Z., 2007. Iterative control approach to compensate for both the hysteresis and the dynamics effects of piezo actuators. *IEEE Transactions on Control Systems Technology* 15**,** 936-944.

Yanding, Q., Yanling, T., Dawei, Z., Shirinzadeh, B. and Fatikow, S., 2013. A novel direct inverse modeling approach for hysteresis compensation of piezoelectric actuator in feedforward applications. *IEEE/ASME Transactions on Mechatronics* 18**,** 981-989.

Yang, X.F., Li, W., Wang, Y.Q. and Ye, G., 2008. Modeling hysteresis in piezo actuator based on neural networks. *In: 3rd International Conference on Intelligence Computation and Applications*. Wuhan, China, pp. 290–296.

Yi, K.A. and Veillette, R.J., 2005. A charge controller for linear operation of a piezoelectric stack actuator. *IEEE Transactions on Control Systems Technology* 13(4), 517–526.

Yu, Y. H., Naganathan, N. and Dukkipati, R., 2002. Preisach modeling of hysteresis for piezoceramic actuator system. *Mechanism and Machine Theory* 37(1), 49-59.

Zareinejad, M., Ghidary, S. S., Rezaei, S. M. and Abdullah, A., 2010. Precision control of a piezo-actuated micro telemanipulation system. *International Journal of Precision Engineering and Manufacturing* 11(1), 55-65.

Zhang, X. L., Tan, Y. H., Su, M. Y. and Xie, Y. Q., 2010. Neural networks based identification and compensation of rate-dependent hysteresis in piezoelectric actuators. *Physica B: Physics of Condensed Matter* 405(12), 2687-2693.

Zhang, Y. D., Fang, Y. C., Zhou, X. W. and Dong, X. K., 2009. Image-based hysteresis modeling and compensation for an AFM piezo-scanner. *Asian Journal of Control* 11(2), 166-174.

Zhao, Y.D. and Jayasuriya, S., 1995. Feedforward controllers and tracking accuracy in the presence of plant uncertainties. *Journal of Dynamic Systems Measurement and Control-Transactions of the ASME* 117**,** 490-495.

3 Digital Charge Amplifier

3.1 Introduction

As mentioned in the previous chapter, analog charge amplifiers are expensive to implement due to the complexity of the analog circuitry. This chapter presents a novel digital charge amplifier (DCA) which is the foundation development of this thesis. The design and analysis of the DCA is presented and it is shown that the DCA can reduce hysteresis and improve the linearity of piezoelectric actuators. In order to evaluate the performance of the DCA, the behaviour of the DCA in respect of linearity, frequency response and voltage drop are presented in the experimental results.

This easily-implemented, digital charge drive approach opens up the possibility of integration with other displacement control techniques such as model-based methods to improve the performance of the displacement controller.

3.2 Implementation and analysis of an innovative digital charge amplifier for hysteresis reduction in piezoelectric stack actuators

Submitted to Review of Scientific Instruments.

Statement of Authorship

Title of Paper	Implementation and analysis of an innovative digital charge amplifier for hysteresis reduction in piezoelectric stack actuators
Publication Status	○ Published ○ Accepted for Publication ● Submitted for Publication ○ Publication Style
Publication Details	Bazghaleh, M., Grainger, S., Cazzolato, B. & Lu, T.F. (2013). Implementation and analysis of an innovative digital charge amplifier for hysteresis reduction in piezoelectric stack actuators. Review of Scientific Instruments. Under-review.

Author Contributions

By signing the Statement of Authorship, each author certifies that their stated contribution to the publication is accurate and that permission is granted for the publication to be included in the candidate's thesis.

Name of Principal Author (Candidate)	Mr. Mohsen Bazghaleh		
Contribution to the Paper	Developed theory, performed experimental work, analyzed data and wrote the manuscript.		
Signature		Date	25/10/2013

Name of Co-Author	Dr. Steven Grainger		
Contribution to the Paper	Supervised the research, contributed in academic discussion and reviewed manuscript.		
Signature		Date	25/10/13

Name of Co-Author	Dr. Ben Cazzolato		
Contribution to the Paper	Supervised the research, contributed in academic discussion and reviewed manuscript.		
Signature		Date	25/10/13

Name of Co-Author	Dr. Tien-Fu Lu		
Contribution to the Paper	Supervised the research, contributed in academic discussion and reviewed manuscript.		
Signature		Date	25/10/13

Implementation and analysis of an innovative digital charge amplifier for hysteresis reduction in piezoelectric stack actuators

Mohsen Bazghaleh, Steven Grainger, Ben Cazzolato and Tien-Fu Lu

Abstract. *Smart actuators are the key components in a variety of nanopositioning applications, such as scanning probe microscopes and atomic force microscopes. Piezoelectric actuators are the most common smart actuators due to their high resolution, low power consumption and wide operating frequency but they suffer hysteresis which affects linearity. In this paper, an innovative digital charge amplifier is presented to reduce hysteresis in piezoelectric stack actuators. Compared to traditional analog charge drives, experimental results show that the piezoelectric stack actuator driven by the digital charge amplifier has less hysteresis. It is also shown that the voltage drop of the digital charge amplifier is significantly less than the voltage drop of conventional analog charge amplifiers.*

Keywords: *Piezoelectric actuators; digital implementation; hysteresis; charge control***.**

1 Introduction

Piezoelectric stack actuators have been widely used in many applications ranging from fuel injection systems (MacLachlan *et al*., 2004) to vibration cancellation in disk drives (Ma and Ang, 2000). Aside from being compact in size, they are capable of nanometre resolution in displacement, have high stiffness, provide excellent operating bandwidth and high force output

(Devasia *et al.*, 2007). A piezoelectric stack actuator is assembled using multiple layers of piezoelectric materials which are placed in series and wired in parallel as shown in Figure 1. The sign of the applied voltage, *V*, determines whether the actuator should expand or contract.

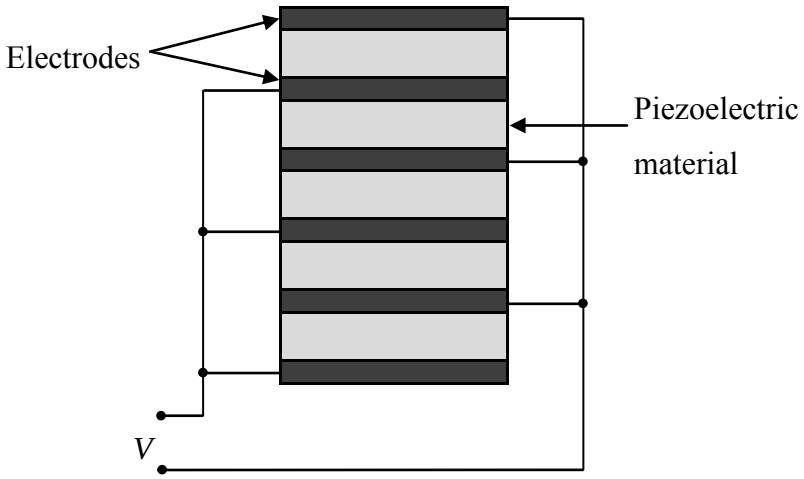

Figure 1: Piezoelectric stack actuator construction

Typically piezoelectric stack actuators are driven by voltage, however voltage driven methods suffer from hysteresis and creep which are nonlinear in nature and reduce the positioning accuracy (Leang and Devasia, 2002).

Creep is the result of the remnant polarization which continues to change after the applied signal reaches its final value and is normally an issue at low frequencies (Meeker, 1996). Hysteresis is due to the polarization of microscopic particles (Damjanovic, 2005) and depends on both the currently applied voltage as well as that previously applied (Kuhnen and Janocha, 1998). Physically it means that, for a similar voltage input, the piezoelectric actuator may have different displacement values. The relationship between applied voltage and displacement also changes subject to the amplitude and the frequency of the applied voltage, thus it is both non-linear and dynamic in nature (Adriaens, 2000).

A variety of approaches have been used to tackle the hysteresis of piezoelectric actuators. Feed-forward control uses an inverse-model, such as the Preisach model (Ge and Jouaneh, 1995) or Maxwell resistive model (Goldfarb and Celanovic, 1997b), to compensate for hysteresis. But due to uncertainties in the piezo parameters, the feedforward inverse-model technique can suffer from a lack of robustness. Another approach is displacement feedback control (Shieh *et al*., 2004) but this is limited by sensor-induced noise, high cost, additional complexity and limited bandwidth (Fleming and Leang, 2008).

Charge regulator and capacitor insertion techniques have also been used (Minase *et al*., 2010). The capacitor insertion method (Kaizuka and Siu, 1988) involves using a capacitor in series with the piezoelectric actuator and, while it is effective in dealing with hysteresis, significantly reduces the operating range because of the voltage drop across the capacitor. Charge regulation was first introduced by Comstock (1981) who showed that by regulating the charge across a piezoelectric actuator the hysteresis is reduced significantly. However a charge amplifier approach has historically been complicated and expensive to implement due to the complexity of the analog circuitry required to meet stringent performance targets (Fleming and Moheimani, 2005). Additionally, in the ideal charge amplifier, the load capacitor is charged up because of the uncontrolled nature of the output voltage and once the output voltage reaches the power supply rails, the charge amplifier saturates. To avoid this undesirable effect additional methods have been used which increases the implementation complexity (Fleming and Moheimani, 2004). Comstok (1981) used an initialization circuit to short circuit the sensing capacitor periodically; however, it causes undesirable disturbances at high frequencies. Fleming and Moheimani (2004) used an additional voltage feedback loop to improve the low

frequency response. But it works as a voltage amplifier at low frequencies. Therefore the piezo still suffers from hysteresis at low frequencies.

In this paper, a new digital charge amplifier is presented. It significantly reduces the hysteresis effect of piezoelectric actuators. It is more cost effective than analog charge amplifiers and this new design significantly addresses the reduced voltage drop. The design and analysis of the digital charge amplifier are presented in Section 2. Experimental investigations are in Section 3 followed by a conclusion in Section 4.

2 Design and analysis

In a typical analog charge amplifier, sensing capacitors are used for integrating electric currents. However, since these capacitors are not ideal they suffer from dielectric charge leakage which is one of the reasons for drift and saturation of loads (Clayton *et al*., 2006). The main operating principle in the digital charge amplifier is to calculate the charge signal by digitally integrating the electric current passing the piezoelectric actuator. The sensing capacitor is replaced by a sensing resistor whose voltage drop can be measured to provide a signal from which the electric current can be deduced and thereby avoids the dielectric charge leakage of capacitors.

2.1 Digital charge amplifier configuration

Figure 2 shows the digital charge amplifier that forms the basis of this work. It consists of a voltage amplifier, digital to analog converter (DAC), analog to digital converter (ADC) and a digital signal processor (DSP). A sensing resistor is placed in series with the piezoelectric stack actuator.

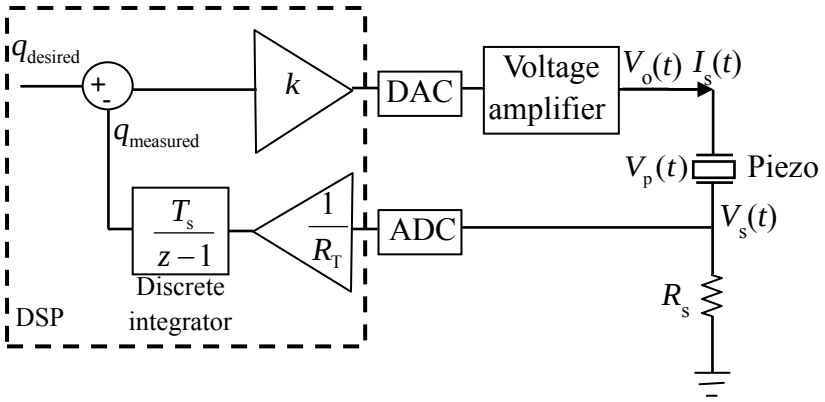

Figure 2: Circuit of the digital charge amplifier

The DSP unit calculates the charge across the piezoelectric actuator, $q_p(t)$, by integrating the piezoelectric actuator current.

$$q_p(t) = \int I_s(t)dt. \tag{1}$$

Because of the ADC input resistance $R_{inputADC}$, the piezoelectric actuator current is given by

$$I_s(t) = \frac{V_s(t)}{R_s \| R_{inputADC}} \tag{2}$$

where $V_s(t)$ is the sensing voltage across the sensing resistor.

Substituting (2) into (1) gives

$$q_p(t) = \int \frac{V_s(t)}{R_s \| R_{inputADC}} dt. \tag{3}$$

The input resistance is in parallel with sensing resistor R_s so the total resistance is

$$R_{\mathrm{T}}=R_{\mathrm{s}}\|R_{\mathrm{inputADC}}. \tag{4}$$

Substituting (4) in (3) gives

$$q_{\mathrm{p}}(t)=\frac{1}{R_{\mathrm{T}}}\int V_{\mathrm{s}}(t)dt. \tag{5}$$

Therefore the charge across the piezoelectric actuator is equal to the integral of the voltage across the sensing resistor divided by the total resistance. A high gain feedback loop is used to equate the actual charge with the desired charge.

2.2 Transfer function of the digital charge amplifier

The transfer function can now be derived. By considering a capacitor, C_{L}, as a model of the piezoelectric actuator (Fleming and Moheimani, 2005, Huang *et al*., 2010), the transfer function between the output of the voltage amplifier $V_{\mathrm{o}}(t)$ and sensing voltage $V_{\mathrm{s}}(t)$ is:

$$H(s)=\frac{V_{\mathrm{s}}(s)}{V_{\mathrm{o}}(s)}=\frac{R_{\mathrm{T}}C_{\mathrm{L}}s}{R_{\mathrm{T}}C_{\mathrm{L}}s+1} \tag{6}$$

By taking the Z transform, the discrete transfer function will be:

$$H(z)=\frac{V_{\mathrm{s}}(z)}{V_{\mathrm{o}}(z)}=\frac{z\text{-}1}{z\text{-}\mathrm{e}^{-\frac{T_{\mathrm{s}}}{R_{\mathrm{T}}C_{\mathrm{L}}}}}} \tag{7}$$

where T_{s} is the sampling time. Moreover, the transfer function of the digital charge drive algorithm is

$$V_{\mathrm{o}}(z) = k(q_{\mathrm{desired}}(z) - \frac{T_{\mathrm{s}}}{(z-1)R_{\mathrm{T}}} V_{\mathrm{s}}(z)) \tag{8}$$

where k is the closed loop gain and $q_{\mathrm{desired}}(z)$ is the desired charge. Substituting (8) in (7) results in

$$\frac{z - e^{-\frac{T_{\mathrm{s}}}{R_{\mathrm{T}}C_{\mathrm{L}}}}}{z-1} V_{\mathrm{s}}(z) = k(q_{\mathrm{desired}}(z) - \frac{T_{\mathrm{s}}}{(z-1)R_{\mathrm{T}}} V_{\mathrm{s}}(z)). \tag{9}$$

By considering $V_{\mathrm{s}}(z) = \frac{q_{\mathrm{actual}}(z) R_{\mathrm{T}}(z-1)}{T_{\mathrm{s}}}$, where $q_{\mathrm{actual}}(z)$ is the actual charge across the piezoelectric actuator, the discrete transfer function from the input (desired charge) to the output (actual charge) is given by

$$\frac{q_{\mathrm{actual}}(z)}{q_{\mathrm{desired}}(z)} = \frac{\frac{T_{\mathrm{s}}k}{R_{\mathrm{T}}}}{z - e^{-\frac{T_{\mathrm{s}}}{R_{\mathrm{T}}C_{\mathrm{L}}}} + \frac{T_{\mathrm{s}}k}{R_{\mathrm{T}}}}. \tag{10}$$

For a typical piezoelectric stack actuator with a capacitance of 3.4 μF using the digital charge amplifier with a 100 Ω sensing resistor and sampling frequency 40 kHz, the frequency response has zero dB gain with approximately zero phase-shift up to 10 kHz. This is the theoretical bandwidth. In Section 3 the practical bandwidth will be shown.

3 Experimental investigations

3.1 Experimental setup

The proposed technique was validated experimentally by using a piezoelectric stack actuator AE0505D44H40 from NEC. The displacement

of the piezoelectric stack actuator was measured using a strain gauge from Vishay Electronics (EA-06-125TG-350), which is solely used to evaluate the performance of the DCA. All digital algorithms, estimation and control functions were written in Matlab/Simulink then compiled for a dSPACE DS1104 development platform. Matlab/Simulink was also used for actuator characterization (Figure 3).

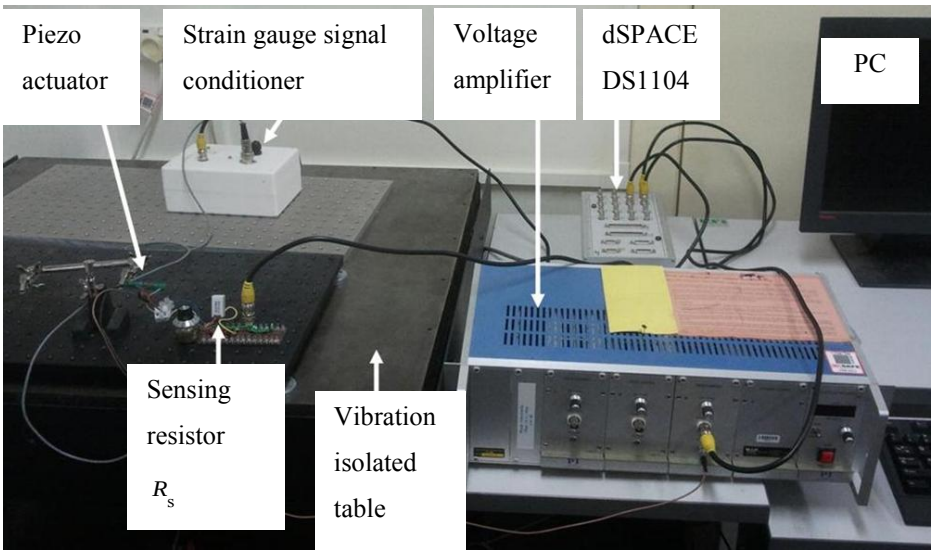

Figure 3: The experimental setup

3.2 DCA linearity results

Figure 4 illustrates the improvement in linearity offered by the new digital charge amplifier compared to a standard voltage amplifier. Figure 4a shows the hysteresis loop when the piezo is driven by a voltage amplifier and Figure 4b shows the results when the piezo is driven by the DCA. It can be seen that the hysteresis loop is significantly reduced in the DCA. For a displacement range of 11.54μm, the digital charge amplifier has maximum hysteresis of 144 nm while it is 1598 nm for the voltage amplifier for a

driving frequency of 10 Hz. Therefore, the digital charge amplifier has reduced the hysteresis by 91%.

Figure 5 illustrates the displacement trajectories and tracking errors under voltage drive and DCA. A 5 Hz triangle wave with three different displacement ranges (4 μm, 8 μm and 20 μm) were chosen which correspond to 10%, 20% and 50% of the maximum displacement range.

Table 1 shows a comparison of the maximum absolute errors for voltage drive and DCA. For displacement range of 4 μm, 8 μm and 20 μm, the voltage-driven displacement errors were reduced by 77.15%, 89.54% and 91.14% using the DCA.

Table 1: Comparison of errors between the voltage drive and the DCA

	Maximum absolute error		
Displacement range	Voltage drive	DCA	Reduction
4 μm	3.35%	0.76%	77.15%
8 μm	5.02%	0.52%	89.54%
20 μm	7.18%	0.64%	91.14%

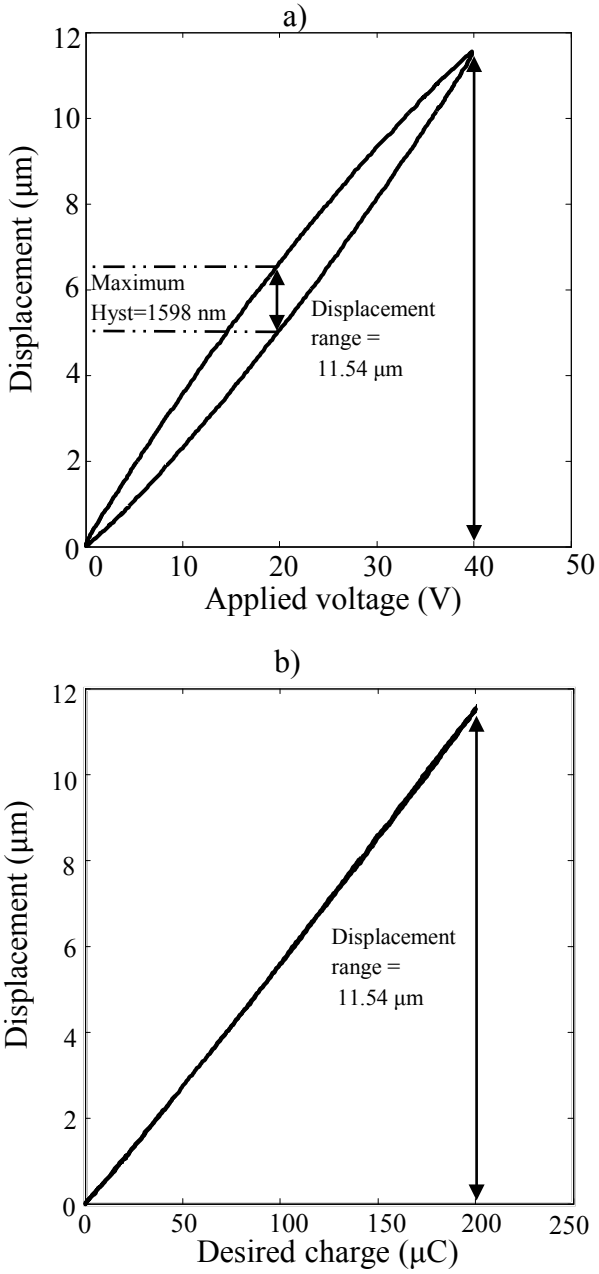

Figure 4: Experimental hysteresis loop of a piezoelectric stack actuator AE0505D44H40 subjected to a 10 Hz sine wave driven by a) a voltage amplifier and b) DCA

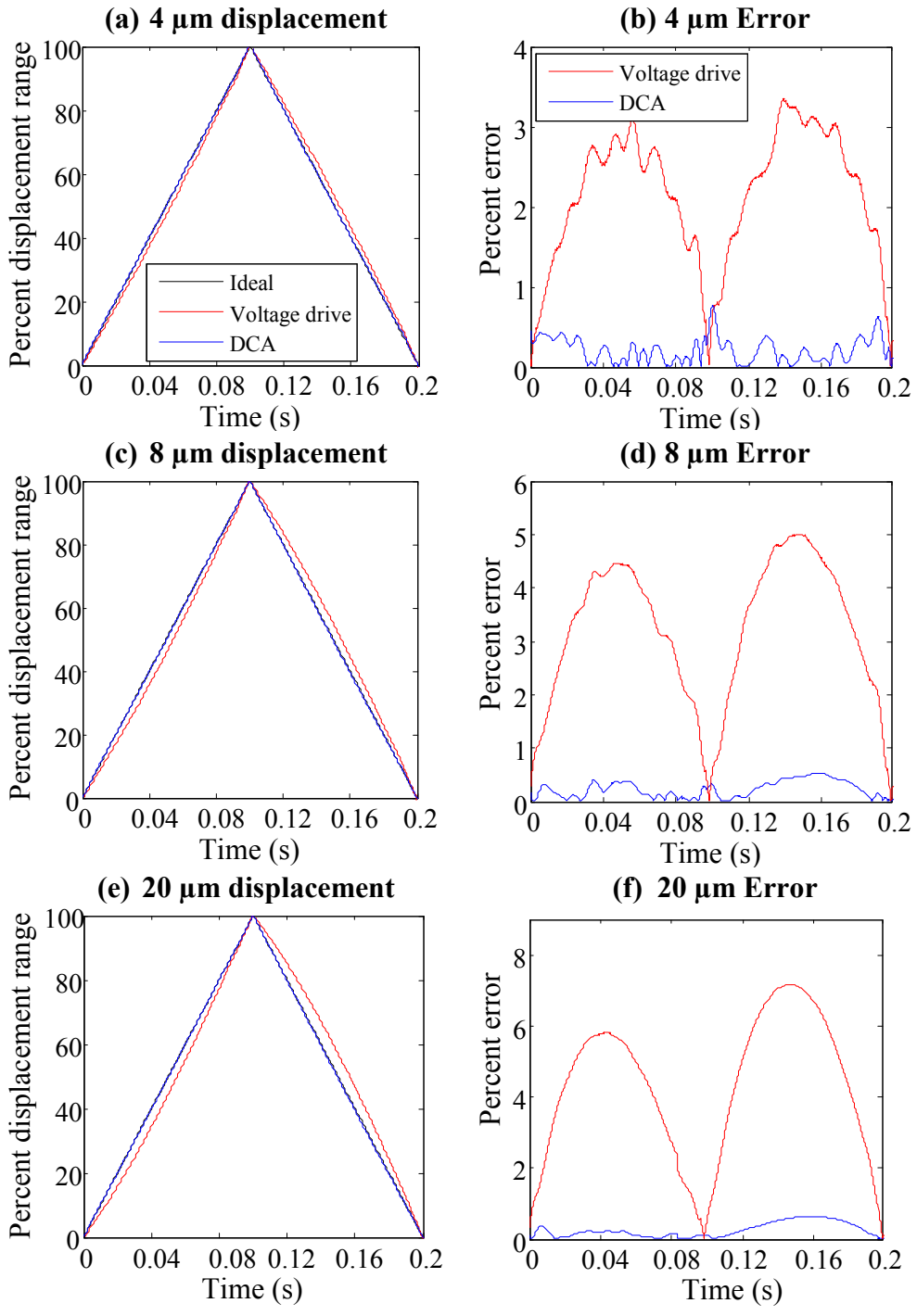

Figure 5: The percentage of displacements and errors for 5 Hz triangle waves with 4, 8 and 20 µm displacement ranges

3.3 Frequency response of the output displacement to input charge

Figure 6 illustrates experimentally measured displacement versus charge at different frequencies. This shows that at higher frequencies the area within the loop between charge and displacement increases. This loop is not hysteresis but rather a linear phase shift. Figure 7 illustrates the frequency response of displacement output to charge input for the stack piezo. It can be seen that for frequencies higher than 100Hz the phase lag starts to increase, which makes it undesirable for higher frequency tracking applications. As described by Goldfarb and Celanovic (1997a) the relation between the charge and the displacement of the piezo introduces a phase lag as shown in Figure 7 from the nature of the piezoelectric actuator itself.

3.4 Low frequency limitation of the DCA

Because of the RC circuit formed by the sensing resistor and the piezo, at low frequencies the voltage drop across the sensing resistor decreases significantly. This causes a reduction in the signal-to-noise ratio (SNR) which is shown in Figure 8. To make the data comparable, the displacement range is set to be ±5 μm. Therefore the accuracy of measured charge decreases with decreasing frequency, which causes an increase in the error of the output displacement. As shown in Figure 8, increasing the sensing resistance can increase the voltage across the sensing resistor and therefore improve the SNR. However, increasing the sensing resistor can cause the sensing voltage to reach the maximum ADC input voltage at lower frequencies and therefore limits the bandwidth of the DCA.

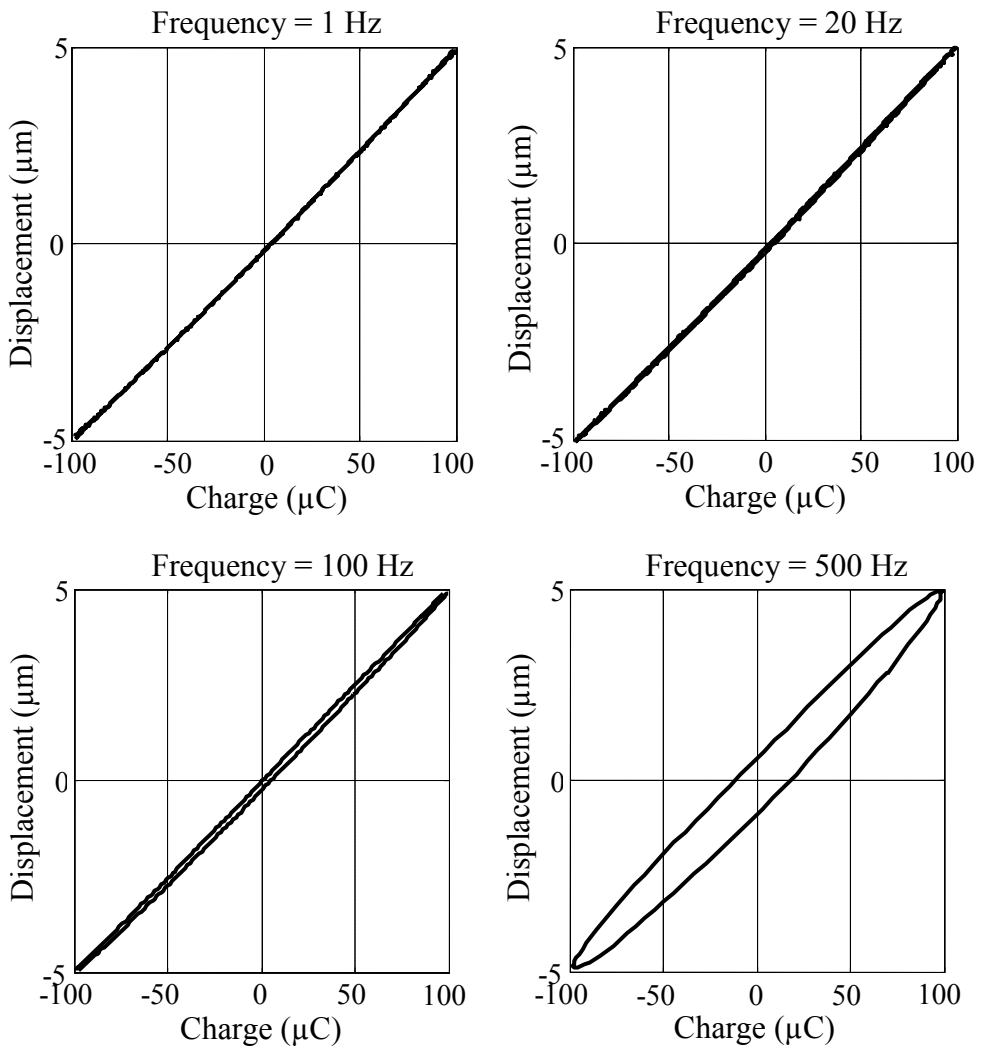

Figure 6: Measured displacement versus charge for a sinusoidal input of 1 Hz, 20 Hz, 100 Hz and 500 Hz

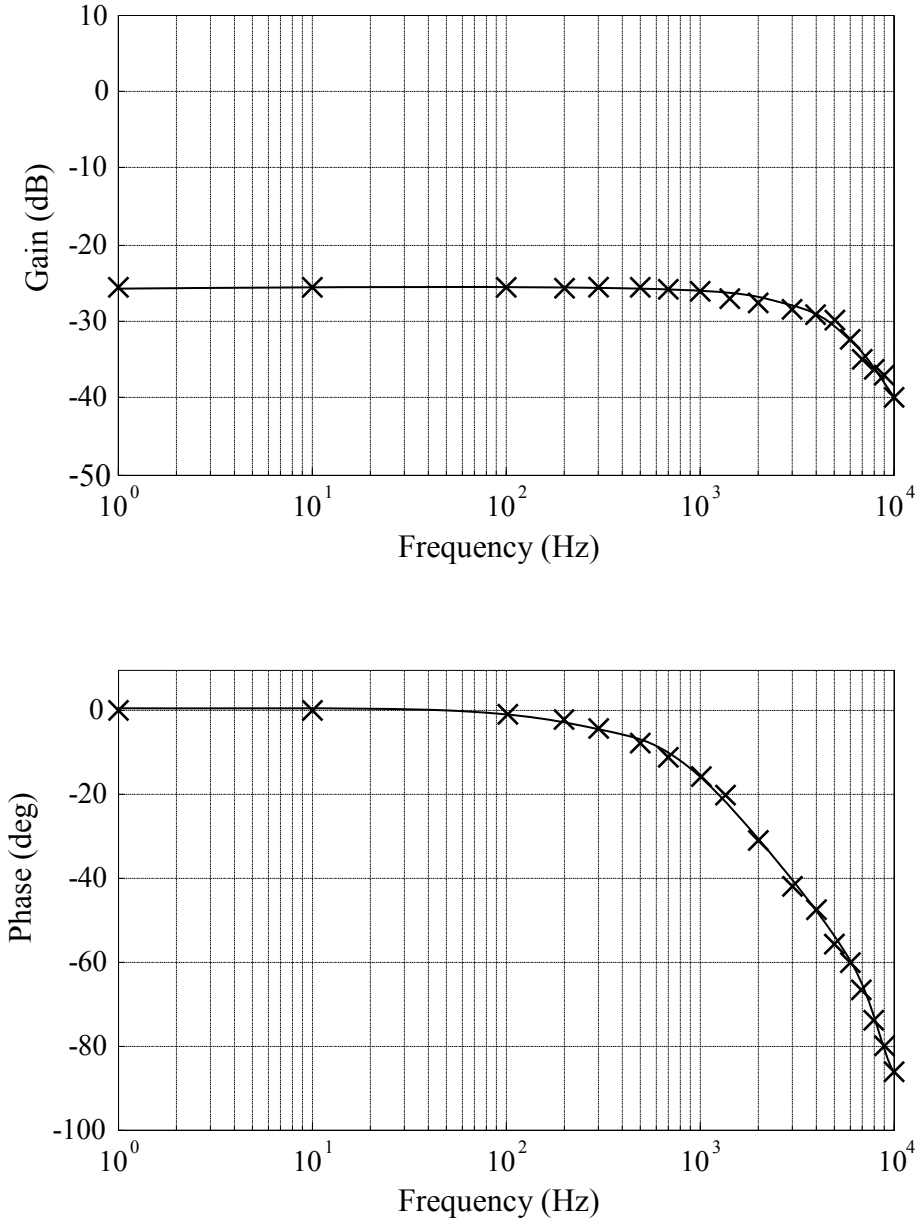

Figure 7: Measured frequency response of the output displacement to input charge

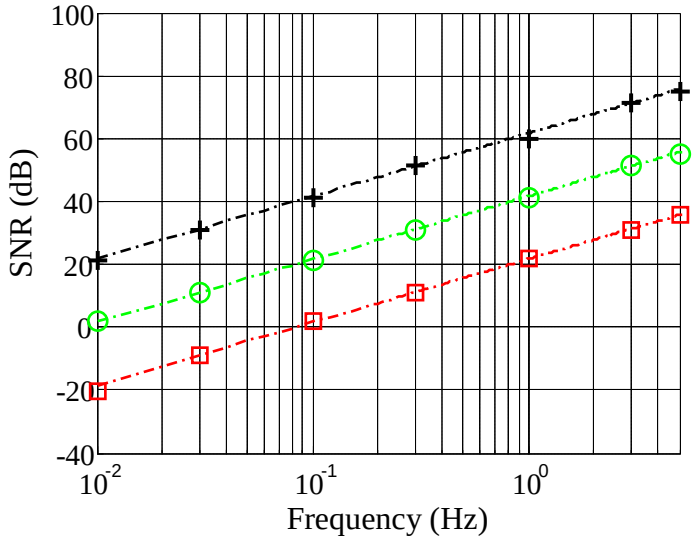

Figure 8: Signal to noise ratio (SNR) of the sensing voltage for R_s equal to 50 Ω (Red), 500 Ω (Green) and 5 KΩ (Black)

3.5 Voltage drop

The voltage drop across any sensing element limits the piezoelectric actuator voltage range. Table 2 compares the maximum voltage drop for two hysteresis linearization techniques from the literature that have been evaluated experimentally (a grounded charge amplifier (Fleming and Moheimani 2005, Minase *et al*., 2010), capacitor insertion (Kaizuka and Siu, 1988, Minase *et al*., 2010)) and the DCA at different frequencies. To make the data comparable, the displacement range is set to be ±5μm. It can be seen that at lower frequencies the DCA voltage drop is significantly smaller than the voltage drop of the grounded charge amplifier or capacitor insertion method, thus maximizing the displacement that can be achieved for a given supply voltage.

Table 2: Comparison of voltage drop and percentage of voltage drop using three alternative methods at four different frequencies

Frequency	Grounded charge amplifier (C_s = 30 µF)	Capacitor insertion (C_s = 1 µF)	DCA (R_s = 50 Ω)
0.1 Hz	2.72(12%)	51.42(72%)	0.01(0.05%)
1 Hz	2.41(11%)	52.38(72%)	0.02(0.1%)
10 Hz	2.48(11%)	53.28(72%)	0.25(1.2%)
75 Hz	2.32(11%)	53.53(72%)	1.93(8.8%)

3.6 Choosing an appropriate sensing resistor

Choosing the appropriate sensing resistor is an important task when using the DCA. The sensing resistor should not be so small that the noise on the measured charge increases significantly and also it should not be so large that V_s becomes more than the input ADC limitation at the required bandwidth. The value of the sensing resistor should be set for each application. To select the best value for R_s, the maximum displacement at the maximum frequency should be considered. Then R_s should be calculated such that the sensing voltage will not be greater than the maximum ADC voltage. Using the highest possible sensing resistor increases the SNR at low frequencies. As an indicator, if the maximum displacement and the maximum frequency for a particular application are 25 µm and 100 Hz respectively, then R_s should be set to 50 Ω to avoid saturation on the ADC and if the acceptable SNR is taken as 30 dB then from Figure 8, the minimum operational frequency will be 3 Hz.

4 Conclusion

An innovative digital charge amplifier has been introduced to reduce the non-linear behaviour of a piezoelectric actuator. For the experiments

conducted, it was found that the charge amplifier reduced the hysteresis by 91% at 10 Hz. Compared to a grounded charge amplifier, the DCA has less voltage drop, does not need gain tuning and is far more cost effective. This easily implemented, digital charge drive approach opens up the possibility of integration with other displacement control methods such as model-based methods to improve the performance of the displacement controller which will be investigated in future work.

References

Adriaens, H.J.M.T.A., Koning, W.L.D. and Banning R., 2000. Modeling piezoelectric actuators. *IEEE/ASME Transactions on Mechatronics.* 5(4), 331–341.

Bazghaleh, M., Grainger, S., Cazzolato, B. and Lu, T.-F., 2010. An innovative digital charge amplifier to reduce hysteresis in piezoelectric actuators, *In: Australian Robotics and Automation Association (ACRA).* Brisbane, Australia.

Clayton, G., Tien, S., Fleming, A., Moheimani, S. and Devasia, S., 2006. Hysteresis and vibration compensation in piezoelectric actuators by integrating charge control and inverse feedforward. *In: Proceedings of 4th IFAC Conference on Mechatronic Systems*. Heidelberg, Germany.

Comstock, R.H., 1981. Charge control of piezoelectric actuators to reduce hysteresis effects. *USA Patent* No. 4,263,527.

Damjanovic, D., 2005. Hysteresis in piezoelectric and ferroelectric materials *The Science of Hysteresis* 3, 337–465.

Devasia, S., Eleftheriou, E. and Moheimani, S.O.R., 2007. A survey of control issues in nanopositioning. *IEEE Transactions on Control Systems Technology* 15(5), 802–823.

Fleming, A.J. and Leang, K.K., 2008. Evaluation of charge drives for scanning probe microscope positioning stages. *In: American Control Conference.* Seattle, USA, pp. 2028–2033.

Fleming, A.J. and Moheimani, S.O.R., 2004. Hybrid DC accurate charge amplifier for linear piezoelectric positioning. *In: Proceedings of 3th IFAC Conference on Mechatronic Systems*. pp. 283–288.

Fleming, A.J. and Moheimani, S.O.R., 2005. A grounded-load charge amplifier for reducing hysteresis in piezoelectric tube scanners. *Review of Scientific Instruments* 76(7), 73707.

Ge, P. and Jouaneh, M., 1995. Modeling Hysteresis in piezoceramic actuators. *Precision Engineering* 17(3), 211-221.

Goldfarb, M. and Celanovic, N., 1997a. A lumped parameter electromechanical model for describing the nonlinear behavior of piezoelectric actuators. *Journal of Dynamic Systems, Measurement, and Control* 119, 478–485.

Goldfarb, M. and Celanovic, N., 1997b. Modeling piezoelectric stack actuators for control of micromanipulation. *IEEE Control Systems Magazine* 17, 69–79.

Huang, L., Ma, Y.T., Feng, Z.H. and Kong, F.R., 2010. Switched capacitor charge pump reduces hysteresis of piezoelectric actuators over a large frequency range. *Review of Scientific Instruments* 81(9), 094701.

Kaizuka, H. and Siu, B., 1988. A simple way to reduce hysteresis and creep when using piezoelectric actuators. *Japanese Journal of Applied Physics* 27(5), 773–776.

Kuhnen, K. and Janocha, H., 1998. Compensation of the creep and hysteresis effects of piezoelectric actuators with inverse systems. *In: The 6th International Conference on New Actuators.* pp. 426–429.

Leang, K.K. and Devasia, S., 2002. Hysteresis, creep, and vibration compensation for piezoactuators: Feedback and feedforward control paper. *In: The 2nd IFAC Conference on Mechatronic Systems*. Berkeley, CA, pp. 283–289.

Ma, J. and Ang, M., 2000. High-bandwidth macro/microactuation for hard-disk drive. *In: Proceedings of the SPIE*. pp. 94–102.

Maclachlan B.J., Elvin, N., Blaurock, C. and Keegan, N.J., 2004. Piezoelectric valve actuator for flexible diesel operation. *In: Smart Structures and Materials, International Society for Optics and Photonics.* pp. 167-178.

Meeker, T. R., 1996. Publication and proposed revision of ANSI/IEEE standard 176-1987. ANSI/IEEE Standard on Piezoelectricity. *IEEE Transactions on Ultrasonics Ferroelectrics and Frequency Control* 43(5), 717-718.

Minase, J., Lu, T.F., Cazzolato, B. and Grainger, S.,2010. A review, supported by experimental results, of voltage, charge and capacitor insertion method for driving piezoelectric actuators. *Precision Engineering: Journal*

of International Society for Precision Engineering and Nanotechnology 34(4), 692–700.

Shieh, H.J., Lin, F. J., Huang, P.K. and Teng, L.T., 2004. Adaptive tracking control solely using displacement feedback for a piezo-positioning mechanism. *IEE Proceedings-Control Theory and Applications* 151(5), 653–660.

4 Non-linear Modelling of Piezoelectric Actuators

4.1 Introduction

The DCA, which has been presented in the previous chapter, shows some improvement in performance compared to traditional analog charge drives. However, the principal difficulty in using this technique is drift of the displacement output. In the digital charge amplifier, the analog to digital converter (ADC) is not ideal and suffers from offset voltage and drift. This issue, together with dielectric leakage of the piezoelectric actuator, causes a bias voltage across the sensing resistor and due to the integration of the voltage bias the measured charge will drift, resulting in miscalculation of the actual charge across the piezoelectric actuator. The output voltage will also drift until it reaches the power supply rails.

In order to find a drift-free method, which later will be integrated with the DCA to remove the displacement drift of the DCA, non-linear modelling of piezoelectric actuators is presented in this chapter.

There are many different methods for modeling piezoelectric actuators. However, universal approximators are available with proven ability in

system modeling; hence, the modeling technique is no longer such a critical issue. In this chapter, Nonlinear Auto-Regressive models with eXogenous inputs (NARX), which is commonly used for classical system identification, is utilized. In addition, to reduce complexity and increase the accuracy of the NARX model, appropriate inputs to the model must be selected.

To assess the significance of the possible inputs, a subtractive clustering derived neuro-fuzzy network is used which provides visibility of the internal operation and lets the researcher understand the role of each input in the model in comparison with other inputs. This method is very helpful in finding the most appropriate input arrangement. The first paper in this chapter, entitled “Fuzzy Modeling of a Piezoelectric Actuator”, is focused on this assessment.

In order to use the NARX model for position estimation, the accuracy of the estimated displacement is an important factor. One of the phenomena that reduce the accuracy of modelling is error accumulation. Because piezoelectric actuators are dynamic systems, the current value of their displacement is dependent on previous values of displacement. Therefore in dynamic models, in addition to piezoelectric-voltage-based signals, previously estimated values of displacement are also used as inputs to the model. Therefore, the current output error depends on previous output errors and hence the estimation error may accumulate. Error accumulation is a problem in a NARX model and in an extreme situation the model can become unstable. The second paper, entitled “A new hybrid method for sensorless control of piezoelectric actuators”, proposes a novel hybrid method to deal with the error accumulation phenomena. This is achieved through the use of a method that employs a velocity signal, which is related to the electric current passing through the piezoelectric actuator, to reduce

the effect of error accumulation on the output displacement of the model. This method is then theoretically and experimentally verified.

4.2 Fuzzy modeling of a piezoelectric actuator

Published in International Journal of Precision Engineering and Manufacturing.

Statement of Authorship

Title of Paper	Fuzzy modeling of a piezoelectric actuator
Publication Status	● Published ○ Accepted for Publication ○ Submitted for Publication ○ Publication Style
Publication Details	Mohammadzaheri, M., Grainger, S., & Bazghaleh, M. (2012). Fuzzy modeling of a piezoelectric actuator. International Journal of Precision Engineering and Manufacturing, 13(5) 663-670.

Author Contributions

By signing the Statement of Authorship, each author certifies that their stated contribution to the publication is accurate and that permission is granted for the publication to be included in the candidate's thesis.

Name of Principal Author	Dr. Morteza Mohammadzaheri		
Contribution to the Paper	Supervised modeling and drafted paper		
Signature		Date	11/6/2013

Name of Co-Author	Dr. Steven Grainger		
Contribution to the Paper	Initiated research and drafted paper		
Signature		Date	11/9/13

Name of Co-Author (Candidate)	Mr. Mohsen Bazghaleh		
Contribution to the Paper	Developing model, performed experimental and theoretical analyses and drafted paper.		
Signature		Date	11/9/13

Fuzzy modeling of a piezoelectric actuator

Morteza Mohammadzaheri, Steven Grainger and Mohsen Bazghaleh

Abstract. *In this research, a piezoelectric actuator was modeled using fuzzy subtractive clustering and neuro-fuzzy networks. In the literature, the use of various modeling techniques (excluding techniques used in this article) and different arrangements of inputs in black box modeling of piezoelectric actuators for the purpose of displacement prediction has been reported. Nowadays, universal approximators are available with proven ability in system modeling; hence, the modeling technique is no longer such a critical issue. Appropriate selection of the inputs to the model is, however, still an unsolved problem, with an absence of comparative studies. While the extremum values of input voltage and/or displacement in each cycle of operation have been used in black box modeling inspired by classical phenomenological methods, some researchers have ignored them. This article focuses on addressing this matter. Despite the fact that classical artificial neural networks, the most popular black box modeling tools, provide no visibility of the internal operation, neuro-fuzzy networks can be converted to fuzzy models. Fuzzy models comprise of fuzzy rules which are formed by a number of fuzzy or linguistic values, and this lets the researcher understand the role of each input in the model in comparison with other inputs, particularly, if fuzzy values (sets) have been selected through subtractive clustering. This unique advantage was employed in this research together with consideration of a few critical but subtle points in model verification which are usually overlooked in black box modeling of piezoelectric actuators.*

Keywords: *Piezoelectric actuators; fuzzy; ANFIS; input and output extrema; input arrangement; black box modeling.*

NOMENCLATURE

A= a fuzzy set
B = a fuzzy set
C = centre of a cluster
D = density function
f = the output of fuzzy rules and FISs
f = function
m = the number of rules of a FIS
n = the number of inputs to a FIS
p, *q*, *r* = parameters of FIS consequent s
r_a = range of influence
r_b = squash factor
r_u, r_y = input and output order
S = integration area
t = time (*s*)
u = input (V)
x = a datum in clustering
w = the weight of a rule in a FIS
y = output (μm)

Greek Letters
α, *β* = input variables in the Preisach model
μ (.) = membership grade in FISs
μ (.,.) = a weight function in (1)

Indices
d = delay
s = sampling
i = counter

1 Introduction

Piezoelectric actuators are being increasingly studied and used in different areas of science and technology due to their nanometre displacement resolution, wide bandwidth, fast response and high stiffness (Zhang *et al.*, 2010). As a result of this broad application, mathematical modeling of these devices has become an important task for engineers and scientists. This article concerns models that predict the displacement of a stack piezoelectric actuator based on its voltage.

Finite element techniques have been used to model piezoelectric actuators (Soderkvist, 1998, Han *et al.*, 1999, Wang and Wereley, 1998); however, models derived through this method do not suit real time control (Boukari *et al.*, 2011) which is a very important application for models of piezoelectric actuators (Xie *et al.*, 2009, Zhang *et al.*, 2007). The IEEE standard on

piezoelectricity (Meeker, 1987) led to some linear lumped-parameter models for piezoelectric actuators suitable for control purposes. These linear models proved inadequate in many instances due to the significant nonlinearities in piezoelectric actuator behavior (Song and Li, 1999). In the 1990's, some physics-based nonlinear models were introduced but these had limitations such as inability to model minor hysteresis loops (Jung and Kim, 1994), vulnerability to measurement noise (Leigh and Zimmerman, 1991), and difficult parameter identification procedures (Rakotondrabe, 2011).

In 1995, the Preisach phenomenological model originally devised by the German physicist in 1935 to describe hysteresis phenomenon in magnetic systems (Preisach, 1935), was used to model piezoelectric actuators (Ge and Jouaneh, 1995) and is now widely accepted (Boukari *et al.*, 2011, Liaw and Shirinzadeh, 2011, Zhang *et al.*, 2009). The Prandtl-Ishlinskii model was derived from the Presiach model which fails to model asymmetric hysteresis loops (Zareinejad *et al.*, 2010). Extended and modified versions of the Preisach model have also been published (Song and Li, 1999, Li and Tan, 2004, Dupre *et al.*, 2001, Ge and Jouaneh, 1997, Han and Zhu, 2009, Yu *et al.*, 2002).

In the Preisach model, numeric values of some parameters that cannot be determined merely based on a phenomenological description of the system are estimated using input-output (voltage-displacement) data. Due to this fact, some authors have categorized the Preisach model as a black box model (Makaveev *et al.*, 2001, Sixdenier *et al.*, 2008). This model needs a 'whole domain' solution, that is, model equations (i.e. a double integral) must be solved in an area including the very first moment. In classical black box modeling, this deficiency can be avoided and more computationally efficient models can be made. A variety of black box models have been

used for this purpose such as Multi-Layer Perceptrons (MLPs) (Zhang *et al.*, 2010, Dong *et al.*, 2008, Yang *et al.*, 2008), Radial Basis Function Networks (RBFNs) (Dang and Tan, 2007), Recurrent Fuzzy Neural Networks (RFNNs) (Lin *et al.*, 2006a), wavelet neural networks (Lin *et al.*, 2006b), Nonlinear Auto-Regressive Moving Average models with eXogenous inputs (NARMAX) (Deng and Tan, 2009) and non-standard artificial neural networks (Hwang *et al.*, 2001). With the availability of universal approximators (Ying, 1998a, Ying, 1998b, Chen and Chen, 1995a, Chen and Chen, 1995b, Chen *et al.*, 1995c, Park and Sandberg, 1993), the modeling approach or the arrangement of inputs is more important than modeling techniques. In this article, fuzzy subtractive clustering and adaptive neuro fuzzy inference systems (ANFISs, also known as nuero-fuzzy networks) are employed to explore the most appropriate arrangement of inputs to a black box model of a piezoelectric stack actuator. Subtractive-clustering-based-neuro-fuzzy networks result in fuzzy models which can indicate the importance of each model input; this possibility is very helpful in finding the most appropriate input arrangement. Other universal approximators (e.g. MLPs and RBFNs) lack this critical advantage.

2 Background theory

2.1 Preisach Model

Let us consider a one-dimensional piezoelectric actuator with a varying input voltage. In Figure 1, vertical and horizontal axes of the (b) diagram, α and β, both present input (voltage, u in this paper). According to the Preisach model, the displacement (y) at any point can be calculated as (Yang *et al.*, 2008):

$$y(t) = \iint_{\beta \geq \alpha} \mu(\alpha, \beta) d\alpha d\beta. \tag{1}$$

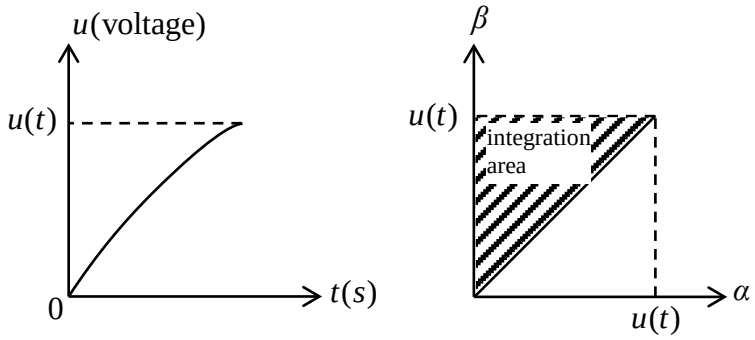

Figure 1: A varying input voltage (u) applied to the actuator (a), and its corresponding integration area for the Preisach model of (1), (b)

In the Preisach model, (1) will be converted to the following equations (Song and Li, 1999):

$$\begin{aligned} y(t) = & \iint_{S(0 \to u_{\min})} \mu(\alpha, \beta) d\alpha d\beta \\ & + \iint_{S(u_{\min} \to u)} \mu(\alpha, \beta) d\alpha d\beta (\textit{ascending}), \end{aligned} \tag{2}$$

$$\begin{aligned} y(t) = & \iint_{S(0 \to u_{\max})} \mu(\alpha, \beta) d\alpha d\beta \\ & - \iint_{S(u_{\max} \to u)} \mu(\alpha, \beta) d\alpha d\beta (\text{descending}). \end{aligned} \tag{3}$$

where S is integration area. (2) and (3) can be rewritten as (Zhang *et al.*, 2009):

$$y(t) = y_{\min} + \iint_{S(u_{\min} \to u)} \mu(\alpha, \beta) d\alpha d\beta \text{ (ascending)}, \tag{4}$$

$$y(t) = y_{\max} - \iint_{S(u_{\max} \to u)} \mu(\alpha, \beta) d\alpha d\beta \text{ (descending)}. \tag{5}$$

where y_{max} is the last local maximum when descending and y_{min} is the last local minimum when ascending. (4) and (5) show that the current input (voltage), last extremum of the input ($u_{ext} = u_{min}$ or u_{max}) and its corresponding output ($y_{ext} = y_{min}$ or y_{max}) are used in estimating the current output ($y(t)$) according to the Preisach model. Hence, these extremum values can be used in black box modeling including neuro-fuzzy modeling.

2.2 Neuro-fuzzy Networks

Figure 2 shows the structure of a linear Sugeno type fuzzy inference system (FIS) with two inputs and two fuzzy sets (values) for each input. In this structure, the 'antecedent' of each fuzzy rule contains fuzzy sets and the 'consequent' of each rule is a first order polynomial. *x* and *y* are numeric inputs to the FIS. X and Y are input variables (e.g. length). *x*, a value of X, is the input to A_1 and A_2 and leads to two membership grades of $\mu_{A_1}(x)$ and $\mu_{A_2}(x)$, similarly, *y*, a value of Y, is the input to B_1 and B_2 and leads to two membership grades of $\mu_{B_1}(y)$ and $\mu_{B_2}(y)$. All the membership grades of a rule should pass AND function to result in the weight of that rule. For the FIS shown in Figure 2(a),

$$w_1 = \text{AND}(\mu_{A_1}(x), \mu_{B_1}(y)), \tag{6}$$

and

$$w_2 = \text{AND}(\mu_{A_2}(x), \mu_{B_2}(y)), \tag{7}$$

where w_1 and w_2 are the weight of rules shown in Figure 2(a). In Sugeno-type FISs, the consequent is totally independent of inputs. A consequent can

have the order of zero or one and generates the output of a rule. For a system with n inputs, a first order consequent has n+1 parameters. For the FIS shown in Figure 2(a),

$$\mathrm{f}_i = p_i x + q_i y + r_i, \tag{8}$$

where p_i and q_i and r_i are consequent parameters and f_i is the rule output. The output of the FIS is the weighted sum of the outputs of the rules.

$$\mathrm{f} = \frac{\sum_{i=1}^{m} \mathrm{f}_i w_i}{\sum_{i=1}^{m} w_i}, \tag{9}$$

where m is the number of rules and f is the output of the FIS.

A sugeno type FIS as shown in Figure 2(a) can be converted to a neuro-fuzzy network (or ANFIS) shown in Figure 2(b). In neuro fuzzy networks, activation functions (i.e. membership functions) are adjusted during training rather than weights. The first layer of nodes of a neuro-fuzzy network uses membership functions of the corresponding FIS as activation functions. The second layer nodes use AND function (product in this case) as the activation function and the activation function of the third layer nodes are weighted sum functions. In the nodes of the fourth layer, rule outputs are calculated and the last layer includes a node with a sum activation function. The training procedure involves gradient error back propagation to adjust the coefficients of the activation functions of the second layer (i.e. fuzzy membership functions) and least square of error to adjust the coefficients of the activation functions of the fourth layer (i.e. FIS consequent parameters) (Ghaffari *et al.*, 2007, Jang *et al.*, 2006).

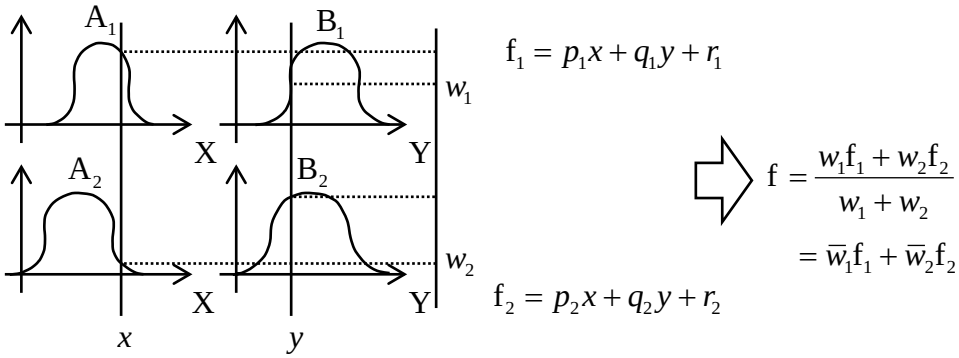

(a)

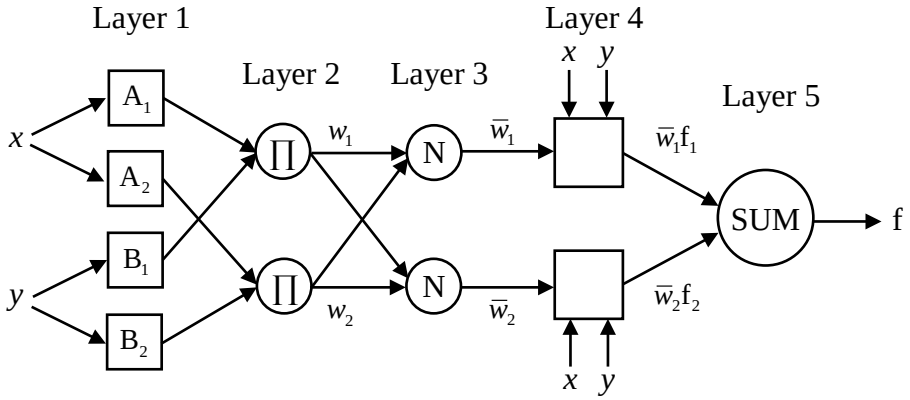

(b)

Figure 2: (a) A Sugeno-type fuzzy inference system (Ghaffari *et al.*, 2007) (b) A Sugeno-type neuro-fuzzy network (Ghaffari *et al.*, 2007)

2.3 Subtractive clustering

In fuzzy inference systems, if all the inputs have an identical number of fuzzy sets (values), the number of fuzzy rules in the model equals the number of fuzzy sets allocated to each input (e.g. 3) raised to the power of the number of inputs. Therefore, sometimes, too many rules are needed to cover all the input space. In order to reduce the number of fuzzy rules with

minimum loss of accuracy, 'subtractive clustering' is applied (Ghaffari *et al.*, 2007, Jang *et al.*, 2006, Mathworks, 2011).

In this method, for each set of input data $(x_i, i = 1,..,n)$ in an *m*-dimensional space, a density value is calculated:

$$D_i = \sum_{j=1}^{n} \exp\left(-\frac{\left\| x_i - x_j \right\|^2}{\left(r_a / 2 \right)^2} \right), \tag{10}$$

where

$$\left\| x_i - x_j \right\| = \sqrt{\sum_{k=1}^{m} (x_i^k - x_j^k)^2} \text{ (distance)}, \tag{11}$$

and r_a = Range of Influence (a positive number).

The point with the highest density is defined as the centre of the first cluster. The centre of the first cluster is named *C*1, and its density is named D_{C1}. A cluster is a hyper sphere with a centre of *Ci* and radius of r_a in an *m*-dimensional space. Later, each cluster is used as the antecedent of a fuzzy rule. After the definition of the centre of the first cluster, the density of other points is redefined as

$$D_i = D_i - D_{C1} \exp\left(-\frac{\left\| x_i - x_{C1} \right\|^2}{\left(r_b / 2 \right)^2} \right), \tag{12}$$

where r_b = Squash Factor.

If the redefined density of any point exceeds the 'Accept Ratio', it is defined as the centre of a cluster, and then, the density of other points are redefined again:

$$D_i = D_i - \sum_{j=1}^{p} D_{C\,j} \exp\left(-\frac{\left\| x_i - x_{C\,j} \right\|^2}{\left(r_b/2 \right)^2} \right), \tag{13}$$

where p = the number of already defined clusters.

After any stage of redefinition, the density of the centres of previously defined clusters are re-calculated. If their density yields lower than 'Reject Ratio', those clusters are eliminated. This process continues till the clusters do not change between two sequential stages. The model derived from subtractive clustering is used as the initial neuro-fuzzy model for training.

3 Data gathering

The set up includes a NEC AE0505D44H40 stack piezoelectric actuator and a PHILTECH D20 optical sensor connected to a PC through dSPACE and voltage amplifiers. The system was excited by three triangle waves of voltage with maximum and minimum amplitude of ±20 V and slopes of ±80 V/s, ±800 V/s and ±8000 V/s, for a period of 2s each. Furthermore, it was excited by a repeating stair function, shown in Figure 3, and a chirp function, both in the range of ±20 V and for a time period of 2s. Data gathered through these excitations were used as the training data. The data obtained through the excitation of the set up with 20sin10 V was used as the validation data.

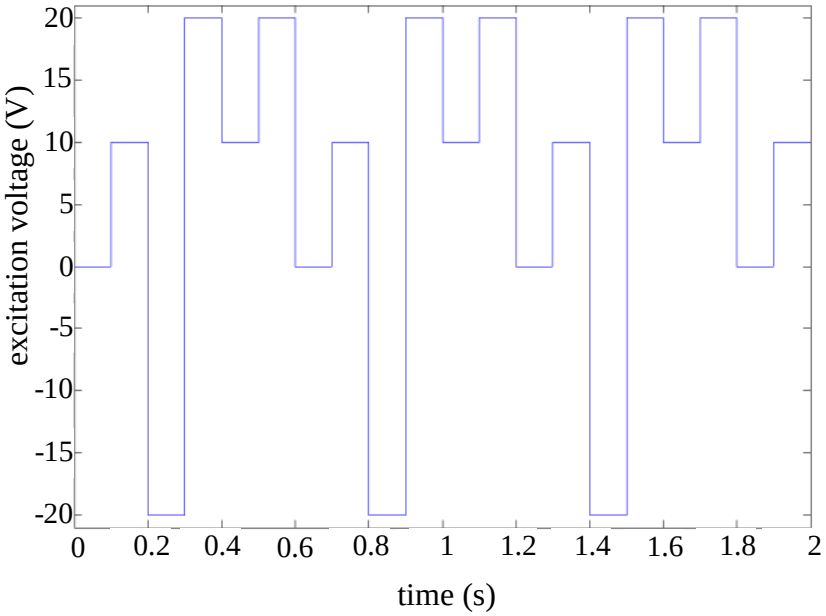

Figure 3: Repeating stair function used for system excitation

4 Modeling

4.1 Model structure

Nonlinear Auto-Regressive models with eXogenous inputs (NARX models) are commonly used for classical system identification (Nelles, 2001). According to the NARX structure, for a single input-single output system like a one-dimensional piezoelectric actuator (Nelles, 2001),

$$y(t) = f\begin{pmatrix} u(t-t_{\mathrm{d}}), u(t-t_{\mathrm{d}}-T_{\mathrm{s}}), \ldots, u(t-t_{\mathrm{d}}-r_{\mathrm{u}}T_{\mathrm{s}}), \\ y(t-T_{\mathrm{s}}), y(t-2T_{\mathrm{s}}), \ldots, y(t-r_{\mathrm{y}}T_{\mathrm{s}}) \end{pmatrix}, \tag{14}$$

where t_{d} is delay time, and r_{u} and r_{y} are input and output orders respectively. f is an approximated nonlinear function. The sampling time of 0.001 s, the delay time of 0.001 s and orders up to three were selected based

on a previous successful black box modeling work on stack piezoelectric actuators (Zhang *et al.*, 2009). However, inspired by the Preisach model (see (4) and (5)), the extrema of the system's input and output have been also used as inputs to the model together with the classical inputs to NARX models. In this article, the involvement of extrema in black box modeling of a piezoelectric stack actuator is particularly addressed.

4.2 Different approaches to model validation

In system identification, there are two different approaches for validating models: one-step prediction and simulation. One-step prediction is the normal way of assessing black box models of piezoelectric actuators in the literature (Zhang *et al.*, 2010, Song and Li, 1999, Li and Tan, 2004, Dong *et al.*, 2008, Yang *et al.*, 2008, Dang and Tan, 2007, Zhang *et al.*, 2009). In this approach, all the inputs to the model are recalled from the memory, or their real values are assumed to be available:

$$\hat{y}(t) = f\begin{pmatrix} u(t-t_{\mathrm{d}}), u(t-t_{\mathrm{d}}-T_{\mathrm{s}}), \ldots, u(t-t_{\mathrm{d}}-r_{\mathrm{u}}T_{\mathrm{s}}), \\ y(t-T_{\mathrm{s}}), y(t-2T_{\mathrm{s}}), \ldots, y(t-r_{\mathrm{y}}T_{\mathrm{s}}) \end{pmatrix}, \tag{15}$$

where the variable(s) with a hat represent estimated values. In one-step prediction, all real values of model inputs during an operation are given to the model, and the output of the model is compared to the recorded value of the system output.

However, if the model is used in predictive control (with a horizon of two or more) (Mohammadzaheri and Chen, 2010) sensor-less control or process simulation, the delayed outputs will not be available, so one-step prediction is not applicable; thus, previously estimated values of system output(s) are

needed to be used as model inputs. This is called model validation for simulation:

$$\hat{y}(t) = f\begin{pmatrix} u(t-t_{\mathrm{d}}), u(t-t_{\mathrm{d}}-T_{\mathrm{s}}), \ldots, u(t-t_{\mathrm{d}}-r_{\mathrm{u}}T_{\mathrm{s}}), \\ \hat{y}(t-T_{\mathrm{s}}), \hat{y}(t-2T_{\mathrm{s}}), \ldots, \hat{y}(t-r_{\mathrm{y}}T_{\mathrm{s}}) \end{pmatrix}. \quad (16)$$

As a result, the inevitable error of estimated outputs returns to the validation process and increases the resultant error repeatedly. This phenomenon is called ‘error accumulation’ (Mohammadzaheri and Chen, 2010, Mohammadzaheri *et al.*, 2010).

Due to error accumulation, a high number of delayed outputs can decrease the accuracy in simulation and increase the accuracy in one-step prediction, especially in the case of deficiencies in the modeling structure or algorithm. This explains why the Preisach model, which is independent of delayed outputs, is used successfully in real-time control applications in spite of its deficiency. In summary, as a result of error accumulation, the decrease of the error in model validation for one step prediction does not necessarily lead to the decrease of the estimation error for simulation or real time application. This statement is confirmed by the results listed in Table 1. Only highly accurate models can both benefit from delayed outputs as their inputs and overcome the error accumulation for a significant period of time.

Table 1: Simulation (left hand side number) and one-step prediction errors (right hand side number) for a number of fuzzy models with different output orders (r_y). All models have been made by subtractive clustering and neuro-fuzzy modeling. Modeling and verification data were explained in Section 3

Output order	Error without extrema (μm)	Error with u_{ex} (μm)	Error with both extrema (μm)
r_y=1	2.2227/0.0837	0.2184/0.0222	0.2421/0.0290
r_y=2	8.0331/0.0339	0.1145/0.0185	0.1866/0.0292
r_y=3	1.2911/0.0362	0.1747/0.0194	0.1025/0.0259

4.3 Modeling results

In black box modeling of piezoelectric actuators, the extrema of input (voltage) (Deng and Tan, 2009, Zhang *et al.*, 2009, Zhang and Tan, 2010, Kim *et al.*, 2009) and the output (displacement) (Yang *et al.*, 2008) have sometimes been used as the inputs to black box models, in some other works, these variables have not been utilized in modeling (Dong *et al.*, 2008). In the literature there is no comparison to indicate the superiority of any of these approaches. In this section, fuzzy subtractive clustering (see Section 2.3) is employed to address this matter. In subtractive clustering, a higher number of fuzzy sets are allocated to the inputs which are more influential on forming clusters or operation areas (an operation area is a cluster or an antecedent of a fuzzy rule). If an input has only one fuzzy set, repeated in all rules, it will have no effect on the result, and that input can be overlooked in modeling (Jang *et al.*, 2006). This is sometimes interpreted as: the inputs with more fuzzy sets have a more important role on the behavior of the system (Ahmadpour *et al.*, 2009). This statement is not general, and the operation areas of rules need to be checked before finalizing the judgment about the importance of model inputs.

In this research, with a series of experimental data, a number of Sugeno-type fuzzy models were made through subtractive clustering. Membership

functions (fuzzy sets) are Gaussian and the consequent is a first order polynomial, AND method is product, and OR method is algebraic sum (Jang *et al.*, 2006, Mathworks, 2011). The input arrangement of the fuzzy model is shown in (17):

$$\hat{y}(t) = f\begin{pmatrix} u(t-0.001), u(t-0.002), u(t-0.003), u_{\text{ex}}, \\ y(t-0.001), y(t-0.002), y(t-0.003), y_{\text{ex}} \end{pmatrix}. \qquad (17)$$

Range of Influence and Squash Factor were retained fixed at 1.25 and 0.5 in modeling; Accept and Reject Ratios were subject to change. Different pairs of Accept and Reject Ratios would result in different numbers of fuzzy sets allocated to each input. The results are listed in Table 2. Standard data preparation (Mohammadzaheri *et al.*, 2009) was done prior to modeling.

According to Table 2, it appears that the extrema have a low number of fuzzy sets, and thus a low grade of importance in modeling, and they can be ignored. However, it is not correct. Figure 4 shows a fuzzy inference system of Table 2 with 10 rules. The first six inputs have similar fuzzy sets in the rules, differing from the last two inputs. It means, if a number of the first six inputs (with high numbers of fuzzy sets) are eliminated, they might be replaced by others, but if both extrema are neglected, their role cannot be fulfilled by the first six inputs. As an example, in the FIS shown in Figure 4, the operation areas (antecedents) of rules 2 and 10 will be almost the same without the extrema. As a result, involving the extrema (both or one of them) has a critical role in defining operation areas, and the extrema should not be overlooked. Results listed in Table 1 confirm this conclusion.

Table 2: Number of fuzzy rules resulting from a pair of Accept and Reject Ratios (in parentheses in the first column) and the number of fuzzy sets allocated to each model input

No. of rules	$u(t\text{-}3t_s)$	$u(t\text{-}2t_s)$	$u(t\text{-}t_s)$	$y(t\text{-}3t_s)$	$y(t\text{-}2t_s)$	$y(t\text{-}t_s)$	u_{ex}	y_{ex}
31(0.05,0.01)	20	20	22	22	24	20	5	8
24(0.2,0.05)	19	19	19	21	18	19	4	7
20(0.5,0.15)	15	16	16	18	16	17	3	5
13(0.8,0.3)	13	13	13	12	12	12	3	4
10(0.95,0.5)	10	10	9	10	9	10	3	3

The results listed in Table 1 and shown in Figures. 5 ((a) and (b)) have been gathered through subtractive clustering followed by neuro-fuzzy modeling. An effort has been made to achieve the best results with each arrangement of inputs; however, neuro fuzzy networks are a subset of artificial neural networks (ANNs), and it is a difficult and unsolved problem to find the best ANN structure for each specific application; thus, a fairly large ANN is usually employed to deal with relatively complex approximation problems (Deng *et al.*, 2008, Mohammadzaheri *et al.*, 2012).

In this research, around 20 fuzzy rules were used for modeling; a higher number of rules did not lead to higher accuracy. The resolution of the measurement system (the lowest measurable value of the displacement) is 0.09 μm. Thus, errors below this value are not meaningful and can be assumed equal to 0.09 μm. Simulation errors, which are a few times higher than the resolution for a time period of 2s (2000 instants), correspond to highly accurate models.

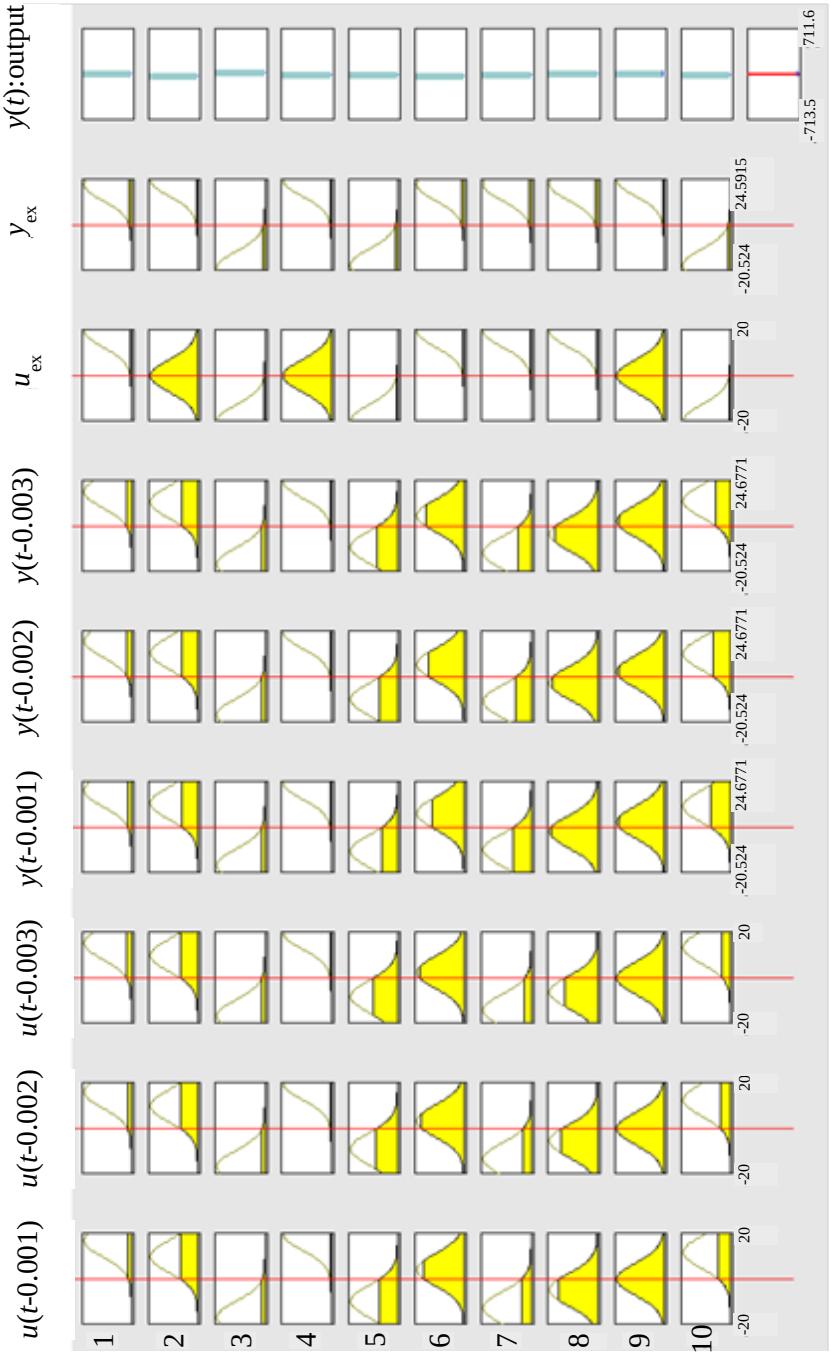

Figure 4: A fuzzy model of a piezoelectric actuator with 10 rules

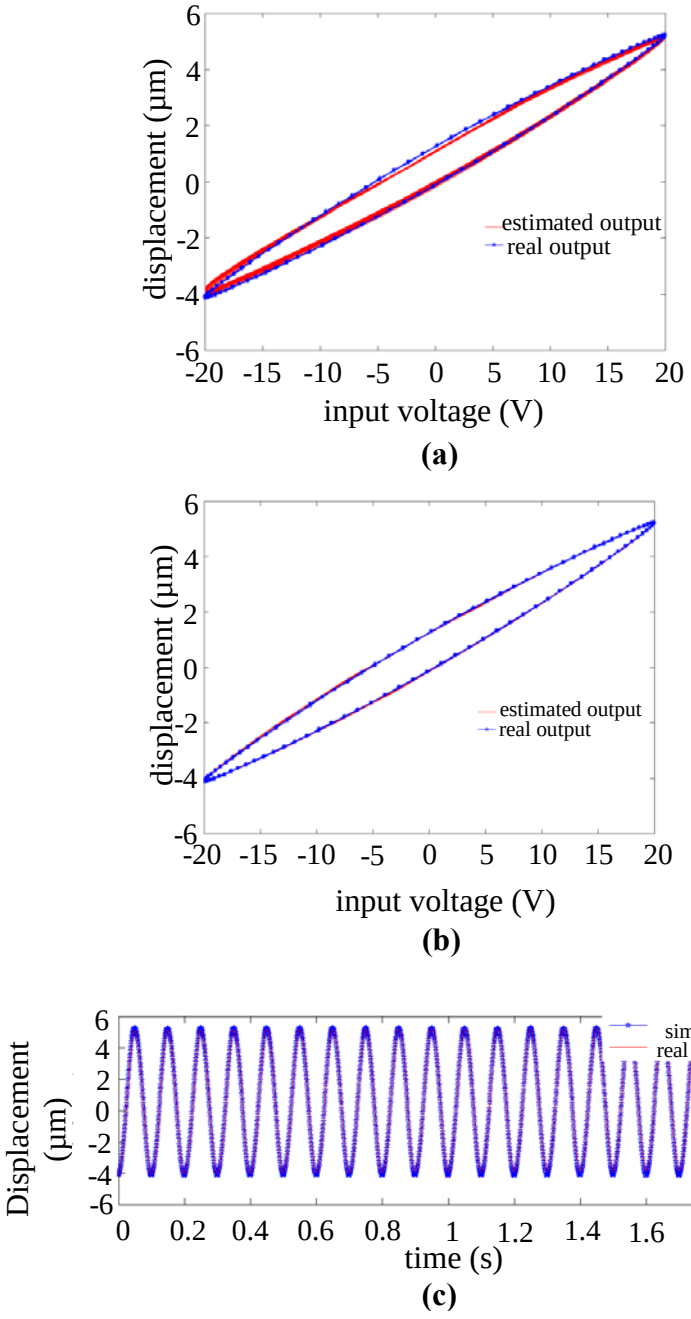

Figure 5: Verification results in the form of hysteresis diagrams of 20 cycles of simulation (a) and one-step prediction (b), and in the form of time response of simulation (c) for a fuzzy model with orders of three for both inputs and outputs and with both the extrema and 20 fuzzy rules. The model has been made for the piezoelectric actuator detailed in Section 3

5 Conclusion

This article addresses the use of subtractive-clustering-based fuzzy modeling for piezoelectric actuators, which gives an insight to the model and makes it possible to assess the significance of the inputs to models. In this research, a number of experiments were undertaken on a stack piezoelectric actuator. After preparation, these data were used in fuzzy subtractive clustering, then in neuro fuzzy modeling which resulted in a number of fuzzy models. The aforementioned modeling method is a black box method, not using the laws of nature. However, its outcomes, fuzzy models, mainly formed by linguistic or fuzzy values, convey valuable information about the model. This helps significantly in assessing how critical each model input is. In this research fuzzy modeling was followed by a thorough model validation, with data different from training data, both for one-step prediction and simulation. This research not only resulted in a number of accurate fuzzy models for piezoelectric actuators, but also provided a guideline for future modeling works especially for real time applications.

References

Ahmadpour, M., Yue, W. L. and Mohammadzaheri, M., 2009. Neuro-fuzzy modelling of workers trip production. *In: The 32nd Australasian Transport Research Forum*. Auckland, New Zealand.

Boukari, A. F., Carmona, J. C., Moraru, G., Malburet, F., Chaaba, A. and Douimi, M., 2011. Piezo-actuators modeling for smart applications. *Mechatronics* 21(1), 339-349.

Chen, T. P. and Chen, H., 1995a. Approximation capability to functions of several variables, nonlinear functionals, and operators by radial basis function neural networks. *IEEE Transactions on Neural Networks* 6(4), 904-910.

Chen, T. P. and Chen, H., 1995b. Universal approximation to nonlinear operators by neural networks with arbitrary activation functions and its application to dynamical-systems. *IEEE Transactions on Neural Networks* 6(4), 911-917.

Chen, T. P., Chen, H. and Liu, R. W., 1995c. Approximation capability in C((R)over-Bar(N)) by multilayer feedforward networks and related problems. *IEEE Transactions on Neural Networks* 6(1), 25-30.

Dang, X. J. and Tan, Y. H., 2007. RBF neural networks hysteresis modelling for piezoceramic actuator using hybrid model. *Mechanical Systems and Signal Processing* 21(1), 430-440.

Deng, H., Li, H. X. and Wu, Y. H., 2008. Feedback-linearization- based neural adaptive control for unknown nonaffine nonlinear discrete-time systems. *IEEE Transactions on Neural Networks* 19(9), 1615-1625.

Deng, L. and Tan, Y. H., 2009. Modeling hysteresis in piezoelectric actuators using NARMAX models. *Sensors and Actuators A: Physical* 149(1), 106-112.

Dong, R., Tan, Y. H., Chen, H. and Xie, Y. Q., 2008. A neural networks based model for rate-dependent hysteresis for piezoceramic actuators. *Sensors and Actuators A: Physical* 143(2), 370-376.

Dupre, L., Van Keer, R. and Melkebeek, J., 2001. Generalized scalar preisach model for grain oriented materials excited along arbitrary directions. *Journal of Applied Physics* 89(11), 7245-7247.

Ge, P. and Jouaneh, M., 1997. Generalized preisach model for hysteresis nonlinearity of piezoceramic actuators. *Precision Engineering* 20(2), 99-111.

Ge, P. and Jouaneh, M., 1995. Modeling hysteresis in piezoceramic actuators. *Precision Engineering* 17(3), 211-221.

Ghaffari, A., Mehrabian, A. R. and Mohammad-Zaheri, M., 2007. Identification and control of power plant de-superheater using soft computing techniques. *Engineering Applications of Artificial Intelligence* 20(2), 273-287.

Han, J. H., Cho, K. D., Youn, S. H. and Lee, I., 1999. Vibration and actuation characteristics of composite structures with a bonded piezo-ceramic actuator. *Smart Materials and Structures* 8(1), 136-143.

Han, Y. and Zhu, J., 2009. Implementation procedure for the generalized moving preisach model based on a first order reversal curve diagram. *Rare Metals* 28(4), 355-360.

Hwang, C. L., Jan, C. and Chen, Y. H., 2001. Piezomechanics using intelligent variable-structure control. *IEEE Transactions on Industrial Electronics* 48(1), 47-59.

Jang, J.-S. R., Sun, C.-T. and Mizutani, E., 2006. Neuro-fuzzy and soft computing: A computational approach to learning and machine intelligence. *Prentice Hall.*

Jung, S. B. and Kim, S. W., 1994. Improvement of scanning accuracy of pzt piezoelectric actuators by feedforward model-reference control. *Precision Engineering* 16(1), 49-55.

Kim, I., Kim, Y. S. and Park, E. C., 2009. Sliding mode control of the inchworm displacement with hysteresis compensation. *International Journal of Precision Engineering and Manufacturing* 10(3), 43-49.

Leigh, T. D. and Zimmerman, D. C., 1991. An implicit method for the nonlinear modelling and simulation of piezoceramic actuators displaying hysteresis. *In: 112th ASME Winter Annual Meeting*. pp. 57-63.

Li, C. and Tan, Y., 2004. A neural networks model for hysteresis nonlinearity. *Sensors and Actuators A: Physical* 112(1), 49-54.

Liaw, H. C. and Shirinzadeh, B., 2011. Robust adaptive constrained motion tracking control of piezo-actuated flexure-based mechanisms for micro/nano manipulation. *IEEE Transactions on Industrial Electronics* 58(4), 1406-1415.

Lin, F. J., Shieh, H. J., Huang, P. K. and Teng, L. T., 2006a. Adaptive control with hysteresis estimation and compensation using RFNN for piezo-actuator. *IEEE Transactions on Ultrasonics Ferroelectrics and Frequency Control* 53(9), 1649-1661.

Lin, F. J., Shieh, H. J. and Huang, P. K., 2006b. Adaptive wavelet neural network control with hysteresis estimation for piezo-positioning mechanism. *IEEE Transactions on Neural Networks* 17(2), 432-444.

Makaveev, D., Dupre, L., De Wulf, M. and Melkebeek, J., 2001. Modeling of quasistatic magnetic hysteresis with feed-forward neural networks. *Journal of Applied Physics* 89(11), 6737-6739.

Mathworks, 2011. *Fuzzy logic toolbox™ user's guide*.

Meeker, T. R., 1996. Publication and proposed revision of ANSI/IEEE standard 176-1987. ANSI/IEEE Standard on Piezoelectricity. *IEEE Transactions on Ultrasonics Ferroelectrics and Frequency Control* 43(5), 717-718.

Mohammadzaheri, M. and Chen, L., 2010. Intelliegnt predictive control of model helicopters' yaw angle. *Asian Journal of Control* 12(6), 1-13.

Mohammadzaheri, M., Chen, L. and Grainger, S., 2012. A critical review of the most popular types of neuro control. *Asian Journal of Control* 14(1), 1-11.

Mohammadzaheri, M., Chen, L., Ghaffari, A. and Willison, J., 2009. A combination of linear and nonlinear activation functions in neural networks for modeling a de-superheater. *Simulation Modelling Practice and Theory* 17(2), 398-407.

Mohammadzaheri, M., Chen, L., Mirsepahi, A., Ghanbari, M. and Prime, Z., 2010. Hybrid intelligent control of an infrared dryer. *In: The 38th Australasian Conference of Chemical Engineering*. pp. 1-10.

Nelles, O., 2001. Nonlinear System Identification. *Springer-Verlag*. Berlin Heidelberg.

Park, J. and Sandberg, I. W., 1993. Approximation and radial-basis-function networks. *Neural Computation* 5(2), 305-316.

Preisach, F., 1935. Uber die magnetische nachwirkung. *Zeitschrift Für Physik* 94(5-6), 277-302.

Rakotondrabe, M., 2011. Bouc-Wen modeling and inverse multiplicative structure to compensate hysteresis nonlinearity in piezoelectric actuators. *IEEE Transactions on Automation Science and Engineering* 8(2), 428-431.

Sixdenier, F., Scorretti, R., Marion, R. and Morel, L., 2008. Quasistatic hysteresis modeling with feed-forward neural networks: Influence of the last but one extreme values. *Journal of Magnetism and Magnetic Materials* 320(20), E992-E996.

Soderkvist, J., 1998. Using fea to treat piezoelectric low-frequency resonators. *IEEE Transactions on Ultrasonics Ferroelectrics and Frequency Control* 45(3), 815-823.

Song, D. W. and Li, C. J., 1999. Modeling of piezo actuator's nonlinear and frequency dependent dynamics. *Mechatronics* 9(4), 391-410.

Wang, G. and Wereley, N. M., 1998. Frequency response of beams with passively constrained damping layers and piezo-actuators. *In: Proceeding of SPIE* 3327, 44-60.

Xie, W. F., Fu, J., Yao, H. and Su, C. Y., 2009. Neural network-based adaptive control of piezoelectric actuators with unknown hysteresis. *International Journal of Adaptive Control and Signal Processing* 23(1), 30-54.

Yang, X. F., Li, W., Wang, Y. Q. and Ye, G., 2008. Modeling hysteresis in piezo actuator based on neural networks. *Advances in Computation and Intelligence* 5370, 290-296.

Ying, H., 1998a. General Siso Takagi-Sugeno fuzzy systems with linear rule consequent are universal approximators. *IEEE Transactions on Fuzzy Systems* 6(4), 582-587.

Ying, H., 1998b. General Takagi-Sugeno fuzzy systems are universal approximators. *In: IEEE International Conference on Fuzzy Systems Proceedings*. pp. 819-823.

Yu, Y. H., Naganathan, N. and Dukkipati, R., 2002. Preisach modeling of hysteresis for piezoceramic actuator system. *Mechanism and Machine Theory* 37(1), 49-59.

Zareinejad, M., Ghidary, S. S., Rezaei, S. M. and Abdullah, A., 2010. Precision control of a piezo-actuated micro telemanipulation system. *International Journal of Precision Engineering and Manufacturing* 11(1), 55-65.

Zhang, J., Wang, E. and Gao, R., 2008. Neural network predictive control for piezoelectric smart structures. *In: ASME 9th Biennial Conference on Engineering Systems Design and Analysis* 2, Paper No. ESDA2008-59094, pp. 417-421.

Zhang, X. L. and Tan, Y. H., 2010. A hybrid model for rate- dependent hysteresis in piezoelectric actuators. *Sensors and Actuators A: Physical* 157(1), 54-60.

Zhang, X. L., Tan, Y. H. and Su, M. Y., 2009. Modeling of hysteresis in piezoelectric actuators using neural networks. *Mechanical Systems and Signal Processing* 23(8), 2699-2711.

Zhang, X. L., Tan, Y. H., Su, M. Y. and Xie, Y. Q., 2010. Neural networks based identification and compensation of rate-dependent hysteresis in piezoelectric actuators. *Physica B: Physics of Condensed Matter* 405(12), 2687-2693.

Zhang, Y. D., Fang, Y. C., Zhou, X. W. and Dong, X. K., 2009. Image-based hysteresis modeling and compensation for an AFM piezo-scanner. *Asian Journal of Control* 11(2), 166-174.

4.3 A new hybrid method for sensorless control of piezoelectric actuators

Published in Sensors and Actuators A: Physical.

Statement of Authorship

Title of Paper	A new hybrid method for sensorless control of piezoelectric actuators
Publication Status	◉ Published ○ Accepted for Publication ○ Submitted for Publication ○ Publication Style
Publication Details	Bazghaleh, M., Mohammadzaheri, M., Grainger, S., Cazzolato, B. & Lu, T.F. (2013). A new hybrid method for sensorless control of piezoelectric actuators. Sensors and Actuators A: Physical, 194(1) 25-30.

Author Contributions

By signing the Statement of Authorship, each author certifies that their stated contribution to the publication is accurate and that permission is granted for the publication to be included in the candidate's thesis.

Name of Principal Author (Candidate)	Mr. Mohsen Bazghaleh		
Contribution to the Paper	Developed theory, performed experimental work, analyzed data and wrote the manuscript.		
Signature		Date	11/9/13

Name of Co-Author	Dr. Morteza Mohammadzaheri		
Contribution to the Paper	Supervised research, reviewed manuscript.		
Signature		Date	11/6/2013

Name of Co-Author	Dr. Steven Grainger		
Contribution to the Paper	Supervised research, reviewed manuscript.		
Signature		Date	11/9/13

Name of Co-Author	Dr. Ben Cazzolato		
Contribution to the Paper	Supervised research, reviewed manuscript.		
Signature		Date	11/9/13

Name of Co-Author	Dr. Tien-Fu Lu		
Contribution to the Paper	Supervised research, reviewed manuscript.		
Signature		Date	11/09/13

A new hybrid method for sensorless control of piezoelectric actuators

Mohsen Bazghaleh, Morteza Mohammadzaheri, Steven Grainger, Ben Cazzolato and Tien-Fu Lu

Abstract. *This paper offers a new hybrid position estimation method for the sensorless control of piezoelectric actuators. Often mathematical models which map easy to measure signals to displacement are used in this role. The proposed method is aimed at enhancing the accuracy of commonly accepted black box models. Three easy to measure signals are available to be used to estimate displacement. One, the induced voltage, is not suitable for piezoelectric stacks. Two others are more generally usable: the piezoelectric voltage and the sensing voltage. This paper proposes, then theoretically and experimentally verifies a hybrid algorithm that uses the two latter signals to produce estimates of displacement with improved accuracy.*

Keywords: *Piezoelectric actuators; sensorless control; displacement estimation; black box modeling; fuzzy modeling.*

1 Introduction

Sensorless control of the displacement of piezoelectric actuators has attracted much attention to avoid the expense and practical limits of precision displacement sensors (Aphale *et al.*, 2007, Fairbairn *et al.*, 2011, Fleming and Moheimani, 2006, Park and Moon, 2010, Ronkanen *et al.*, 2011). The basis of sensorless control is to estimate displacement using easy

to measure electrical signals. In general, three signals may be used for this purpose: the voltage applied to the piezoelectric actuator or in short, the piezoelectric voltage (see Figure 1) (Aphale *et al.*, 2007), the voltage across the sensing resistor, or at the output of the piezoelectric actuator, explained in Section 2.1 (the sensing voltage (see Figure 1)) (Fleming and Moheimani, 2006), and the induced voltage in electrodes or segments of the piezoelectric actuator which are not subject to the applied voltage (mostly used in piezoelectric tubes) (Kuiper and Schitter, 2010). The use of these signals, the sensing voltage, the induced voltage and the piezoelectric voltage is briefly explained in the following three paragraphs.

The sensing voltage signal can be used to obtain the electrical current passing the piezoelectric actuator (explained in Section 2.1), and the charge is found through integration. The charge that passes the piezoelectric actuator has a direct relation with its displacement in normal operational areas, so is a precise indicator of the displacement (Fleming and Moheimani, 2006, Comstock, 1981). However, in a digital environment, due to the problem of drift, after a while, the calculated charge is not equal to the real charge (Bazghaleh *et al.*, 2010).

The induced voltage signal has been suggested as an indicator of displacement using an arrangement of capacitors (Kuiper and Schitter, 2010), also linear mathematical models have been offered to map the induced voltage to the piezoelectric voltage (Moheimani and Yong, 2008, Yong and Moheimani, 2009); however, to date, no direct mapping between displacement and the induced voltage has been reported in sensorless control of piezoelectric actuators.

The piezoelectric voltage, on the other hand, has been adequately mapped onto displacement through a variety of dynamic mathematical models (Park and Moon, 2010, Li and Tan, 2004, Mohammadzaheri *et al.*, 2012b, Schitter and Stemmer, 2004, Song and Li, 1999, Yang *et al.*, 2008, Yu *et al.*, 2002, Zhang and Tan, 2010, Zhang *et al.*, 2009, Zhang *et al.*, 2010). Analytical models have failed to model this complex relationship, and instead, dynamic phenomenological (e.g. the Presiach or the Rayleigh models) (Park and Moon, 2010, Yu *et al.*, 2002) and classical black box models (e.g. artificial neural networks or neurofuzzy networks) (Yang *et al.*, 2008, Mohammadzaheri *et al.*, 2012c) have been employed to perform this task. It has been shown that static models (those not considering a history of the system input/output) are not adequate tools to model piezoelectric actuators. Alternatively, dynamic models have shown promising outcomes (Mohammadzaheri *et al.*, 2012b).

Piezoelectric actuators are dynamic systems; that is, the current value of their displacement is dependent on previous values of displacement. Therefore, in highly accurate dynamic models, in addition to piezoelectric-voltage-based signals (the history and/or derivatives and/or extrema of the piezoelectric voltage), previously estimated values of displacement are also used as inputs to the model (Mohammadzaheri *et al.*, 2012b). This however, gives rise to the error accumulation phenomenon (explained in Section 2.2) which is a major issue in modeling of dynamic systems in general (Mohammadzaheri *et al.*, 2012b). Many researchers have contributed to sensorless control of piezoelectric actuators through developing new mathematical models to map the piezoelectric voltage onto displacement more effectively. This paper introduces a new approach to decrease the effect of error accumulation in displacement estimation of piezoelectric actuators through an algorithm that also incorporates the sensing voltage.

2 Existing popular approaches towards sensorless control of piezoelectric actuators

Two of the most popular displacement estimation circuits are shown in Figures 1 and 3: $V_{\mathrm{i}}(t)$ is input voltage to the piezoelectric actuator (coming from a voltage amplifier), $V_{\mathrm{s}}(t)$ and R_{s} are the sensing voltage and the sensing resistance respectively. $i_{\mathrm{P}}(t)$ is the electrical current passing the piezoelectric actuator; $V_{\mathrm{p}}(t)$ and $q_{\mathrm{p}}(t)$ are the piezoelectric actuator voltage and charge respectively, and d is the displacement of the piezoelectric actuator.

2.1 Displacement estimation using the sensing voltage

There is a linear relation between the charge and the displacement of the piezoelectric actuator (Fleming and Moheimani, 2005, Newcomb and Flinn, 1982). At higher frequencies, in this case more than 100 Hz, the phase lag between charge and displacement starts to increase which makes it undesirable for higher frequency tracking applications. In this paper, to avoid phase lag the excitation signal is assumed to be less that 100 Hz. Therefore:

$$d(t) = Kq_{\mathrm{p}}(t) \tag{1}$$

According to Figure 1, displacement can be estimated as below

$$\hat{d}(t) = K\int_0^{t_{\mathrm{f}}} i_{\mathrm{P}}(t)\,dt \tag{2}$$

or

$$\hat{d}(t) = \frac{K}{R_s}\int_0^{t_f} V_s(t)\,dt \tag{3}$$

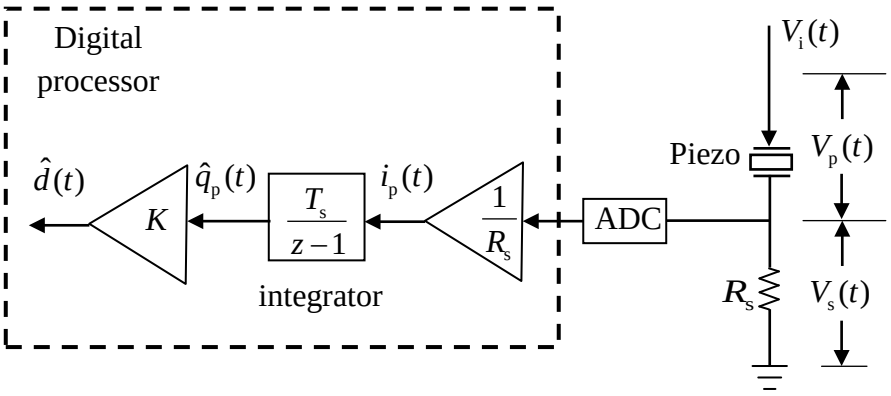

Figure 1: A schematic of a digital circuit that outputs displacement with the input of the sensing voltage

However, in the circuit shown in Figure 1, the analog to digital converter (ADC) is not ideal and its offset voltage together with the dielectric leakage of the piezoelectric actuator introduce a bias voltage term, V_{bias}, and in practice, the estimated displacement is

$$\hat{d}(t) = \frac{K}{R_s}\int_0^{t_f} \left(V_s(t) + V_{\text{bias}}\right) dt, \tag{4}$$

where t_f is the final time of operation. The discrepancy between (3) and (4) leads to an estimation error, namely 'drift'. In the discrete domain, $d(k)$ represents the current displacement and $d(k-i)$ represents the value of displacement at *i* instants ago; the time interval between two consecutive instants is the sampling time of the model, T_s.

If $n_f = \frac{t_f}{t_s}$, then

$$\hat{d}(t) = \frac{K}{R_s} \sum_{k=1}^{n_f+1} \left(V_s(k) + V_{bias} \right). \tag{5}$$

If the number of terms of discrete sum function (n_f) is large, then the resultant error or drift will be considerable even with a small V_{bias}. Drift compensation was not addressed in this research. Figure 2 shows the drift which increases as the operations progresses.

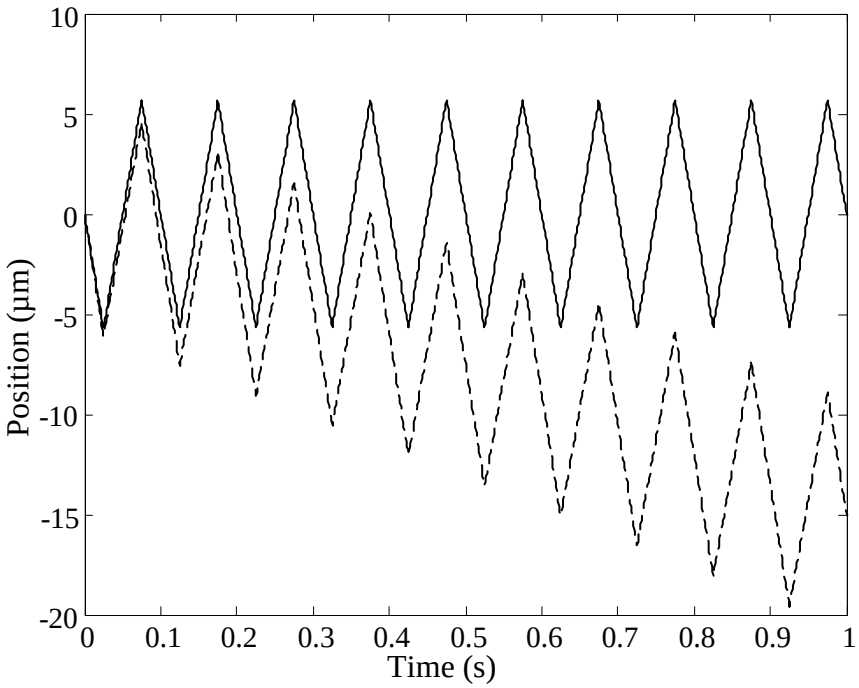

Figure 2: Actual (-) and estimated (--) piezoelectric actuator displacement using the circuit shown in Figure 1 with a sampling time of 0.001 s

2.2 Displacement estimation using the piezoelectric voltage

A variety of dynamic models have been used to map the piezoelectric voltage to displacement. In terms of the essence of inputs to the model, dynamic models are divided into two groups: in some phenomenological models (i.e. different forms of Preisach models), the previous values of displacement are not used as the inputs to the model, although these values definitely influence the current value of displacement. This can be interpreted as the previous values of displacement have been assumed to be indirectly represented by the piezoelectric-voltage-based signals (the history and/or derivatives and/or extrema of the piezoelectric voltage). Preisach models, originally developed by a physicist in the area of magnetism (Preisach, 1935), need a whole-domain solution from the very first instant of operation to estimate the current displacement, moreover phenomenological models focus on hysteresis modeling (e.g. (Yu *et al.*, 2002)), whereas hysteresis is not the main issue in cases such as tube piezoelectric actuators.

The second group of dynamic models in the area are classical black-box models such as universal approximators with mathematically proven capability in system identification (Mohammadzaheri, 2012a). These techniques offer modeling accuracy and computational efficiency (Mohammadzaheri, 2012a). Sensorless control of piezoelectric actuators using highly accurate black box models, shown in Figure 3, is the main focus of this article.

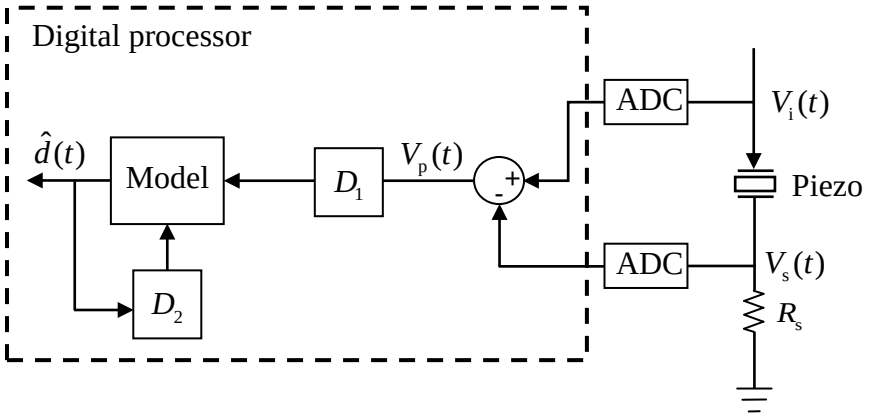

Figure 3: A typical circuit to estimate displacement; the input to the circuit is the piezoelectric voltage. The output of blocks D_1 and D_2 are their input signals together with a number of temporal derivatives and previous extrema of their input signals

As previously mentioned, in order to achieve higher accuracy, the previously estimated values of displacement are used as inputs to this model. As a result, during sensorless operation, the inevitable error in the estimated displacements feeds back to the model and influences the next estimated displacement.

Consider a model of f: $\hat{d}(k) = f\left(\mathbf{V}_{\mathbf{ps}}, d(k-1)\right)$, (6)

where $\mathbf{V}_{\mathbf{ps}}$ is a vector of the present and a number of previous piezoelectric-voltage values. Variables with a hat represent estimated values. The estimation error *e*, is given by

$$e(k) = d(k) - \hat{d}(k). \tag{7}$$

According to these definitions, during operation:

$$e(2) = d(2) - f\left(\mathbf{V}_{\mathbf{ps}}, d(1)\right) \text{ or } d(2) = f\left(\mathbf{V}_{\mathbf{ps}}, d(1)\right) + e(2), \tag{8}$$

So

$$e(3) = d(3) - f\left(\mathbf{V_{ps}}, \overbrace{\left(f\left(\mathbf{V_{ps}}, d(1)\right) + e(2)\right)}^{d(2)}\right), \tag{9}$$

and

$$e(4) = d(4) - f\left(\mathbf{V_{ps}}, \overbrace{f\left(\mathbf{V_{ps}}, \overbrace{\left(f\left(\mathbf{V_{ps}}, d(1)\right) + e(2)\right)}^{d(2)}\right) + e(3)}^{d(3)}\right) \tag{10}$$

and

$$\begin{aligned} e(k) = d(k) - f(\mathbf{V_{ps}}, f(\mathbf{V_{ps}}, \ldots f(\mathbf{V_{ps}}, f(\mathbf{V_{ps}}, f(\mathbf{V_{ps}}, d(1)) \\ + e(2)) + e(3)) + e(4)...) + e(k-1)). \end{aligned} \tag{11}$$

Thus, the resultant error is likely to increase as the operation progresses, that is, larger k very often leads to a larger $e(k)$. This phenomenon is called error accumulation. In other words, the estimation error at each instant affects all future estimated values of displacement. This article addresses this issue and offers an original approach to reduce its effect on displacement estimation of piezoelectric actuators.

3 Proposed hybrid model

In this section, a method is offered to estimate the previous values of the displacement in such a way as to reduce estimation errors. Then these new

estimated values are used as inputs to the black box model, such that the influence of error accumulation will decrease.

If v represents the velocity of the piezoelectric actuator at the point where displacement is measured, for one instant before the current time, as a result of an approximate discrete derivation:

$$\frac{d(k\text{-}1)-d(k\text{-}2)}{T_s}\cong v(k\text{-}1) \text{ or}$$

$$d(k\text{-}1)\cong d(k\text{-}2)+T_s v(k\text{-}1) \tag{12}$$

For two instants before the current time:

$$d(k\text{-}2)\cong d(k\text{-}3)+T_s v(k\text{-}2) \tag{13}$$

(12) and (13) can be combined:

$$d(k\text{-}1)\cong d(k\text{-}3)+T_s\left[v(k\text{-}1)+v(k\text{-}2)\right]. \tag{14}$$

Similarly,

$$d(k\text{-}1)\cong d(k\text{-}4)+T_s\left[v(k\text{-}1)+v(k\text{-}2)+v(k\text{-}3)\right], \tag{15}$$

or in general, for N instants earlier:

$$d(k\text{-}1)\cong d(k\text{-}N)+T_s\left[\sum_{j=1}^{N-1} v(k\text{-}j)\right] \tag{16}$$

where N defines the number of previous displacements used in estimation.

The velocity can be estimated by taking the temporal derivative of (1) in the case of the validity of (1):

$$v = Ki_{\mathrm{p}} \tag{17}$$

Hence,

$$d\left(k\text{-}1\right) \cong d\left(k\text{-}N\right) + KT_{\mathrm{s}}\left[\sum_{j=1}^{N-1} i_{\mathrm{p}}\left(k\text{-}j\right)\right]. \tag{18}$$

During estimation, (18) will be used as

$$\hat{d}\left(k\text{-}1\right) = \hat{d}\left(k\text{-}N\right) + KT_{\mathrm{s}}\left[\sum_{j=1}^{N-1} i_{\mathrm{p}}\left(k\text{-}j\right)\right], \tag{19}$$

$$\text{or } \hat{d}\left(k\text{-}1\right) = \hat{d}\left(k\text{-}N\right) + \frac{KT_{\mathrm{s}}}{R_{\mathrm{s}}}\left[\sum_{j=1}^{N-1}\left(V_{\mathrm{s}}\left(k-j\right) + V_{\mathrm{bias}}\right)\right], \tag{20}$$

V_{bias} is very small and its effect is negligible if N is a small number (see Section 2.1), so it is approximately assumed that:

$$\hat{d}\left(k\text{-}1\right) = \hat{d}(k\text{-}N) + \frac{KT_{\mathrm{s}}}{R_{\mathrm{s}}}\left[\sum_{j=1}^{N-1} V_{\mathrm{s}}\left(k-j\right)\right]. \tag{21}$$

Eq. (21) can be adjusted so as to offer equivalents for $\hat{d}\left(k\text{-}2\right)$ or $\hat{d}\left(k\text{-}3\right)$ or any other displacement-based inputs to the black box model, using earlier estimated values of displacements. Eq. (21) and their aforementioned equivalents are the heart of the proposed idea of this paper.

Displacement estimation with a black box model of (6), with or without use of the proposed method can be compared. Subscripts b and h, respectively, represent use of the black box model solely and use of the proposed hybrid method. The initial value of displacement ($d(1)$) is available (usually $d(1)$ = 0 in practice). For N = 3 and k = 4, without the proposed method, From (10),

$$\hat{d}_{\mathrm{b}}(4) = f\left(\mathbf{V_{ps}}, \overbrace{f\left(\mathbf{V_{ps}}, \overbrace{\left(f\left(\mathbf{V_{ps}}, d(1)\right) + e_{\mathrm{b}}(2)\right)}^{d(2)}\right) + e_{\mathrm{b}}(3)}^{d(3)}\right). \tag{22}$$

Two different estimation errors are involved in the argument of (22). With the proposed method,

$$\hat{d}_{\mathrm{h}}(4) = f\left(\mathbf{V_{ps}}, \overbrace{\left(d(1) + Kt_{\mathrm{s}}\left[\sum_{j=1}^{3} V_{\mathrm{s}}(4-j)\right]\right)}^{d(3)}\right), \tag{23}$$

No estimation error is involved in the argument of (23), if (21) is valid.

Similarly, for k = 7, from (11) and (6), in the case of sole usage of a black box model,

$$\begin{aligned}\hat{d}_{\mathrm{b}}(7) = f(\mathbf{V_{ps}}, \ldots f(\mathbf{V_{ps}}, f(\mathbf{V_{ps}}, f(\mathbf{V_{ps}}, d(1)) \\ + e_{\mathrm{b}}(2)) + e_{\mathrm{b}}(3)) + e_{\mathrm{b}}(4) + \ldots) + e_{\mathrm{b}}(6).\end{aligned} \tag{24}$$

Five estimation errors are involved in the calculation of the estimated displacement.

However, in the case of the proposed hybrid model:

$$\hat{d}_{\mathrm{h}}(7)=f\left(\mathbf{V_{ps}},\overbrace{\left(\overbrace{f\left(\mathbf{V_{ps}},\overbrace{\left(d(1)+Kt_{\mathrm{s}}\left[\sum_{j=1}^{3}V_{\mathrm{s}}(4-j)\right]\right)}^{\hat{d}_{\mathrm{h}}(4)}\right)+e_{\mathrm{h}}(4)}^{d(4)}+Kt_{\mathrm{s}}\left[\sum_{j=1}^{3}V_{\mathrm{s}}(7-j)\right]\right)}^{d(6)}\right) \tag{25}$$

only one estimation error is involved in the calculation of the estimated displacement. Similarly, it can be concluded for the first order model presented in (6), with $N = 3$, $\hat{d}_{\mathrm{h}}(10)$, $\hat{d}_{\mathrm{h}}(13)$, $\hat{d}_{\mathrm{h}}(16)$ and $\hat{d}_{\mathrm{h}}(k)$ have only two, three, four and $(k-4)/3$ estimation errors involved in their estimation calculations, respectively. In general, $(k-N-1)/N$ estimation errors are involved in calculating $\hat{d}_{\mathrm{h}}(k)$ for model (6). This simply means the inevitable estimation error at each instant does not affect all subsequent estimated values of displacement; thus, the influence of error accumulation decreases significantly.

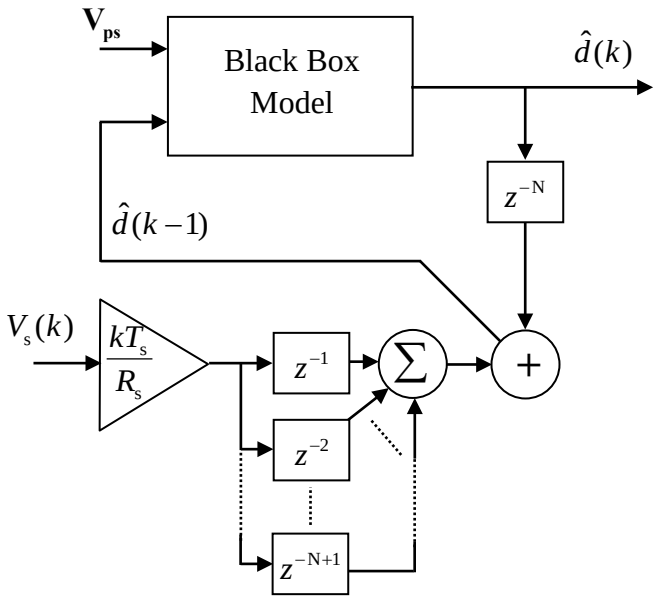

Figure 4: A schematic of the proposed method for the model introduced in (6), Z^{-1} represents a unit delay

However, this conclusion is based on the assumption of the validity of (1) which is true at excitation frequencies below 100 Hz, and is also based on the validity of (21) which is not completely true. Large values of N (introduced in (16)) may lead to a considerable error due to conversion errors (see Section 2.2). In summary, as N increases, error accumulation decreases and the aforementioned error increases. Therefore, the value of N is a trade-off.

4 Data gathering and black box modeling

The set up includes a NEC/TOKIN AE0505D44H40 stack piezoelectric actuator and a PHILTECH D20 optical sensor connected to a PC through a DS1104 dSPACE and a voltage amplifier. The system was excited by three triangle waves with maximum and minimum amplitude of ±20 V and

frequencies of 1 Hz, 10 Hz and 100 Hz, for a period of 2 s each. All experiments were performed under no external forces, so the models are valid under this condition (such as with Atomic Force Microscopy). In scanning devices, the piezoelectric actuators follow a raster pattern (Schitter *et al.*, 2007, Abramovitch *et al.*, 2007, Moheimani, 2008); triangle waves of excitation are employed to generate this pattern of motion; that is, in one direction (let us say *x*), the tube should track a triangular waveform, and in the other direction (let us say *y*), the tube should track a very slowly increasing ramp.

In this research, a Sugeno-type fuzzy model was fitted to the aforementioned data:

$$\hat{d}(k) = f\left(V_{\mathrm{P}}(k-1), V_{\mathrm{P}}(k-2), V_{\mathrm{P}}(k-3), V_{\mathrm{Pext}}, d(k-1)\right), \qquad (26)$$

where V_{Pext} is the last extremum value of the piezoelectric voltage. Antecedent parameters were tuned via the steepest descent method and consequent parameters were tuned using least square of error. The fuzzy model comprises 25 fuzzy rules, initially selected through subtractive clustering. The fuzzy modeling process and its performance have been detailed in (Mohammadzaheri *et al.*, 2012c).

5 Experimental results

The achieved fuzzy model has been tested operating alone (with $\hat{d}(k\text{-}1)$ arising directly from $\hat{d}(k)$) and within the circuit shown in Figure 4 for one second (1000 instants). A variety of triangle waves, the most prevalent wave form in piezoelectric actuation, with the domain of ±20 V and a range of frequencies have been used in the tests. Results (Mean of Absolute Error,

MAE) are presented in Table 1 and depicted in Figures 5 and 6. The improvement in accuracy ranges from 27% to 47% for Table 1. It can be seen there is an optimal value for *N*. This confirms the trade-off mentioned in Section 3. It is expected the optimal *N* is dependent upon the noise properties of the sensing voltage used to determine velocity and is the subject of future research. The results indicate the capability of the method to estimate displacement at the given range of frequency. Due to the RC circuit between the sensing resistor and the piezoelectric actuator, at low frequencies, the voltage drop across the sensing resistor decreases significantly. This causes a significant reduction in the signal-to-noise ratio (SNR) of the sensing voltage, $V_s(t)$, introduced in Section 2, which means this signal cannot be measured accurately. Therefore, this method is not suitable to estimate displacement when the applied voltage is low frequency or a DC signal.

Table 1: Mean of absolute values of estimation error for one second (1000 instants) in micro meters. The range of voltage is [-20, +20] V and the range of displacement is approximately [-5, +5] micro meters.

	Fuzzy	Hybrid *N*=2	Hybrid *N*=3	Hybrid *N*=4	Hybrid *N*=5	Hybrid *N*=6	Hybrid *N*=7	Hybrid *N*=8
15Hz	0.6242	0.5102	0.4774	0.4601	0.4549	0.4588	0.4541	0.4677
20Hz	0.4586	0.3151	0.2787	0.2818	0.3360	0.3170	0.3589	0.3900
50Hz	0.6824	0.5260	0.5213	0.5332	0.4349	0.4528	0.3777	0.6854
75Hz	1.6075	1.0656	1.0219	1.1294	1.1741	1.1046	0.8524	1.7515

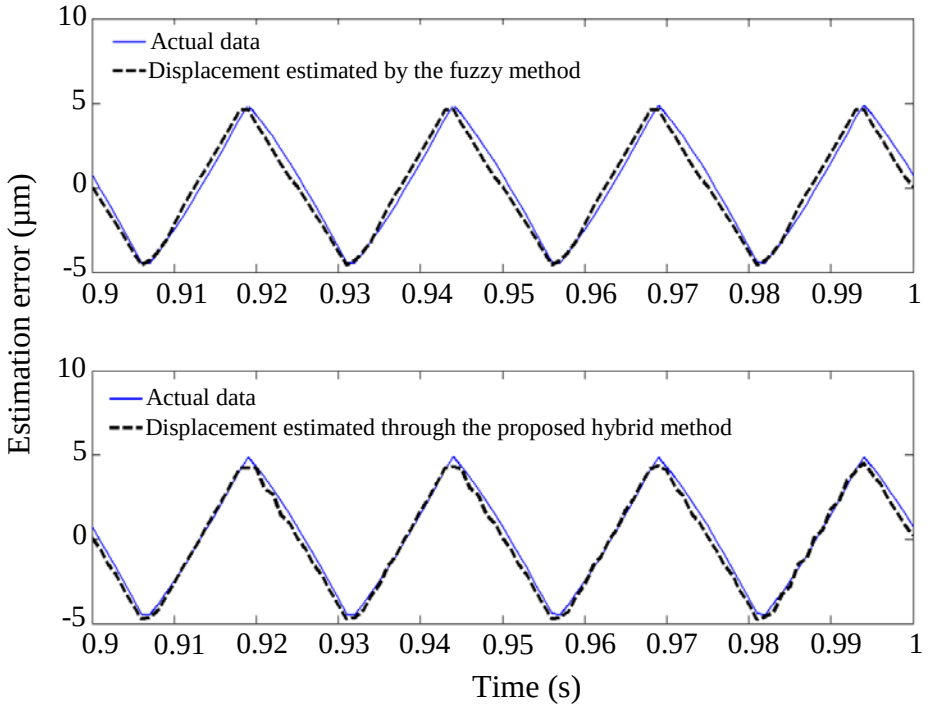

Figure 5: The accuracy of solely the fuzzy model and the hybrid algorithm (with N=6) to predict displacement generated by a triangle excitation voltage wave at the frequency of 40 Hz and the domain of 20V after 0.9 seconds of operation

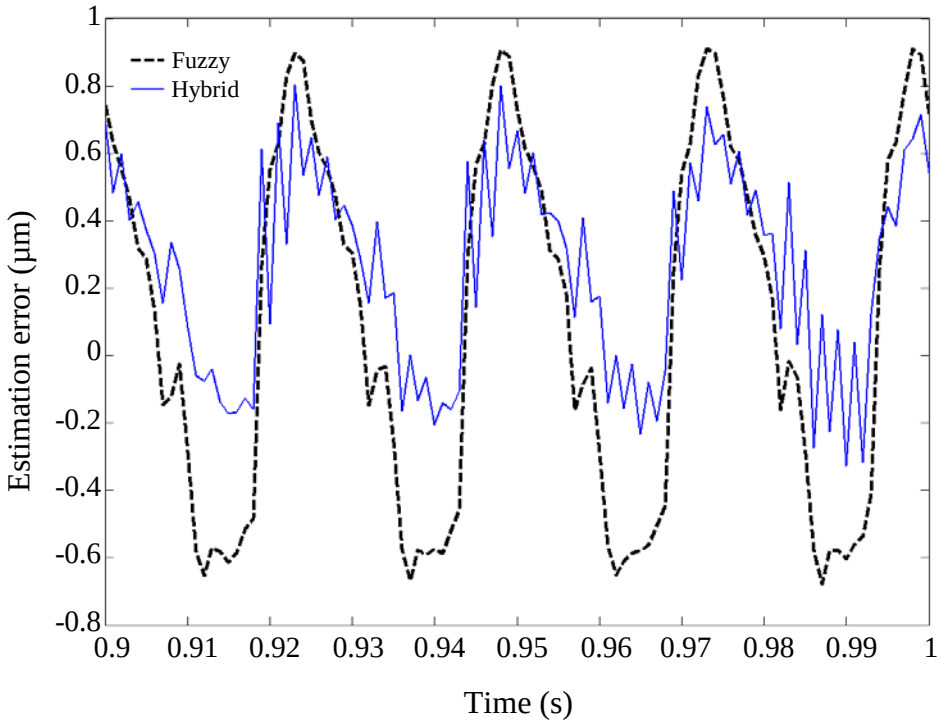

Figure 6: The estimation error for the fuzzy model and hybrid method as detailed in Figure 5 for the same time period

6 Conclusion

In this paper, a new method has been introduced for sensorless control of piezoelectric stack actuators that increases the estimation accuracy of black box models of these actuators through reducing the effect of error accumulation. This is achieved through the use of a method that employs two electrical signals (amongst three known signals for this purpose which one of them is not applicable on piezoelectric stack actuators). The method employs a black box model which maps the piezoelectric voltage onto displacement together with a complementary algorithm that uses the sensing voltage.

References

Abramovitch, D.Y., Andersson, S.B., Pao, L.Y. and Schitter, G., 2007. A tutorial on the mechanisms, dynamics, and control of atomic force microscopes. *In: American Control Conference* 7, pp. 3488-3502.

Aphale, S., Fleming, A.J. and Moheimani, S.O.R., 2007. High speed nano-scale positioning using a piezoelectric tube actuator with active shunt control. *Micro and Nano Letters* 2(1), 9–12.

Bazghaleh, M., Grainger, S., Cazzolato, B. and Lu, T.-F., 2010. An innovative digital charge amplifier to reduce hysteresis in piezoelectric actuators, *In: Australian Robotics and Automation Association (ACRA).* Brisbane, Australia.

Comstock, R.H., 1981. Charge control of piezoelectric actuators to reduce hysteresis effects. *USA Patent* No. 4,263,527.

Fairbairn, M.W., Moheimani, S.O.R. and Fleming, A.J., 2011. Q control of an atomic force microscope microcantilever: A sensorless approach. *Journal of Microelectromechanical Systems* 20, 1372–1381.

Fleming, A.J. and Moheimani, S.O.R., 2005. A grounded-load charge amplifier for reducing hysteresis in piezoelectric tube scanners. *Review of Scientific Instruments* 76(7), 0737071–737075.

Fleming, A.J. and Moheimani, S.O.R., 2006. Sensorless vibration suppression and scan compensation for piezoelectric tube nanopositioners. *IEEE Transactions on Control Systems Technology* 14(1), 33–44.

Kuiper, S. and Schitter, G., 2010. Active damping of a piezoelectric tube scanner using self-sensing piezo actuation, *Mechatronics* 20(6), 656–665.

Li, C. and Tan, Y., 2004. A neural networks model for hysteresis nonlinearity. *Sensors and Actuators A-Physical* 112(1), 49–54.

Mohammadzaheri, M., Chen, L. and Grainger, S., 2012a. A critical review of the most popular types of neuro control. *Asian Journal of Control* 16, 1–11.

Mohammadzaheri, M., Grainger, S. and Bazghaleh, M., 2012b. A comparative study on the use of black box modelling for piezoelectric actuators. *The International Journal of Advanced Manufacturing Technology* 1–9.

Mohammadzaheri, M., Grainger, S. and Bazghaleh, M., 2012c. Fuzzy modeling of a piezoelectric actuator. *International Journal of Precision Engineering and Manufacturing* 13(5), 663–670.

Moheimani, S.O.R. and Yong, Y.K., 2008. Simultaneous sensing and actuation with a piezoelectric tube scanner. *Review of Scientific Instruments* 79(7), 073702.

Moheimani, S.O.R., 2008. Invited review article: Accurate and fast nanopositioning with piezoelectric tube scanners: Emerging trends and future challenges. *Review of Scientific Instruments* 79(7), 071101.

Newcomb, C.V. and Flinn, I., 1982. Improving the linearity of piezoelectric ceramic actuators. *Electronics Letters* 18(11), 442–444.

Park, J.K. and Moon, W.K., 2010. Sensorless control for hysteresis compensation of AFM scanner by modified Rayleigh model. *Journal of Central South University of Technology* 17, 1243–1246.

Preisach, F., 1935. Uber Die Magnetische Nachwirkung. *Zeitschrift Für Physik* 94(5-6), 277–302.

Ronkanen, P., Kallio, P., Vilkko, M. and Koivo, H.N., 2011. Displacement control of piezoelectric actuators using current and voltage. *IEEE-ASME Transactions on Mechatronics* 16, 160–166.

Schitter, G., Astroem, K.J., Demartini, B.E., Thurner, P.J., Turner, K.L. and Hansma, P.K., 2007. Design and modeling of a high-speed AFM-scanner. *IEEE Transactions on Control Systems Technology* 15(5), 906–915.

Schitter, G., Stemmer, A., 2004. Identification and open-loop tracking control of a piezoelectric tube, scanner for high-speed scanning-probe microscopy. *IEEE Transactions on Control Systems Technology* 12, 449–454.

Song, D.W. and Li, C.J., 1999. Modeling of piezo actuator's nonlinear and frequency dependent dynamics. *Mechatronics* 9(4), 391–410.

Yang, X.F., Li, W., Wang, Y.Q. and Ye, G., 2008. Modeling hysteresis in piezo actuator based on neural networks. *In: 3rd International Conference on Intelligence Computation and Applications*. Wuhan, China, pp. 290–296.

Yong, Y.K. and Moheimani, S.O.R., 2009. Vibration control of a novel tube scanner using piezoelectric strain-induced voltage. *In: IEEE/ASME International Conference on Advanced Intelligent Mechatronics (AIM)*. pp. 1070–1075.

Yu, Y.H., Naganathan, N. and Dukkipati, R., 2002. Preisach modeling of hysteresis for piezoceramics actuator system. *Mechanism and Machine Theory* 37(1), 49–59.

Zhang, X.L. and Tan, Y.H., 2010. A hybrid model for rate-dependent hysteresis in piezoelectric actuators. *Sensors and Actuators A-Physical* 157, 54–60.

Zhang, X.L., Tan, Y.H. and Su, M.Y., 2009. Modeling of hysteresis in piezoelectric actuators using neural networks. *Mechanical Systems and Signal Processing* 23, 2699–2711.

Zhang, X.L., Tan, Y.H., Su, M.Y. and Xie, Y.Q., 2010. Neural networks based identification and compensation of rate-dependent hysteresis in piezoelectric actuators. *Physica B-Condensed Matter* 405, 2687–2693.

5 Model-based Drift Correction of the Digital Charge Amplifier

5.1 Introduction

While the DCA, proposed in Chapter 3, significantly reduced hysteresis and improved the linearity of piezoelectric actuators, it suffers from drift which reduces the positioning accuracy over a considerable period of time.

This chapter proposes a model-based drift correction technique for removal of the drift and to improve the tracking performance of the DCA. It is shown how the model, developed in Chapter 4, and which crucially does not suffer from drift, can be integrated with a charge amplifier in order to remove the charge amplifier's inherent drift, while the charge amplifier itself tackles the issue of hysteresis. In this respect, data fusion is utilized to integrate the reliability and short term accuracy of the DCA, with the long term accuracy of the non-linear model to obtain the benefit of both techniques.

Experimental results clearly show the elimination of drift and improvements in tracking performance.

5.2 A digital charge amplifier for hysteresis elimination in piezoelectric actuators

Published in Smart Materials and Structures.

Statement of Authorship

Title of Paper	A digital charge amplifier for hysteresis elimination in piezoelectric actuators
Publication Status	● Published ○ Accepted for Publication ○ Submitted for Publication ○ Publication Style
Publication Details	Bazghaleh, M., Grainger, S., Mohammadzaheri, M., Cazzolato, B. & Lu, T.F. (2013). A digital charge amplifier for hysteresis elimination in piezoelectric actuators. Smart materials and structures, 22(7) 075016.

Author Contributions

By signing the Statement of Authorship, each author certifies that their stated contribution to the publication is accurate and that permission is granted for the publication to be included in the candidate's thesis.

Name of Principal Author (Candidate)	Mr. Mohsen Bazghaleh		
Contribution to the Paper	Developed the model, performed experimental work, analyzed data and wrote the manuscript.		
Signature		Date	11/9/13

Name of Co-Author	Dr. Steven Grainger		
Contribution to the Paper	Supervised research, reviewed manuscript.		
Signature		Date	11/9/13

Name of Co-Author	Dr. Morteza Mohammadzaheri		
Contribution to the Paper	Supervised research, reviewed manuscript.		
Signature		Date	11/6/2013

Name of Co-Author	Dr. Ben Cazzolato		
Contribution to the Paper	Supervised research, reviewed manuscript.		
Signature		Date	11/9/13

Name of Co-Author	Dr. Tien-Fu Lu		
Contribution to the Paper	Supervised research, reviewed manuscript.		
Signature		Date	11/09/13

A digital charge amplifier for hysteresis elimination in piezoelectric actuators

Mohsen Bazghaleh, Steven Grainger, Morteza Mohammadzaheri, Ben Cazzolato and Tien-Fu Lu

Abstract. *Piezoelectric actuators are commonly used for nanopositioning due to their high resolution, low power consumption and wide operating frequency but they suffer hysteresis which affects linearity. In this paper, a novel digital charge amplifier is presented. Results show that hysteresis is reduced by 91% compared with a voltage amplifier but over long operational periods the digital charge amplifier approach suffers displacement drift. A non-linear ARX model with long-term accuracy is used with a data fusion algorithm to remove the drift. Experimental results are presented.*

Keywords: *Piezoelectric actuators; digital implementation; hysteresis; charge control; data fusion; drift; non-linear ARX model.*

1 Introduction

The most commonly used nanopositioner is the piezoelectric actuator. Aside from being compact in size, they are capable of nanometre resolution in displacement, have high stiffness, provide excellent operating bandwidth and high force output (Devasia *et al.*, 2007). Consequently they have been widely used in many applications ranging from scanning tunneling microscopes (STM) (Wiesendanger, 1994) to vibration cancellation in disk drives (Ma and Ang, 2000). Typically piezoelectric actuators are driven by

voltage, however voltage driven methods suffer from hysteresis and creep which are nonlinear in nature and reduce the positioning accuracy (Leang and Devasia, 2002).

Creep is the result of the remnant polarization which continues to change after the applied signal reaches its final value and typically is an issue at low frequencies (IEEE Standard on Piezoelectricity, 1987). Hysteresis is due to the polarization of microscopic particles (Damjanovic, 2005) and depends on both the currently applied voltage as well as that previously applied (Kuhnen and Janocha, 1998). Physically it means that, for similar voltage input, the piezoelectric actuator may have different displacement values. The relationship between applied voltage and displacement also changes subject to the amplitude and the frequency of the applied voltage, thus it is both non-linear and dynamic in nature (Adriaens *et al.*, 2000).

A variety of approaches have been used to tackle the hysteresis of piezoelectric actuators. Feed-forward control uses an inverse-model, such as the Preisach model (Ge and Jouaneh, 1995) or Maxwell resistive model (Goldfarb and Celanovic, 1997b), to compensate for hysteresis. Because of uncertainties in the piezo parameters, the feedforward inverse-model technique can suffer from lack of robustness. Another approach is displacement feedback control (Shieh *et al.*, 2004) but this is limited by sensor-induced noise, high cost, additional complexity and limited bandwidth (Fleming and Leang, 2008).

Charge regulator and capacitor insertion techniques have also been used (Minase *et al.*, 2010). The capacitor insertion method (Kaizuka and Siu, 1988) involves using a capacitor in series with the piezoelectric actuator and, while it is effective in dealing with hysteresis, significantly reduces the

operating range because of the voltage drop across the capacitor. Charge regulation was first introduced by Comstock (1981) who showed that by regulating the charge across a piezoelectric actuator the hysteresis is reduced significantly. However a charge amplifier approach has historically been complicated and expensive to implement due to the complexity of the analog circuitry required to meet stringent performance targets (Fleming and Moheimani, 2005). Additionally, in the generic charge amplifier, the load capacitor is charged up because of the uncontrolled nature of the output voltage and once the output voltage reaches the power supply rails, the charge amplifier saturates. To avoid this undesirable effect additional methods have been used which increases the implementation complexity (Fleming and Moheimani, 2004). Comstock (1981) used an initialization circuit to short circuit the sensing capacitor periodically; however, it causes undesirable disturbances at high frequencies. Fleming and Moheimani (2004) used two additional amplifiers to synthesize charge operation at low frequencies.

This paper presents a novel digital charge amplifier with model-based drift compensation for the elimination of hysteresis. In Section 2 the digital charge amplifier is described. Piezoelectric actuator modeling and the model-based drift correction are discussed in Section 3. The experimental setup and results are in Section 4. Conclusions are provided in Section 5.

2 A digital charge amplifier

Figure 1 shows the digital charge amplifier that forms the basis of this work. It consists of a voltage amplifier, digital to analog converter (DAC), analog to digital converter (ADC) and a digital signal processor (DSP). A sensing

resistor is placed in series with the piezoelectric stack actuator and a protection circuit protects the ADC from high voltage.

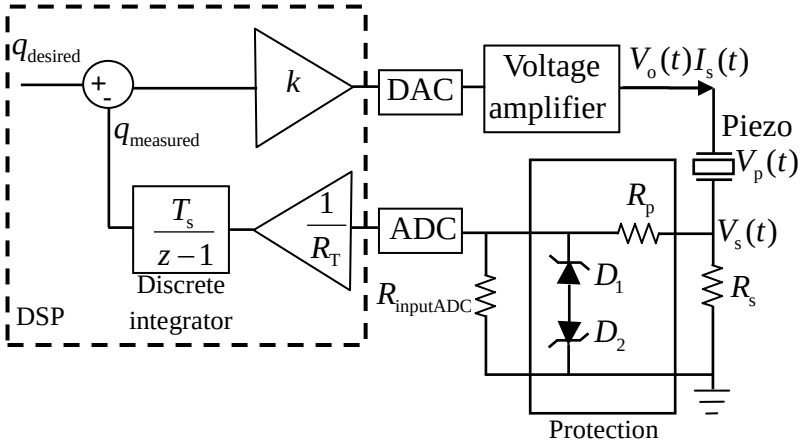

Figure 1: Circuit of the digital charge amplifier

The DSP unit calculates the charge across the piezoelectric actuator, q_p, by integrating the piezoelectric actuator current.

$$q_p = \int I_s(t)dt. \tag{1}$$

Because of the protection circuit resistor R_p and the ADC input resistance $R_{inputADC}$, the piezoelectric actuator current is given by

$$I_s(t) = \frac{V_s(t)}{R_s \parallel (R_p + R_{inputADC})} \tag{2}$$

where V_s is the sensing voltage across the sensing resistor.

Substituting (2) into (1) gives

$$q_{\mathrm{p}} = \int \frac{V_{\mathrm{s}}(t)}{R_{\mathrm{s}} \,\|\, (R_{\mathrm{P}} + R_{\mathrm{inputADC}})} dt. \tag{3}$$

The protection resistor and input resistance are in series and together they are in parallel with sensing resistor R_{s}, so the total resistance is

$$R_{\mathrm{T}} = R_{\mathrm{s}} \,\|\, (R_{\mathrm{P}} + R_{\mathrm{inputADC}}). \tag{4}$$

Substituting (4) in (3) gives

$$q_{\mathrm{p}} = \frac{1}{R_{\mathrm{T}}} \int V_{\mathrm{s}}(t) dt. \tag{5}$$

Therefore the charge across the piezoelectric actuator is equal to the integral of the voltage across the sensing resistor divided by the total resistance. A high gain feedback loop is used to equate the desired charge with the actual charge.

The transfer function can now be derived. By considering a capacitor C_{L} as a model of the piezoelectric actuator (Fleming and Moheimani, 2005, Huang *et al.*, 2010), the transfer function is:

$$H(s) = \frac{V_{\mathrm{s}}(s)}{V_{\mathrm{o}}(s)} = \frac{R_{\mathrm{T}} C_{\mathrm{L}} s}{R_{\mathrm{T}} C_{\mathrm{L}} s + 1} \tag{6}$$

By taking the Z transform, the discrete transfer function between the output of the voltage amplifier $V_{\mathrm{o}}(z)$ and sensing voltage $V_{\mathrm{s}}(z)$ will be

$$H(z) = \frac{V_{\mathrm{s}}(z)}{V_{\mathrm{o}}(z)} = \frac{z - 1}{z - e^{-\frac{T_{\mathrm{s}}}{R_{\mathrm{T}} C_{\mathrm{L}}}}} \tag{7}$$

where T_s is the sampling time. Moreover, the transfer function of the digital charge drive algorithm is

$$V_o(z) = k(q_{\text{desired}} - \frac{T}{(z-1)R_T}V_s(z)) \tag{8}$$

where k is the closed loop gain and $q_{\text{desired}}(z)$ is the desired charge. Substituting (8) in (7) results in

$$\frac{z - e^{-\frac{T_s}{R_T C_L}}}{z-1}V_s(z) = k(q_{\text{desired}}(z) - \frac{T_s}{(z-1)R_T}V_s(z)). \tag{9}$$

By considering $V_s(z) = \frac{q_{\text{actual}}(z)R_T(z-1)}{T_s}$, where $q_{\text{actual}}(z)$ is the actual charge across the piezo, the discrete transfer function from the input (desired charge) to the output (actual charge) is given by

$$\frac{q_{\text{actual}}(z)}{q_{\text{desired}}(z)} = \frac{\frac{T_s k}{R_T}}{z - e^{-\frac{T_s}{R_T C_L}} + \frac{T_s k}{R_T}}. \tag{10}$$

For a typical piezoelectric stack actuator with a capacitance of 3.4 μF using the digital charge amplifier with a 100 Ω sensing resistor and sampling frequency 40 kHz, the frequency response has zero dB gain with approximately zero phase-shift up to 10 kHz. This is the theoretical bandwidth. In Section 4 the practical bandwidth will be shown.

The principal difficulty in using this technique is drift of the displacement output. In the digital charge amplifier, because the ADC is not ideal, it

suffers from current leakage. This can lead to a bias voltage V_{bias} at the input and is the main reason for the drift in the measured charge which is given by

$$q_{\text{measured}} = \frac{1}{R_{\text{T}}} \int (V_{\text{s}}(t) + V_{\text{bias}}) dt. \tag{11}$$

Due to the integration of the voltage bias, the measured charge will drift resulting in miscalculation of the actual charge across the piezoelectric actuator. The output voltage $V_{\text{o}}(t)$, which is equal to $k.(q_{\text{desired}} - q_{\text{measured}})$, will also drift until it reaches the power supply rails.

Some drift removal methods have been proposed including the use of a low-pass filter (LPF) bias estimator, the integrator reset method and a modified integrator. These have been discussed in detail in previous work (Bazghaleh *et al.*, 2010). The LPF bias estimator is easy to implement but does not work at frequencies lower than its cut-off frequency. The modified integrator has less drift compared to a LPF bias estimator but it has some signal distortion at high frequencies and the integrator reset is only useful if it is known that the signal crosses zero regularly. None of these methods have been shown to be successful in removing drift over a wide range of frequencies. In the next section a model-based drift correction method is described to improve the performance of the DCA.

3 Model-based drift correction

This section describes how the model-based drift correction operates. The block diagram is shown in Figure 2 and comprises an integrator unit, a nonlinear autoregressive exogenous model (NARX) and a data fusion block.

With reference to Figure 1, I_s is calculated by dividing V_s by R_s and V_p is calculated by subtracting V_s from V_o.

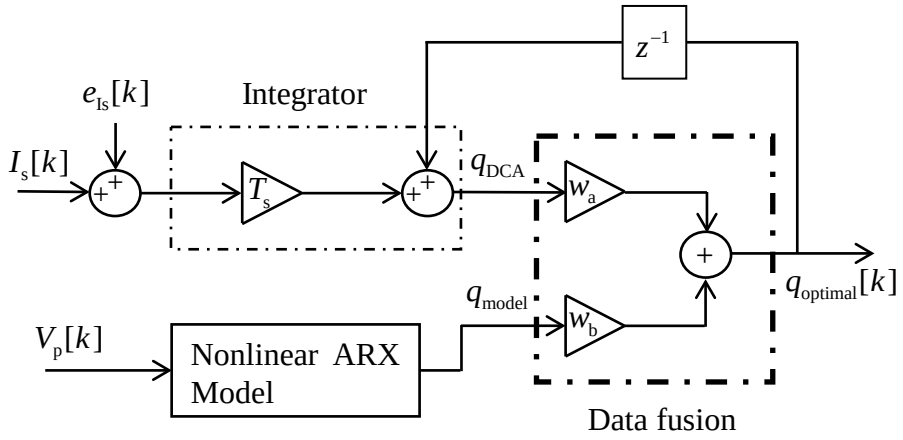

Figure 2: Model-based drift correction block diagram

The integrator unit is used to integrate current passing through the piezo to calculate the charge. As described before, using the digital charge amplifier alone can provide an accurate estimate of charge but it will drift over time due to small errors in the voltage measurement and hence calculated current. As the new charge is calculated iteratively using the previous charge, the charge errors are accumulated and the error grows over time.

Data fusion is used to combine the reliability and short term accuracy of the digital charge amplifier with the long term accuracy of the model to remove the drift on the DCA and improve the accuracy of positioning.

3.1 Nonlinear autoregressive exogenous model (NARX)

The charge on the piezo actuator has a non-linear relationship with the applied piezo voltage and to model this, a black-box NARX model was

used. A NARX model determines the current value of a time series (in this case the charge output of the model) as a non-linear function of both past values of the time series and current and past inputs. The non-linear function is determined through training the black-box model. In this instance the model charge output is determined from the previous charge output of the model and present and past piezo voltages V_{p}.

The model was trained by exciting the piezo with three triangle waves with slopes of ±80 V/s, ±800 V/s and ±8000 V/s with maximum and minimum amplitude of ±20 V for a duration of 2s each. Furthermore, the piezo was excited by a ±20 V chirp function with a frequency range of 1 Hz to 100 Hz for a time period of 2 s. Data gathered through these excitations was used as the training data.

The voltage to displacement relationship of piezoelectric actuators exhibits rate-dependant behavior. This makes modeling difficult and therefore the NARX model is not accurate at all rates as shown in the first column of Figure 9. Later it will be described how this model can be used to remove the drift as the model's important feature is that it is drift free.

3.2 Data fusion

The data fusion comprises two weighting coefficients w_{a} and w_{b} for the digital charge amplifier and the NARX model respectively. The sum of the weighting coefficients is unity. If w_{a} is one and w_{b} is zero, the system is a pure integrator and if w_{a} is zero and w_{b} is one, the system only relies on the model. Choosing w_{a} between zero and one can combine the benefits of both techniques. As illustrated in Figure 2, the optimal output charge is

$$q_{\text{optimal}}[k] = w_{\text{a}} q_{\text{DCA}}[k] + w_{\text{b}} q_{\text{model}}[k] \tag{12}$$

and the output of the integrator is given by

$$q_{\text{DCA}}[k] = q_{\text{optimal}}[k-1] + T_{\text{s}}(I_{\text{s}}[k] + e_{\text{Is}}[k]), \tag{13}$$

where T_{s} is the sampling time, I_{s} is the piezoelectric current and e_{Is} is the current error. Considering q_{actual} as the actual charge on the piezo and e_{m} as the error at the output of the NARX model, the charge in the model is estimated as

$$q_{\text{model}}[k] = q_{\text{actual}}[k] + e_{\text{m}}[k]. \tag{14}$$

Substituting (13) and (14) into (12) gives

$$\begin{aligned} q_{\text{optimal}}[k] = {} & w_{\text{a}} q_{\text{optimal}}[k-1] + w_{\text{a}} T_{\text{s}} I_{\text{s}}[k] \\ & + w_{\text{a}} T_{\text{s}} e_{\text{Is}}[k] + w_{\text{b}} q_{\text{actual}}[k] + w_{\text{b}} e_{\text{m}}[k]. \end{aligned} \tag{15}$$

Considering $e_{\text{q\_opt}}$ as the error in the optimal output charge,

$$q_{\text{optimal}}[k] = q_{\text{actual}}[k] + e_{\text{q\_opt}}[k]. \tag{16}$$

Substituting (16) in (15) gives

$$\begin{aligned} q_{\text{actual}}[k] + e_{\text{q\_opt}}[k] = {} & w_{\text{a}} (q_{\text{actual}}[k-1] + e_{\text{q\_opt}}[k-1]) \\ & + w_{\text{a}} T_{\text{s}} I_{\text{s}}[k] + w_{\text{a}} T_{\text{s}} e_{\text{Is}}[k] + w_{\text{b}} q_{\text{actual}}[k] + w_{\text{b}} e_{\text{m}}[k] \end{aligned} \tag{17}$$

Considering $q_{\text{actual}}[k] = q_{\text{actual}}[k-1] + T_{\text{s}} I_{\text{s}}[k]$,

$$q_{\text{actual}}[k] + e_{\text{q\_opt}}[k] = q_{\text{actual}}[k] + w_{\text{a}} e_{\text{q\_opt}}[k-1] + w_{\text{a}} T_{\text{s}} e_{\text{Is}}[k] + w_{\text{b}} e_{\text{m}}[k] \tag{18}$$

By cancelling $q_{\text{actual}}[k]$ and simplifying (18) the following expression for the error in the optimal charge output is given by

$$e_{\text{q\_opt}}[k] = w_{\text{a}} e_{\text{q\_opt}}[k-1] + w_{\text{a}} T_{\text{s}} e_{\text{Is}}[k] + w_{\text{b}} e_{\text{m}}[k]. \tag{19}$$

Taking the z-transform of both sides of (19) and assuming zero-state conditions

$$e_{\text{q\_opt}}[z](1 - w_{\text{a}} z^{-1}) = w_{\text{a}} T_{\text{s}} e_{\text{Is}}[z] + (1 - w_{\text{a}}) e_{\text{m}}[z]. \tag{20}$$

Rearranging (20) gives

$$e_{\text{q\_opt}}[z] = w_{\text{a}} T_{\text{s}} \frac{e_{\text{Is}}[z]}{(1 - w_{\text{a}} z^{-1})} + (1 - w_{\text{a}}) \frac{e_{\text{m}}[z]}{(1 - w_{\text{a}} z^{-1})}. \tag{21}$$

Taking the inverse z-transform of (21) gives

$$e_{\text{q\_opt}}[k] = (1 - w_{\text{a}})\left(\sum_{n=0}^{k-1} w_{\text{a}}^{n} e_{\text{m}}[k-n]\right) + T_{\text{s}}\left(\sum_{n=0}^{k-1} w_{\text{a}}^{n+1} e_{\text{Is}}[k-n]\right). \tag{22}$$

It can be seen in the second term of (22) that as long as w_{a} is less than unity the effects of previous current errors diminishes over time. Simplifying this equation, the error on the optimal output will be

$$e_{\text{q\_opt}}[k] = \sum_{n=0}^{k-1} (w_{\text{a}}^{n} (T_{\text{s}} w_{\text{a}} e_{\text{Is}}[k - n] + (1 - w_{a}) e_{m}[k - n])). \tag{23}$$

Because of the central limit theorem, the input current error e_{Is} is considered to have a normal distribution with mean μ_1 and standard deviation σ_1 and the model error e_{m} is assumed to have a normal distribution with mean μ_2 and standard deviation σ_2 (Rice, 1995). The sum of two normally distributed signals is also normally distributed. Therefore (23) will be

$$e_{\text{q\_opt}}[k] = \sum_{n=0}^{k-1} (w_{\text{a}}^{n} (f(k - n)) \tag{24}$$

where $f(k - n)$ has a normal distribution with mean

$$\mu_{\text{f}} = T_{\text{s}} w_{\text{a}} \mu_1 + (1 - w_{\text{a}}) \mu_2 \tag{25}$$

and variance

$$\sigma_f^2 = T_{\text{s}}^2 w_{\text{a}}^2 \sigma_1^2 + (1 - w_{\text{a}})^2 \sigma_2^2. \tag{26}$$

Eqn. (24) has a normal distribution with mean and variance

$$\mu_{\text{e\_opt}} = \mu_{\text{f}} \sum_{n=0}^{k-1} w_{\text{a}}^{n} \tag{27}$$

$$\sigma_{\text{e\_opt}}^2 = \sigma_{\text{f}}^2 \sum_{n=0}^{k-1} (w_{\text{a}}^{2n}) \tag{28}$$

If the system is a pure integrator, w_a is equal to one and (27) and (28) will diverge, the error will be accumulated and the output will drift. If w_a is between zero and one, (27) and (28) will converge and therefore there will not be drift of the output and

$$\mu_{e\_opt} = \frac{(T_s w_a \mu_1 + (1 - w_a)\mu_2)}{1 - w_a} \tag{29}$$

$$\sigma^2{}_{e\_opt} = \frac{(T_s^2 w_a^2 \sigma_1^2 + (1 - w_a)^2 \sigma_2^2)}{1 - w_a^2}, \tag{30}$$

The mean square error (MSE) on the optimal output is

$$MSE_{e\_opt} = \mu^2{}_{e\_opt} + \sigma^2{}_{e\_opt}. \tag{31}$$

The optimal value w_a is achieved when the MSE is minimized. In Section 4, the experimental results will show this method eliminates drift and reduces the error.

4 Experimental results and discussion

4.1 Experimental setup

The proposed technique was validated experimentally by using a piezoelectric stack actuator AE0505D44H40 from NEC. The displacement of the piezoelectric stack actuator was measured using a strain gauge from Vishay Electronics (EA-06-125TG-350), which is only used to evaluate the performance of the DCA. All digital algorithms, estimation and control functions were written in Matlab/Simulink then compiled for a dSPACE DS1104 development platform. Matlab/Simulink was also used for actuator characterization (Figure 3).

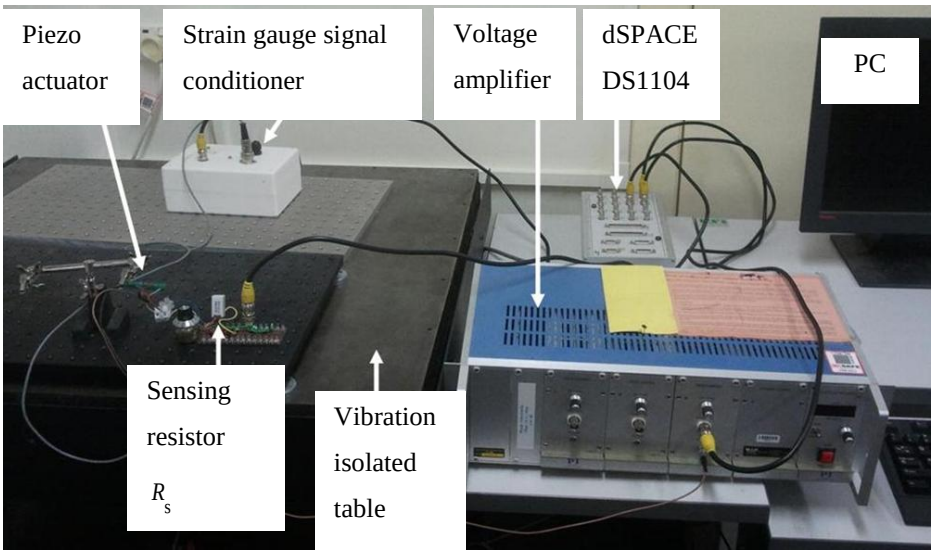

Figure 3: The experimental equipment

4.2 DCA linearity results

Figure 4 illustrates the improvement in linearity offered by the new digital charge amplifier compared to a standard voltage amplifier. Figure 4a shows the hysteresis loop when the piezo is driven by a voltage amplifier and Figure 4b shows the results when the piezo is driven by the DCA. It can be seen that the hysteresis loop is significantly reduced in the DCA. For a displacement range of 11.54 μm, the digital charge amplifier has maximum hysteresis of 144 nm while it is 1598 nm for the voltage amplifier for a driving frequency of 10 Hz. Therefore, the digital charge amplifier has reduced the hysteresis by 91%.

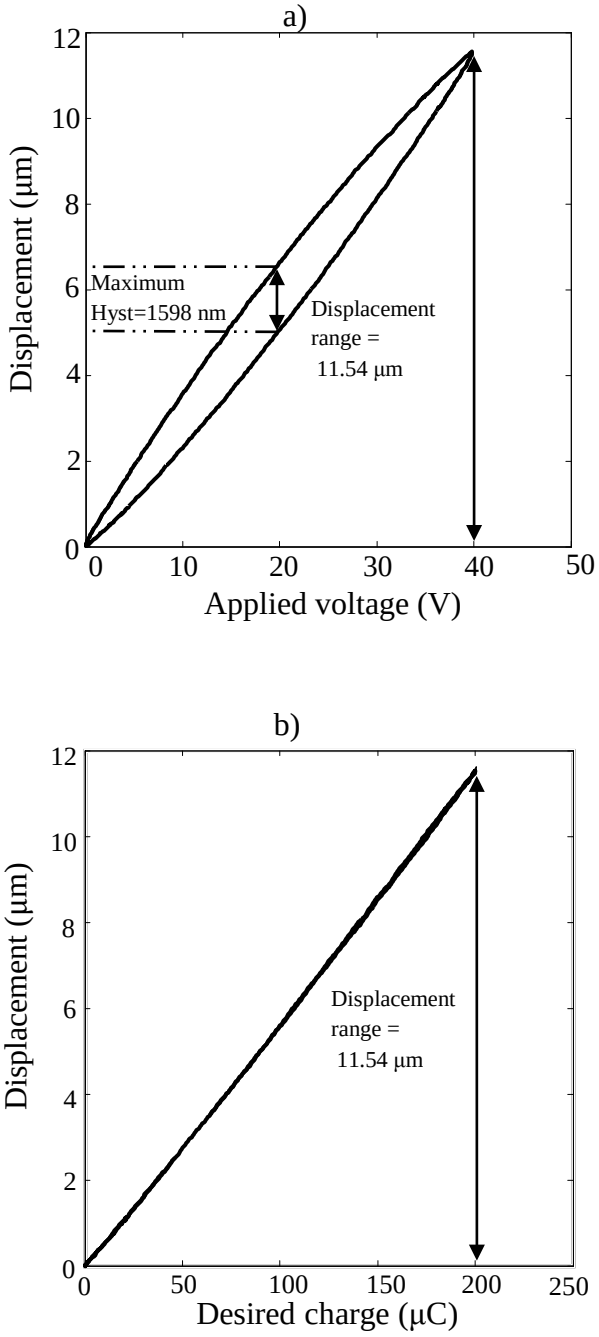

Figure 4: Experimental hysteresis loop of a piezoelectric stack actuator AE0505D44H40 subjected to a 10 Hz sine wave driven by a) a voltage amplifier and b) DCA

4.3 Drift and model-based drift correction results

Figure 5 shows experimentally the drift effect on the displacement of the piezoelectric actuator when it is driven by the digital charge amplifier with no drift removal and when the model-based drift correction method is used. It clearly shows no drift on displacement when it is driven using the model-based drift correction method.

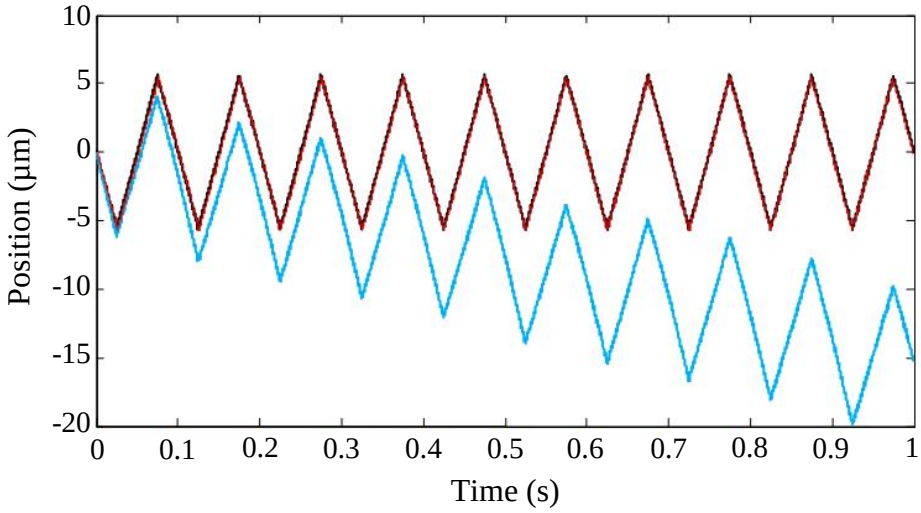

Figure 5: Experimental results for displacement of a piezoelectric actuator driven by the DCA, showing desired displacement (Black) versus the displacement when no drift removal technique (Blue) is used and when the model-based drift correction method (Red) is used

In this experimental setup, μ_1 = -0.00041 A, $\sigma_1 = 8.023\times10^{-5}$, which are the mean and standard deviation of input current noise respectively, and the model error has mean and standard deviation, $\mu_2 = 1\times10^{-5}$ C and $\sigma_2 = 4\times10^{-6}$ respectively. These values were obtained experimentally through statistical analysis of the ADC input and model output when driven

by a 10 Hz triangle waveform. By setting sampling time T_s = 0.0001 s, then (31) can be written as

$$MSE_{e\_opt}(w_a) = \frac{(-4.1\times10^{-8}w_a + 1\times10^{-5}(1-w_a))^2}{(1-w_a)^2} + \frac{(1.68\times10^{-15}w_a^2 + 1\times10^{-5}(1-w_a)^2)}{1-w_a^2}. \quad (32)$$

It can be seen in (32) that the MSE is only dependent on w_a. Figure 6 shows MSE plotted against values of w_a.

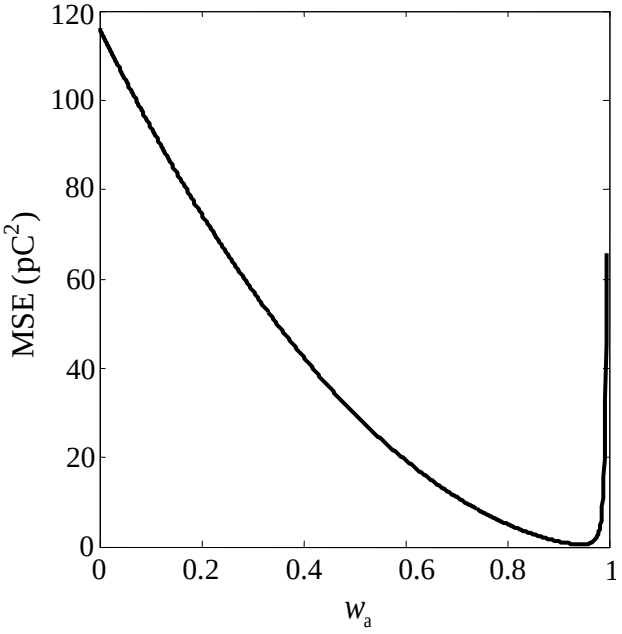

Figure 6: Mean square error plot for different w_a

The MSE has a minimum value 4.76×10^{-13} C^2 when w_a is 0.9460. This value is chosen for w_a to minimize the MSE. Compared to the model alone which has a MSE 1.16×10^{-10} C^2, the model based drift correction method

has reduced the MSE by a factor 243 while it has removed the drift on the digital charge amplifier completely.

4.4 Frequency response of the output displacement to input charge

Figure 7 illustrates experimentally measured displacement versus charge at different frequencies. This shows that at higher frequencies the area within the loop between charge and displacement increases. This loop is not hysteresis but rather a linear phase shift. Figure 8 illustrates the frequency response of displacement output to charge input for the stack piezo. It can be seen that for frequencies higher than 100 Hz the phase lag starts to increase, which makes it undesirable for higher frequency tracking applications. As described by Goldfarb and Celannovic (1997a, 1997b) the relation between the charge and the displacement of the piezo introduces a phase lag as shown in Figure 8, and arises from the nature of the piezoelectric actuator itself.

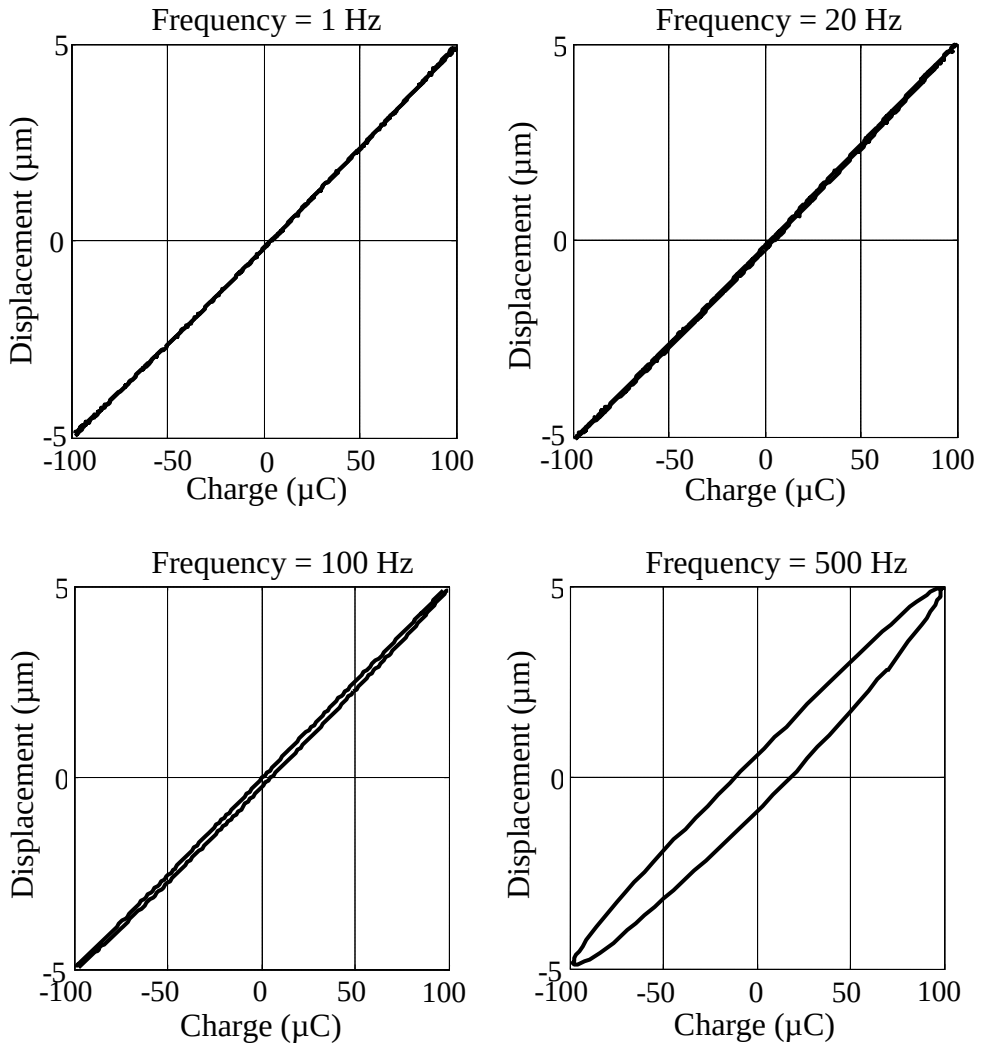

Figure 7: Measured displacement versus charge for a sinusoidal input of 1 Hz, 20 Hz, 100 Hz and 500 Hz

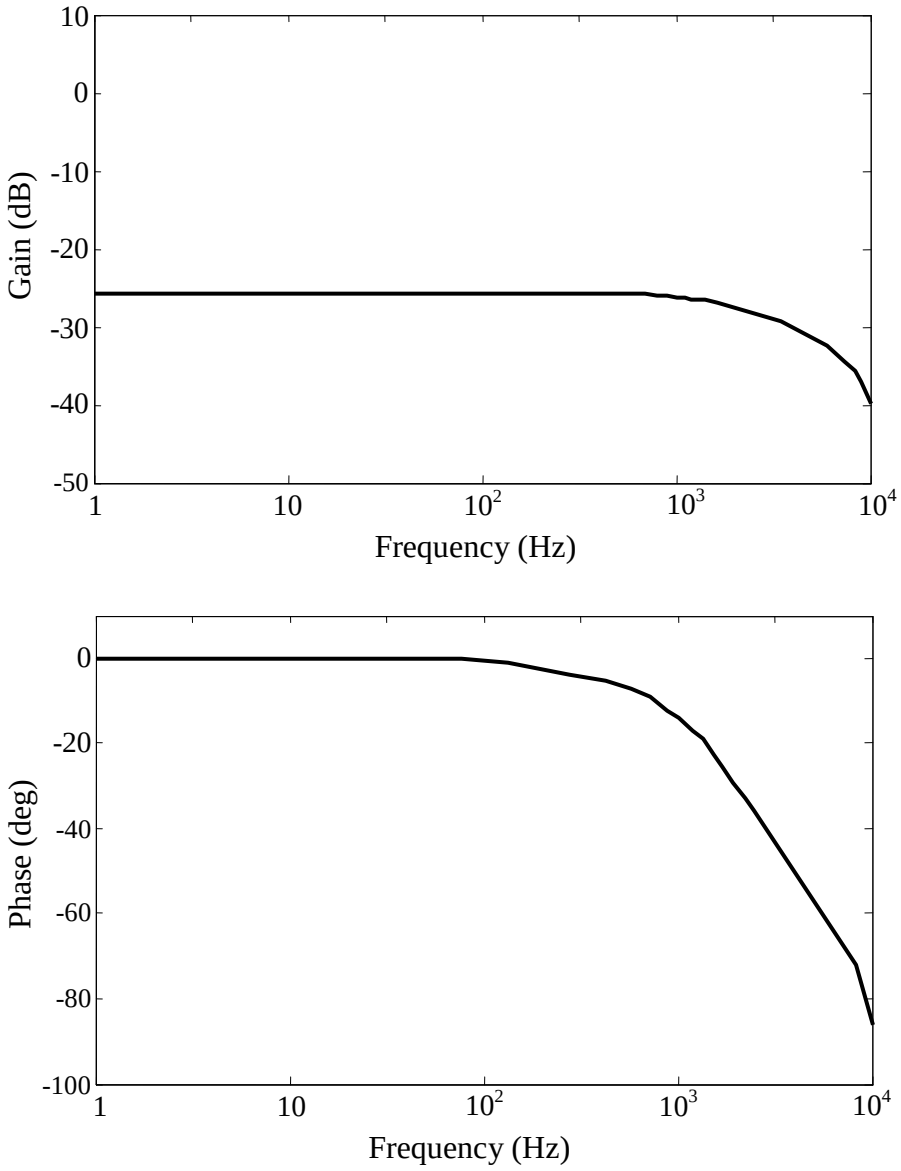

Figure 8: Measured frequency response of the output displacement to input charge

4.5 SNR

Table 1: Signal to noise ratio (SNR) of the sensing voltage for R_s equal to 10 Ω, 200 Ω and 400 Ω and at frequencies 0.01 Hz, 0.1 Hz, 1 Hz and 10 Hz.

Frequency	SNR(dB)		
	R_s =10 Ω	R_s =200 Ω	R_s =400 Ω
0.01 Hz	-20.91	-4.97	0.15
0.1 Hz	-18.94	14.34	19.97
1 Hz	3.92	34.27	39.81
10 Hz	24.65	40.98	41.29

Because of the RC circuit between the sensing resistor and the piezo, at low frequencies the voltage drop across the sensing resistor decreases significantly. This causes a reduction in the signal-to-noise ratio (SNR) which is shown in Table 1. Therefore the accuracy of measured charge decreases with decreasing frequency, which causes an increase in the error of the output displacement. Increasing the sensing resistance can increase the voltage drop and therefore improve the SNR. However, increasing the sensing resistor can cause the sensing voltage to reach the maximum ADC input voltage at lower frequencies and therefore limits the bandwidth of the DCA.

Choosing the appropriate sensing resistor is an important task when using the DCA. The sensing resistor should not be so small that the noise on the measured charge increases significantly and also it should not be so large that V_s becomes more than the input ADC limitation at the required bandwidth.

The value of the sensing resistor should be set for each application. To select the best value for R_s, the maximum displacement at the maximum

frequency should be considered. Then R_s should be calculated such that the sensing voltage will not be greater than the maximum ADC voltage. Using the highest possible sensing resistor increases the SNR at low frequencies.

4.6 Voltage drop

The voltage drop across any sensing element limits the piezoelectric actuator voltage range. Table 2 compares the maximum voltage drop for two hysteresis linearization techniques from the literature that have been evaluated experimentally (a grounded charge amplifier (Fleming and Moheimani, 2005, Minase *et al.*, 2010), capacitor insertion (Kaizuka and Siu, 1988, Minase *et al.*, 2010)) and the DCA at different frequencies. To make the data comparable, the displacement range is set to be ±5 μm. It can be seen that at lower frequencies the DCA voltage drop is significantly smaller than the voltage drop of the grounded charge amplifier or capacitor insertion method, thus maximizing the displacement that can be achieved for a given supply voltage.

Table 2: Comparison of voltage drop and percentage of voltage drop using three alternative methods at four different frequencies

Frequency	Grounded charge amplifier (C_s = 30 μF)	Capacitor insertion (C_s = 1 μF)	DCA (R_s = 55 Ω)
0.1 Hz	2.72(12%)	51.42(72%)	0.01(0.05%)
1 Hz	2.41(11%)	52.38(72%)	0.02(0.1%)
10 Hz	2.48(11%)	53.28(72%)	0.25(1.2%)
75 Hz	2.32(11%)	53.53(72%)	1.93(8.8%)

4.7 Tracking performance

In Figure 9 the desired displacement is compared against the actual displacement at different frequencies using the model-alone (when w_a is zero and w_b is one) and model-based drift correction.

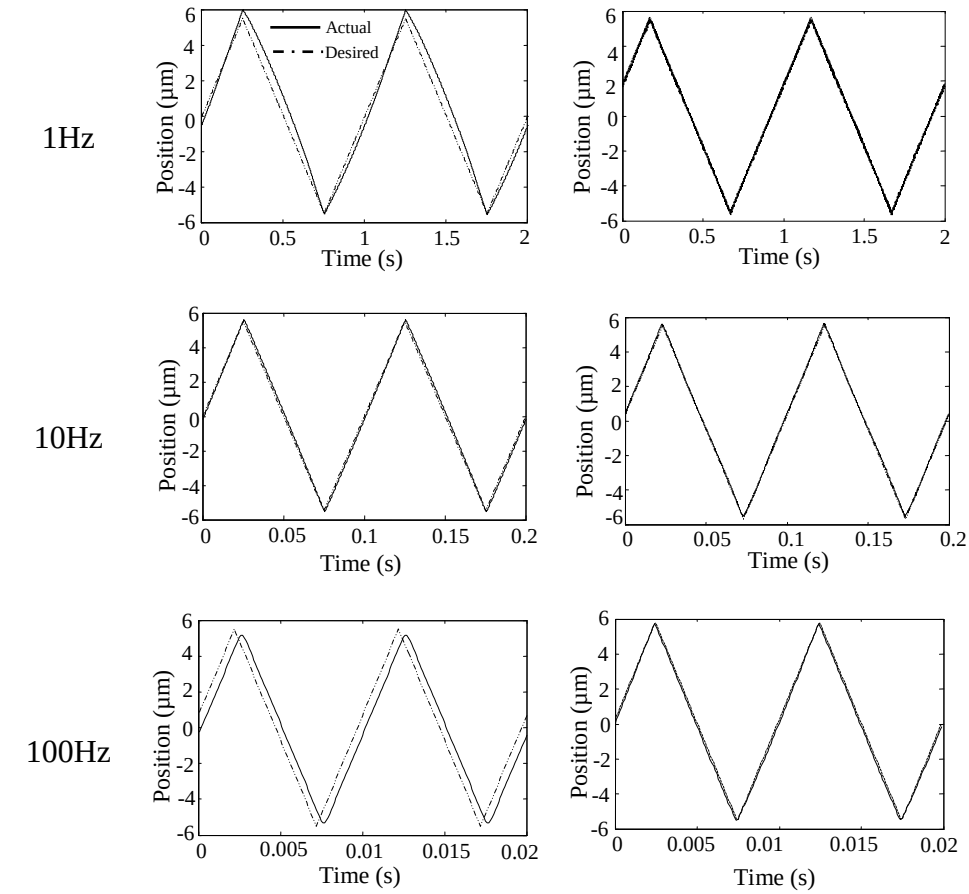

Figure 9: Experimental results of actual and desired charge in 1 Hz, 10 Hz and 100 Hz by using the Model-based drift correction method and the model-alone

It can be seen in Figure 9 that for 1 Hz and 100 Hz the model-alone is not as accurate because the NARX model is tuned at 10 Hz and is unable to track

the rate dependent dynamics of the piezoelectric actuator. As the weighting of the digital charge amplifier is close to one (Section 4.3) the model errors do not significantly impact the tracking performance of the model-based drift correction results.

Figure 10 illustrates the output of the system in three different scenarios: a) when the system only relies on the DCA (w_a is one and w_b is zero) b) when the system only relies on the model (w_a is zero and w_b is one) c) model-based drift correction (when appropriate w_a and w_b are chosen). It clearly can be seen that model-based drift correction removes the drift on the DCA while its accuracy is much better than the model-alone.

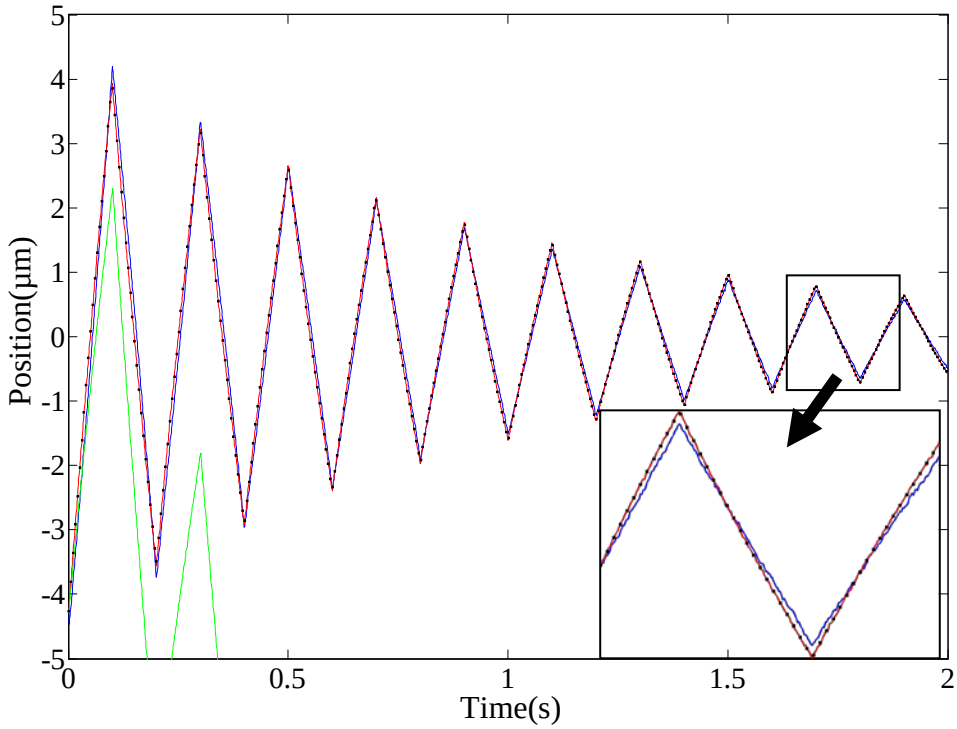

Figure 10: Response to a decaying 5 Hz triangular input signal. The black square marker is desired displacement, the blue line is the displacement when the system only relies on the model (w_a is zero and w_b is one), the green line is when the system only relies on the DCA (w_a is one and w_b is zero) and the red line is the displacement with model-based drift correction (when appropriate w_a and w_b are chosen)

5 Conclusion

An innovative digital charge amplifier has been introduced to reduce the non-linear behavior of a piezoelectric actuator. For the experiments conducted, it was found that the charge amplifier reduced the hysteresis by 91% at 10 Hz. Compared to a grounded charge amplifier, the DCA has less voltage drop, does not need gain tuning and is far more cost effective. Moreover, a model-based drift correction technique has been proposed to remove the drift and improve the tracking performance of the digital charge

amplifier. It uses data fusion to integrate the reliability and short term accuracy of a digital charge amplifier, with the long term accuracy of the NARX model, to realise the benefit of both techniques. This easily implemented, digital charge drive approach overcomes many of the limitations of previous charge drive solutions, opening up new applications where the performance of a charge drive is beneficial such as scanning probe microscopy (Fleming and Leang, 2008). Future work will focus on improving the model and investigating methods to increase the bandwidth, especially at low frequencies.

References

Adriaens, H.J.M.T.A., Koning, W.L.D. and Banning R., 2000. Modeling piezoelectric actuators. *IEEE/ASME Transactions on Mechatronics* 5(4), 331–341.

Bazghaleh, M., Grainger, S., Cazzolato, B. and Lu. T.-F., 2010. An innovative digital charge amplifier to reduce hysteresis in piezoelectric actuators. *In: Australasian Conference on Robotics and Automation*. Brisbane, Australia.

Comstock, R.H., 1981. Charge control of piezoelectric actuators to reduce hysteresis effects. *USA Patent* No. 4,263,527.

Damjanovic, D., 2005. Hysteresis in piezoelectric and ferroelectric materials. *The Science of Hysteresis* 3, 337–465.

Devasia, S., Eleftheriou, E. and Moheimani, S.O.R., 2007. A survey of control issues in nanopositioning. *IEEE Transactions on Control Systems and Technology* 15(5), 802–823.

Fleming, A.J. and Leang, K.K., 2008. Evaluation of charge drives for scanning probe microscope positioning stages. *In: American Control Conference.* Seattle, USA, pp. 2028–2033.

Fleming, A.J. and Moheimani, S.O.R., 2004. Hybrid DC accurate charge amplifier for linear piezoelectric positioning. *In: The 3rd IFAC Symposium on Mechatronic Systems*. pp. 283–288.

Fleming, A.J. and Moheimani, S.O.R., 2005. A grounded-load charge amplifier for reducing hysteresis in piezoelectric tube scanners. *Review of Scientific Instruments.* 76(7), 073707.

Ge, P. and Jouaneh, M., 1995. Modeling hysteresis in piezoceramic actuators. *Precision Engineering* 17, 211–21.

Goldfarb, M. and Celanovic, N., 1997a. A lumped parameter electromechanical model for describing the nonlinear behavior of piezoelectric actuators. *Journal of Dynamic Systems, Measurement, and Control* 119, 478–485.

Goldfarb, M. and Celanovic, N., 1997b. Modeling piezoelectric stack actuators for control of micromanipulation. *IEEE Control Systems Magazine* 17, 69–79.

Huang, L., Ma, Y.T., Feng, Z.H. and Kong, F.R., 2010. Switched capacitor charge pump reduces hysteresis of piezoelectric actuators over a large frequency range. *Review of Scientific Instruments* 81(9), 094701.

IEEE Standard on Piezoelectricity, 1987. *ANSI/IEEE Standard (New York: IEEE)* pp. 176.

Kaizuka, H. and Siu, B., 1988. A simple way to reduce hysteresis and creep when using piezoelectric actuators. *Japanese Journal of Applied Physics* 27(5), 773–776.

Kuhnen, K. and Janocha, H., 1998. Compensation of the creep and hysteresis effects of piezoelectric actuators with inverse systems. *In: The 6th International Conference on New Actuators.* pp. 426–429.

Leang, K.K. and Devasia, S., 2002. Hysteresis, creep, and vibration compensation for piezoactuators: Feedback and feedforward control paper. *In: The 2nd IFAC Conference on Mechatronic Systems*. Berkeley, CA, pp. 283–289.

Ma, J. and Ang, M., 2000. High-bandwidth macro/microactuation for hard-disk drive. *In: Proceedings of the SPIE*. pp. 94–102.

Minase, J., Lu, T.F., Cazzolato, B. and Grainger, S.,2010. A review, supported by experimental results, of voltage, charge and capacitor insertion method for driving piezoelectric actuators. *Precision Engineering: Journal of International Society for Precision Engineering and Nanotechnology* 34(4), 692–700.

Rice, J.A., 1995. Mathematical statistics and data analysis. *2nd edn Belmont: Duxbury Press.*

Shieh, H.J., Lin, F. J., Huang, P.K. and Teng, L.T., 2004. Adaptive tracking control solely using displacement feedback for a piezo-positioning mechanism. *IEEE Proceedings-Control Theory and Applications* 151(5), 653–660.

Wiesendanger, R., 1994. Scanning Probe Microscopy and Spectroscopy: Methods and Applications. *Cambridge: Cambridge University Press*.

6 Bandwidth Extension of the Digital Charge Amplifier

6.1 Introduction

As is mentioned in Chapter 3, the DCA's lowest frequency of operation is limited due to the reduction of signal-to-noise-ratio of the sensing voltage at low frequencies.

In order to extend the DCA's operational bandwidth, a novel hybrid digital method is proposed. As explained in Chapter 5, the relationship between applied voltage and displacement shows rate-dependant behaviour. Thus designing a model that can work over a wide range of operations is a complicated task. In this chapter, a non-linear model was designed and trained to estimate displacement based on the piezoelectric voltage only at low frequencies. The model and charge-based displacement estimators were used together through a complementary filter, to increase the bandwidth of displacement estimation and control. Moreover, the proposed method is designed to be capable of driving grounded-loads such as piezoelectric tube actuators.

Experimental results clearly show that both the tracking performance of the new method is improved and it can also operate over a wider frequency bandwidth.

6.2 A novel digital charge-based displacement estimator for sensorless control of a grounded-load piezoelectric tube actuator

Published in Sensors and Actuators A: Physical.

Statement of Authorship

Title of Paper	A novel digital charge-based displacement estimator for sensorless control of a grounded-load piezoelectric tube actuator
Publication Status	● Published ○ Accepted for Publication ○ Submitted for Publication ○ Publication Style
Publication Details	Bazghaleh, M., Grainger, S., Mohammadzaheri, M., Cazzolato, B. & Lu, T.F. (2013). A novel digital charge-based displacement estimator for sensorless control of a grounded-load piezoelectric tube actuator. Sensors and Actuators A: Physical, 198(1) 91-98.

Author Contributions

By signing the Statement of Authorship, each author certifies that their stated contribution to the publication is accurate and that permission is granted for the publication to be included in the candidate's thesis.

Name of Principal Author (Candidate)	Mr. Mohsen Bazghaleh		
Contribution to the Paper	Developed the model, developed theory, performed experimental work, analyzed data and Wrote the manuscript.		
Signature		Date	11/9/13

Name of Co-Author	Dr. Steven Grainger		
Contribution to the Paper	Supervised research, reviewed manuscript.		
Signature		Date	11/9/13

Name of Co-Author	Dr. Morteza Mohammadzaheri		
Contribution to the Paper	Supervised research, reviewed manuscript.		
Signature		Date	11/6/2013

Name of Co-Author	Dr. Ben Cazzolato		
Contribution to the Paper	Supervised research, reviewed manuscript.		
Signature		Date	11/9/13

Name of Co-Author	Dr. Tien-Fu Lu		
Contribution to the Paper	Supervised research, reviewed manuscript.		
Signature		Date	11/09/13

A novel digital charge-based displacement estimator for sensorless control of a grounded-load piezoelectric tube actuator

Mohsen Bazghaleh, Steven Grainger, Morteza Mohammadzaheri, Ben Cazzolato and Tien-Fu Lu

Abstract. *Piezoelectric tube actuators are widely used in nanopositioning applications, especially in scanning probe microscopes to manipulate matter at nanometre scale. Accurate displacement control of these actuators is critical, and in order to avoid the expense and practical limits of highly accurate displacement sensors, sensorless control has recently attracted much attention. As the electrical charge on these actuators is an accurate indicator of their displacement exhibiting almost no hysteresis over a wide range of frequencies, it suggests that charge measurement can replace displacement sensors. However, charge-based methods suffer from poor low frequency response and voltage drop across the sensing capacitor. In this paper, a displacement estimator is presented that complements a digitally implemented charge amplifier with an artificial neural network (ANN) designed and trained to estimate the piezoelectric tube's displacement using the piezoelectric voltage at low frequencies of excitation where the charge methods fail. A complementary filter combines the grounded-load digital charge amplifier (GDCDE) and the ANN to estimate displacement over a wide bandwidth and to overcome drift. The discrepancy between the desired and estimated displacement is fed back to the piezoelectric actuator using proportional control. Experimental results highlight the effectiveness of the proposed design.*

Keywords: *Piezoelectric tube actuators; sensorless control; displacement estimation; artificial neural network; complementary filter.*

1 Introduction

Scanning Probe Microscopes (SPMs) enable the manipulation of matter at nanometre scale (Moheimani, 2008). In traditional SPMs, a tripod positioner with three stack piezoelectric actuators are employed for movement in the x, y and z directions. Binnig and Smith (1986) used a piezoelectric tube scanner for the first time in 1986. Compared to tripod positioners, piezoelectric tube scanners offer better accuracy, higher bandwidth and an easier manufacturing process (Devasia *et al.*, 2007) while their smaller size simplifies vibration isolation (Chen, 1992). Piezoelectric tubes are the foremost actuators in atomic force microscopy (AFM) (Abramovitch *et al.*, 2007, Kuiper and Schitter, 2010) and are likely to remain the most widely used positioning actuators in other micro-scale and nano-scale positioning tasks for several years (Moheimani, 2008); such as displacement of fiber optics (Leung *et al.*, 2008), ultrasonic applications (Hui *et al.*, 2010) and in ink jet printers (Chen and Tsao, 1977).

In order to avoid the use of expensive highly accurate displacement sensors, sensorless control has recently attracted much attention. The voltage across the piezoelectric tube (piezoelectric voltage) can represent its displacement. However, the relationship between actuator displacement and the piezoelectric voltage suffers from hysteresis and creep which are nonlinear in nature and reduce the positioning accuracy (Leang and Devasia, 2002).

Creep results from remnant polarization which causes the displacement of the piezoelectric actuator to change once the applied voltage is held fixed, and typically is an issue at low frequencies (Minase *et al.*, 2010a). Hysteresis happens due to the polarization of microscopic particles. In practice, it means that, for similar values of the piezoelectric voltage, the

piezoelectric actuator has a variety of displacement values, and this cannot be described with linear models.

Charge regulation and capacitor insertion techniques have been used for linearization (Minase *et al.*, 2010b). Charge regulation relies on the fact that there is almost no hysteresis or other nonlinearity between the charge across the piezo and the displacement of the piezo, so the electrical charge on the piezoelectric can represent displacement more effectively than the applied piezoelectric voltage. Charge regulation was first introduced by Comstock (1981) but has historically been complicated and expensive to implement due to the complexity of the analog circuitry required to meet stringent performance targets (Fleming and Moheimani, 2005).

This paper presents a novel sensorless approach that combines charge-based displacement estimation with mapping of piezoelectric voltage to displacement using an artificial neural network to increase the bandwidth of the developed system and to remove drift. In Section 2 the design principle is described. Section 3 explains the experimental set up. The closed loop control system is analyzed in Section 4. Section 5 addresses ANN model design for low frequency operation. Experimental results are presented in Section 6 and the conclusions are drawn in Section 7.

2 Design principles

Over a wide range of frequencies, the electrical charge (q_p) on a piezoelectric actuator is proportional to its displacement (d) (Fleming and Moheimani, 2005, Newcomb and Flinn, 1982); and may be expressed as

$$d(t) = Kq_\mathrm{p}(t). \tag{1}$$

Figure 1 shows the basis of the proposed grounded-load digital charge-based displacement estimator (GDCDE) which aims to estimate displacement using q_{p}. In GDCDE, a sensing resistor (R_{s}) is placed in series with the piezoelectric tube actuator and an isolation amplifier is used to measure the voltage, V_{s}, across this resistor.

The integral of electrical current equals charge, thus displacement can be estimated by

$$\hat{d}(t) = Kq_{\mathrm{p}}(t) = K\int_0^{t_{\mathrm{f}}} i_{\mathrm{p}}(t)dt = \frac{K}{R_{\mathrm{s}}}\int_0^{t_{\mathrm{f}}} V_{\mathrm{s}}(t)dt, \tag{2}$$

where i_{p} is the electric current passing through the piezoelectric actuator, and t_{f} is the elapsed time.

Due to the RC circuit formed by the sensing resistor and the piezoelectric actuator which may be approximated as a capacitor, at low frequencies the sensing voltage is very small which causes a reduction in its signal to noise ratio (SNR). Also, the analog to digital converter (ADC) is not ideal and suffers from offset voltage and drift. These issues together with dielectric leakage of the piezoelectric actuator causes a bias voltage, V_{bias} and in practice, the estimated displacement is

$$\hat{d}(t) = \frac{K}{R_{\mathrm{s}}}\int_0^{t_{\mathrm{f}}} \left(V_{\mathrm{s}}(t) + V_{\mathrm{bias}}\right) dt. \tag{3}$$

In this paper, at low frequencies, an artificial neural network (ANN) has been designed and trained to map the voltage across the piezoelectric actuator, V_{p}, to displacement. A complementary filter merges these two

displacement estimation methods to increase the bandwidth of the hybrid system. The complementary filter comprises a low pass filter (W_{ANN}) on the output of the ANN and a high pass filter (W_{GDCDE}) on the output of the GDCDE. The high pass and low pass filters used are given by

$$W_{\mathrm{GDCDE}}(s) = \frac{s}{s+\omega_{\mathrm{c}}}, \tag{4}$$

$$W_{\mathrm{ANN}}(s) = \frac{\omega_{\mathrm{c}}}{s+\omega_{\mathrm{c}}}, \tag{5}$$

and

$$W_{\mathrm{ANN}}(j\omega) + W_{\mathrm{GDCDE}}(j\omega) = 1 \tag{6}$$

Where ω_{c} is the cut-off frequency, π rad/s (0.5 Hz). ω_{c} was determined experimentally and is related to the decreasing SNR with frequency. During operation, the complementary filter produces the estimated displacement:

$$\hat{d} = W_{\mathrm{GDCDE}}\hat{d}_{\mathrm{GDCDE}} + W_{\mathrm{ANN}}\hat{d}_{\mathrm{ANN}} \tag{7}$$

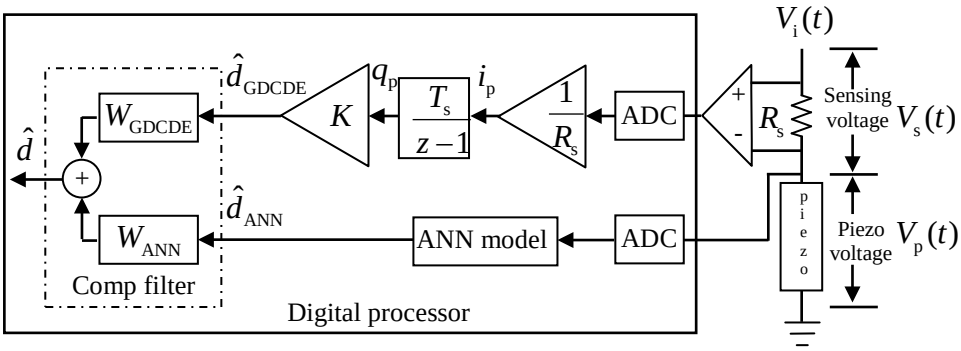

Figure 1: The basis of the proposed displacement estimation system

As shown in Figure 1, in the discrete domain, the charge of the k^{th} sample is estimated as

$$q_{\text{p}}(k) = \frac{T_{\text{s}}}{z-1} i_{\text{p}}(k) = \frac{T_{\text{s}} z^{-1}}{1-z^{-1}} i_{\text{p}}(k). \tag{8}$$

where T_{s} is the sampling time of the system. As a result,

$$q_{\text{p}}(k) = T_{\text{s}} i_{\text{p}}(k-1) + q_{\text{p}}(k-1). \tag{9}$$

In order to improve displacement estimation and remove drift Eq. (9) is replaced by (Bazghaleh *et al.*, 2011)

$$q_{\text{p}}(k) = T_{\text{s}} i_{\text{p}}(k-1) + \frac{\hat{d}(k-1)}{K}. \tag{10}$$

This uses the output of the complementary filter in discrete integration instead of the output of the GDCDE (Figure 2).

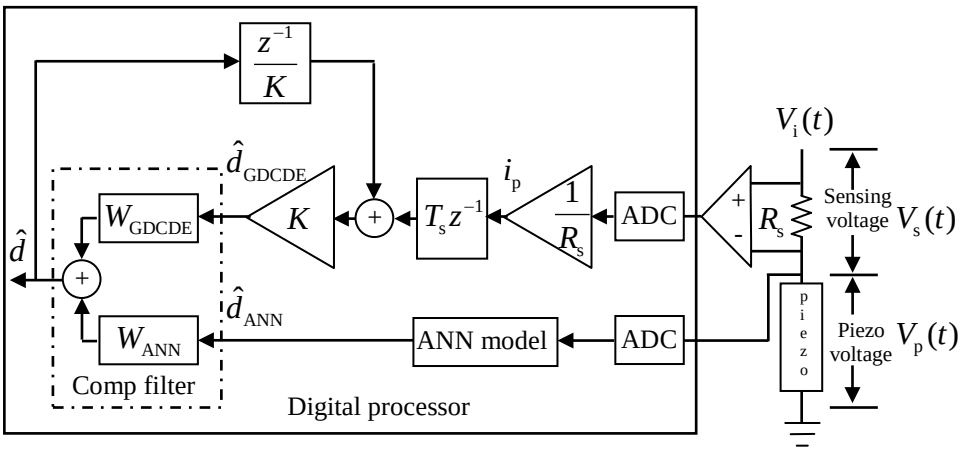

Figure 2: The proposed displacement estimation system

3 Experimental setup

The proposed technique was validated experimentally by using a piezoelectric tube actuator PT130.24 from PI. The tube has one grounded inner electrode and four equally distributed outer electrodes (Figure 3).

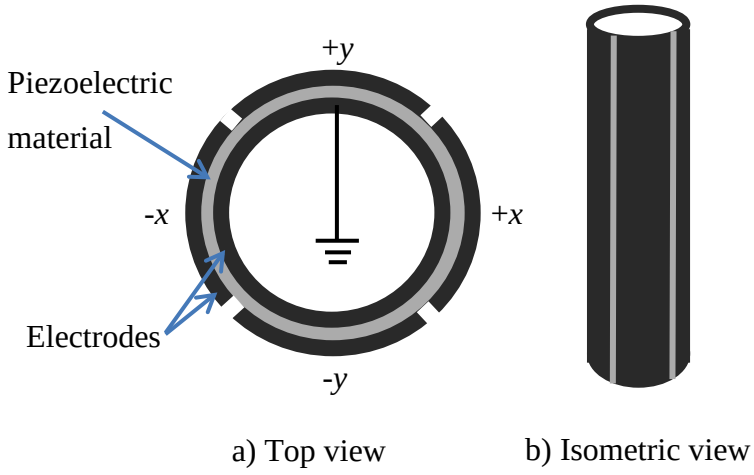

Figure 3: Schematic of piezoelectric tube scanner

PI-D-510 capacitive sensors together with an E-852.10 signal conditioner and a cubical end-effector were used to measure actual displacement. During the experiment, the capacitive sensor is held relative to the tube using an aluminum cylinder (Figure 4).

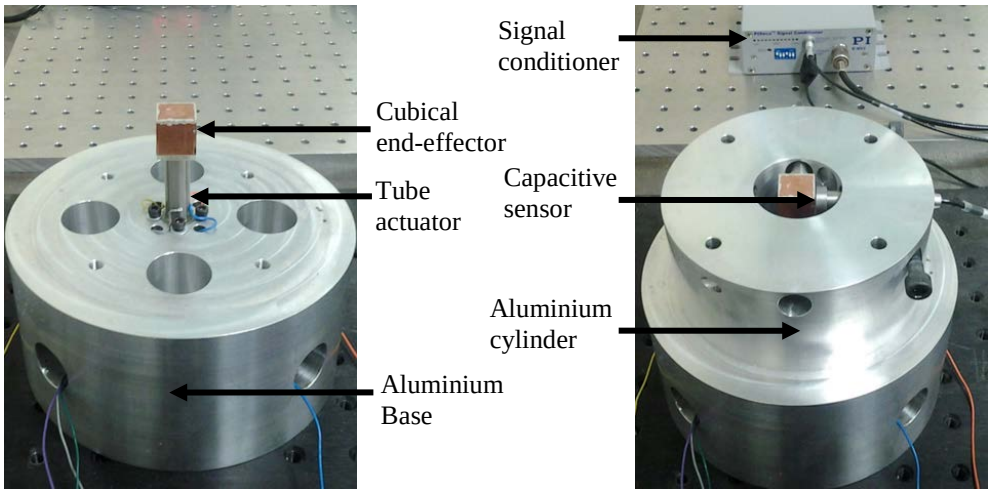

a) b)

Figure 4: The piezoelectric tube actuator setup a) with no cover b) covered by the cylinder holding the capacitive displacement sensors

In scanning devices, the end-effector typically follows a raster pattern (Moheimani, 2008, Abramovitch *et al.*, 2007, Schitter *et al.*, 2007); that is, in one axis (say *x*), the tube should track a triangular waveform, and in the other (say *y*), the tube should track a very slowly increasing ramp, e.g. quasi-static with respect to *x*. For test purposes, the *y* electrode is earthed, replaced by a DC signal or open circuited (Moheimani, 2008, Bhikkaji and Moheimani, 2009, Bhikkaji *et al.*, 2007a, Bhikkaji *et al.*, 2007b). In this research, both *y*+ and *y*- electrodes were earthed and the displacement controller drove one electrode (*x*+) directly and an inverted signal drove *x*- to increase the displacement range (Fleming and Leang, 2008). All algorithms were developed in MATLAB/Simulink then compiled for a dSPACE DS1104 development platform.

Figure 5 shows the control system loop closed on estimated displacement. It consists of a displacement estimation unit, a voltage amplifier, digital to analog converter (DAC) and an analog to digital converter (ADC). The displacement estimation unit is as described before and shown in Figure 2.

The high gain (K_c = 230 V/μm) feedback loop is used to equalize the desired displacement d_r with the estimated displacement $\hat{d}$.

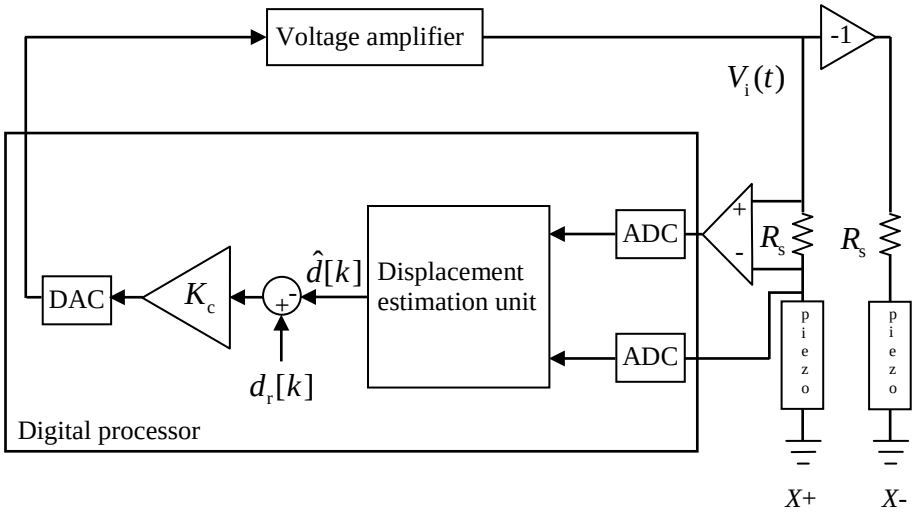

Figure 5: The control system loop closed on estimated displacement

4 Control system analysis with the GDCDE

From Eq. (1) and as the electrical charge is equal to the integral of the electric current:

$$\hat{d}_{GDCDE} = K\frac{V_s}{R_s s} \tag{11}$$

or

$$V_s = \frac{\hat{d}_{GDCDE} R_s s}{K}. \tag{12}$$

By considering a capacitor C_L as an approximate model of the piezoelectric actuator (Fleming and Moheimani, 2005, Huang *et al.*, 2010), the relation

between the input voltage, V_{i}, and the sensing voltage of the *x*+ electrode (as shown in Figure 1), V_{s}, is

$$\frac{V_{\mathrm{i}}}{V_{\mathrm{s}}} = \frac{R_{\mathrm{s}}C_{\mathrm{L}}s+1}{R_{\mathrm{s}}C_{\mathrm{L}}s}. \tag{13}$$

Combining Eqs. (12) and (13) results in the following expression

$$V_{\mathrm{i}} = \frac{R_{\mathrm{s}}C_{\mathrm{L}}s+1}{R_{\mathrm{s}}C_{\mathrm{L}}s}\frac{\hat{d}_{\mathrm{GDCDE}}R_{\mathrm{s}}s}{K} = \frac{R_{\mathrm{s}}C_{\mathrm{L}}s+1}{KC_{\mathrm{L}}}\hat{d}_{\mathrm{GDCDE}}. \tag{14}$$

In the control circuit, shown in Figure 5 with a gain of K_{c}, the input voltage is

$$V_{\mathrm{i}} = K_{\mathrm{c}}(d_{\mathrm{r}} - \hat{d}). \tag{15}$$

If the GDCDE alone is used, then the input voltage is

$$V_{\mathrm{i}} = K_{\mathrm{c}}(d_{\mathrm{r}} - \hat{d}_{\mathrm{GDCDE}}) \tag{16}$$

Equating Eq. (14) with Eq. (16),

$$V_{\mathrm{i}} = \frac{R_{\mathrm{s}}C_{\mathrm{L}}s+1}{KC_{\mathrm{L}}}\hat{d}_{\mathrm{GDCDE}} = K_{\mathrm{c}}(d_{\mathrm{r}} - \hat{d}_{\mathrm{GDCDE}}). \tag{17}$$

Therefore,

$$\left(\frac{R_{\mathrm{s}}C_{\mathrm{L}}s+1}{KC_{\mathrm{L}}} + K_{\mathrm{c}}\right)\hat{d}_{\mathrm{GDCDE}} = K_{\mathrm{c}}d_{\mathrm{r}}. \tag{18}$$

or,

$$\frac{\hat{d}_{\mathrm{GDCDE}}}{d_{\mathrm{r}}} = \frac{K_{\mathrm{c}}}{\frac{R_{\mathrm{s}}C_{\mathrm{L}}s+1}{KC_{\mathrm{L}}}+K_{\mathrm{c}}} = \frac{K_{\mathrm{c}}KC_{\mathrm{L}}}{R_{\mathrm{s}}C_{\mathrm{L}}s+1+K_{\mathrm{c}}KC_{\mathrm{L}}}. \tag{19}$$

As a result, the break (critical) frequency of the displacement estimation loop is

$$f_{\mathrm{critical}} = \frac{1+K_{\mathrm{c}}KC_{\mathrm{L}}}{R_{\mathrm{s}}C_{\mathrm{L}}} \tag{20}$$

The piezoelectric tube PT130.24 has an approximate capacitance of 8.5 nF, and the resistance of the sensing resistor is 50 kΩ. As a result, with $K = K_{\mathrm{c}} = 0$, f_{critical}=374.5 Hz; in other words, f_{critical} > 374.5 Hz (2352 rad/s). This shows a high gain is a satisfactory controller over a wide range of frequencies. The analysis is valid while Eqs. (1) and (11) remain valid.

5 ANN model

The piezoelectric tube was excited by triangular waves with magnitudes of 20 V, 40 V and 60 V at frequencies of 0.1 Hz and 0.5 Hz for 10 s each. The training frequencies were selected to be below those at which the charge displacement estimation operates effectively but above DC. The data gathered with the excitation magnitude of 40 V at 0.5 Hz were used for validation and the rest for ANN modeling. Additional frequencies, as listed in Figure 7, were later used to test the complete control system.

5.1 Model structure

The structure of the model, mapping the piezoelectric voltage represented by V_{P}, to displacement, is Nonlinear Auto-Regressive with eXogenous inputs or NARX (Nelles, 2001); that is

$$d(t) = F\begin{pmatrix} V_{\mathrm{P}}(t - t_{\mathrm{d}}), V_{\mathrm{P}}(t - t_{\mathrm{d}} - T_{\mathrm{s}}), \ldots, V_{\mathrm{P}}(t - t_{\mathrm{d}} - r_{\mathrm{V}}T_{\mathrm{s}}), \\ d(t - T_{\mathrm{s}}), d(t - 2T_{\mathrm{s}}), \ldots, d(t - r_{\mathrm{d}}T_{\mathrm{s}}) \end{pmatrix}, \tag{21}$$

Where t is time, t_{d} is the delay time, T_{s} is the sampling time, r_{V} and r_{d} are the piezoelectric voltage and displacement orders respectively, and F is an artificial neural network. In the discrete domain, the model will be

$$d(k) = F\begin{pmatrix} V_{\mathrm{P}}(k - r_{\mathrm{de}}), V_{\mathrm{P}}(k - r_{\mathrm{de}} - 1), \ldots, V_{\mathrm{P}}(k - r_{\mathrm{de}} - r_{\mathrm{V}}), \\ d(k-1), d(k-2), \ldots, d(k - r_{\mathrm{d}}) \end{pmatrix}, \tag{22}$$

where $r_{\mathrm{de}} = \dfrac{t_{\mathrm{d}}}{T_{\mathrm{s}}}$ and $k = \dfrac{t}{T_{\mathrm{s}}}$. The value of k (index) is higher than the maximum of $(r_{\mathrm{de}} + r_{\mathrm{V}})$ and r_{d}, namely $r_{\max}$.

In the modeling process the values of t_{d}, T_{s}, r_{V} and r_{d} are estimated based on the available knowledge of the system dynamics.

A semi-linear ANN, with both linear and nonlinear activation functions in the hidden layer, especially suiting systems with slight nonlinearities (Mohammadzaheri *et al.*, 2009, Mohammadzaheri *et al.*, 2012a) was employed in this research. Figure 6 shows a typical semi-linear ANN where **T** and **W** vectors/matrices are the weights of connections of the ANN and **b** represents the bias:

$$d(k) = R \times \Big(\sum_{i=r_d+1}^{r_V+r_{de}} W_{Li} V_p(k-i) + \sum_{i=1}^{r_d} T_{Li} d(k-i) + \mathbf{b}_L \Big) + S \times N \Big(\sum_{i=r_d+1}^{r_V+r_{de}} W_{Ni} V_p(k-i) + \sum_{i=1}^{r_d} T_{Ni} d(k-i) + \mathbf{b}_N \Big) + \mathbf{b}. \quad (23)$$

where

$$N(x) = \frac{1}{1+\exp(-x)}. \quad (24)$$

(x represents the input to the activation function N).

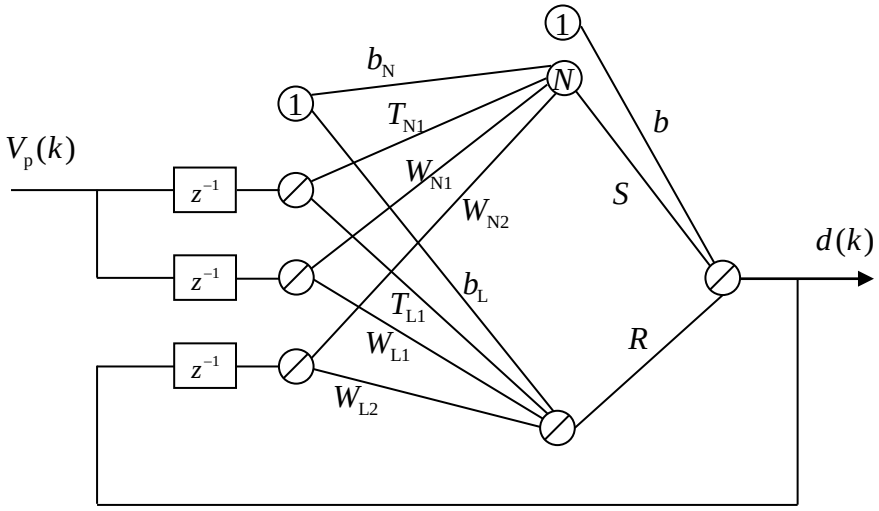

Figure 6: A semi-linear ANN (Mohammadzaheri *et al.*, 2012a)

5.2 Data preparation

In input-output-data-based modeling, if some variables have values with higher magnitudes than others, they are likely to influence the modeling process more significantly (Ghaffari *et al.*, 2007). Therefore, the experimental data are first normalized in black box modeling.

After normalization, the data, which originally have two columns in this case (the piezoelectric voltage and displacement), are rearranged for the purpose of neural network training. The prepared data forms a matrix with $r_{\mathrm{d}} + r_{\mathrm{V}} + 1$ input columns and one output column as shown in Eq. (25) where *n* is the number of data elements in each column of raw data.

$$\left[\begin{array}{cccc|c} \overbrace{\begin{array}{cccc} V_{\mathrm{P}}(k_{\min} - r_{\mathrm{de}}) & V_{\mathrm{P}}(k_{\min} - r_{\mathrm{de}} - 1) & \dots & V_{\mathrm{P}}(k_{\min} - r_{\mathrm{de}} - r_{\mathrm{V}}) \\ V_{\mathrm{P}}(k_{\min} - r_{\mathrm{de}} + 1) & V_{\mathrm{P}}(k_{\min} - r_{\mathrm{de}}) & \dots & V_{\mathrm{P}}(k_{\min} - r_{\mathrm{de}} - r_{\mathrm{V}} + 1) \\ \vdots & \vdots & \ddots & \vdots \\ V_{\mathrm{P}}(n - r_{\mathrm{de}}) & V_{\mathrm{P}}(n - r_{\mathrm{de}} - 1) & \dots & V_{\mathrm{P}}(n - r_{\mathrm{de}} - r_{\mathrm{V}}) \end{array}}^{input} & \cdots & \overbrace{\begin{array}{cccc} d(k_{\min} - 1) & d(k_{\min} - 2) & \dots & d(k_{\min} - r_{\mathrm{d}}) \\ d(k_{\min}) & d(k_{\min} - 1) & \dots & d(k_{\min} - r_{\mathrm{d}} + 1) \\ \vdots & \vdots & \ddots & \vdots \\ d(n-1) & d(n-2) & \dots & d(n - r_{\mathrm{d}}) \end{array}}^{input} & \overbrace{\begin{array}{c} d(k_{\min}) \\ d(k_{\min} + 1) \\ \vdots \\ d(n) \end{array}}^{output} \end{array}\right]$$

(25)

where $k_{\min} = \max((r_{\mathrm{de}} + r_{\mathrm{V}}), r_{\mathrm{d}}) + 1$.

The Nguyen-Widrow algorithm was used for weight initialisation (Nguyen and Widrow, 1990) and Levenberg-Marquardt-Batch-Error-Back-Propagation was employed to train the ANN (Mohammadzaheri *et al.*, 2009).

5.3 Validation

There are two different approaches to validate models: one-step-prediction and simulation. In one-step-prediction, all the inputs to the model are

recalled from memory, or their real values are assumed to be available. For the dynamic model presented in Eq. (21), the one-step-prediction output of the model is

$$\hat{d}(t) = F\begin{pmatrix} V_{\mathrm{P}}(t-t_{\mathrm{d}}), V_{\mathrm{P}}(t-t_{\mathrm{d}}-T_{\mathrm{s}}), \ldots, V_{\mathrm{P}}(t-t_{\mathrm{d}}-r_{\mathrm{V}}T_{\mathrm{s}}), \\ d(t-T_{\mathrm{s}}), d(t-2T_{\mathrm{s}}), \ldots, d(t-r_{\mathrm{d}}T_{\mathrm{s}}) \end{pmatrix}, \quad (26)$$

where the variable(s) with a hat represent estimated values.

However, in simulation of dynamic models, delayed model outputs are used as model inputs after the very first simulation instants and Eq. (21) changes to Eq. (22):

$$\hat{d}(t) = F\begin{pmatrix} V_{\mathrm{P}}(t-t_{\mathrm{d}}), V_{\mathrm{P}}(t-t_{\mathrm{d}}-T_{\mathrm{s}}), \ldots, V_{\mathrm{P}}(t-t_{\mathrm{d}}-r_{\mathrm{V}}T_{\mathrm{s}}), \hat{d}(t-T_{\mathrm{s}}), \\ \hat{d}(t-2T_{\mathrm{s}}), \ldots, \hat{d}(t-r_{\mathrm{d}}T_{\mathrm{s}}) \end{pmatrix}, \quad (27)$$

Therefore, the inevitable error of estimated outputs returns to the validation process and increases the resultant error due to ‘error accumulation’ (Nelles, 2001, Mohammadzaheri *et al.*, 2012b, Bazghaleh *et al.*, 2013). In this research, $t_{\mathrm{d}} = T_{\mathrm{s}} = 0.001\ s$, and $r_{\mathrm{V}} = r_{\mathrm{d}} = 7$ were selected empirically for the neural network model.

6 Experimental results

The voltage drop across any sensing element limits the piezoelectric actuator voltage range. Table 1 compares the maximum voltage drop for two hysteresis linearization techniques from the literature that have been evaluated experimentally (a grounded charge amplifier (Fleming and Moheimani, 2005), capacitor insertion (Kaizuka and Siu, 1988)) and the

GDCDE at different frequencies. To make the data comparable, the displacement range is set to be ±6 μm. It can be seen that at lower frequencies the GDCDE voltage drop is significantly smaller than the voltage drop of the grounded charge amplifier or capacitor insertion method, thus maximizing the displacement that can be achieved for a given supply voltage.

Table 1: Comparison of the maximum voltage drop and its proportion to the input (driver) voltage expressed as a percentage using the three different methods at the frequencies 5, 10, 20 and 50 Hz.

Frequency	Grounded-load charge amplifier (C_s = 78 nF)	Capacitor insertion (C_{series} = 10 nF)	GDCDE (R_s = 20 KΩ)
5 Hz	26 (30%)	82.5 (57%)	0.4147 (0.69%)
10 Hz	14.9 (19%)	82.5 (57%)	0.8294 (1.36%)
20 Hz	10.4 (14%)	82.5 (57%)	1.6588 (2.69%)
50 Hz	8.83 (12.8%)	82.5 (57%)	4.1469 (6.01%)

The value C_{series} for capacitor insertion was chosen from (Minase *et al.*, 2010b) and value C_s for grounded-load charge amplifier was chosen from (Fleming and Moheimani, 2005).

Table 2 compares the lowest operational frequency for each method where displacement is linear with the applied signal. It indicates that this method can extend low frequency operation.

Table 2: Lowest frequency of linear operation

Author, years	Fleming and Moheimani (2004)	Yi and Veillette (2005)	Fleming and Moheimani (2005)	Ru, et al (2008)	This paper
Lowest frequency	2 Hz	1 Hz	0.8 Hz	1 Hz	0.04 Hz

Figure 7 shows the control performance of the proposed GDCDE, the designed ANN and their combination through the complementary filter. The

mean of absolute control error defined as the ratio of the mean of absolute displacement error to the range of displacement varies from 0.5% to 2%. Figure 8 shows the desired displacement versus the actual displacement and the piezoelectric voltage (control input) respectively and Figure 9 illustrates the open-loop frequency response of the piezoelectric tube actuator.

Freq (Hz)	ANN Model	GDCDE	Complementary filter
0.04	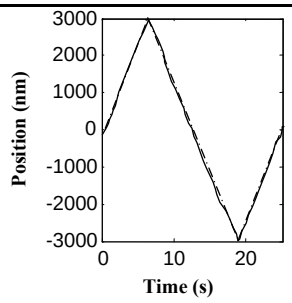	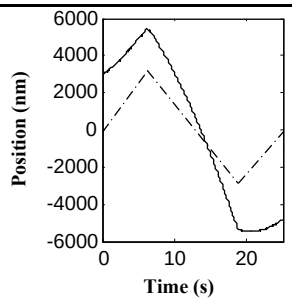	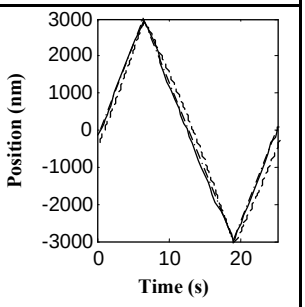
0.07	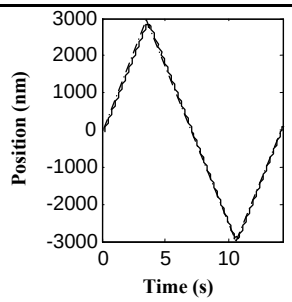	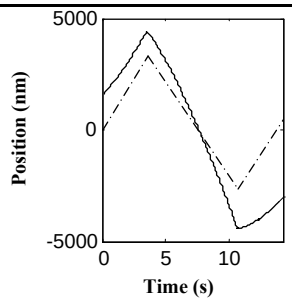	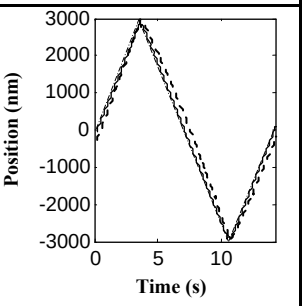
0.1	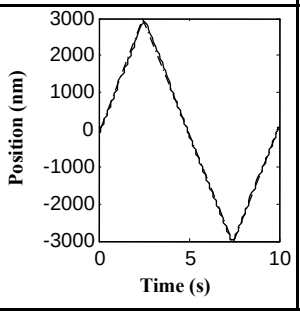	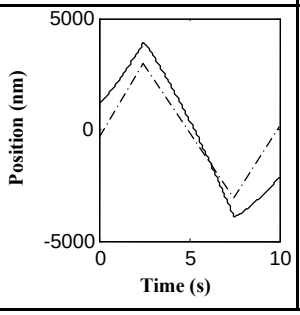	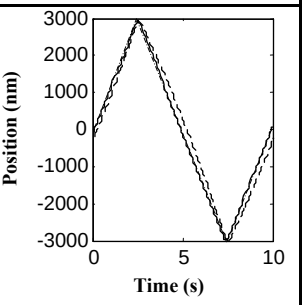

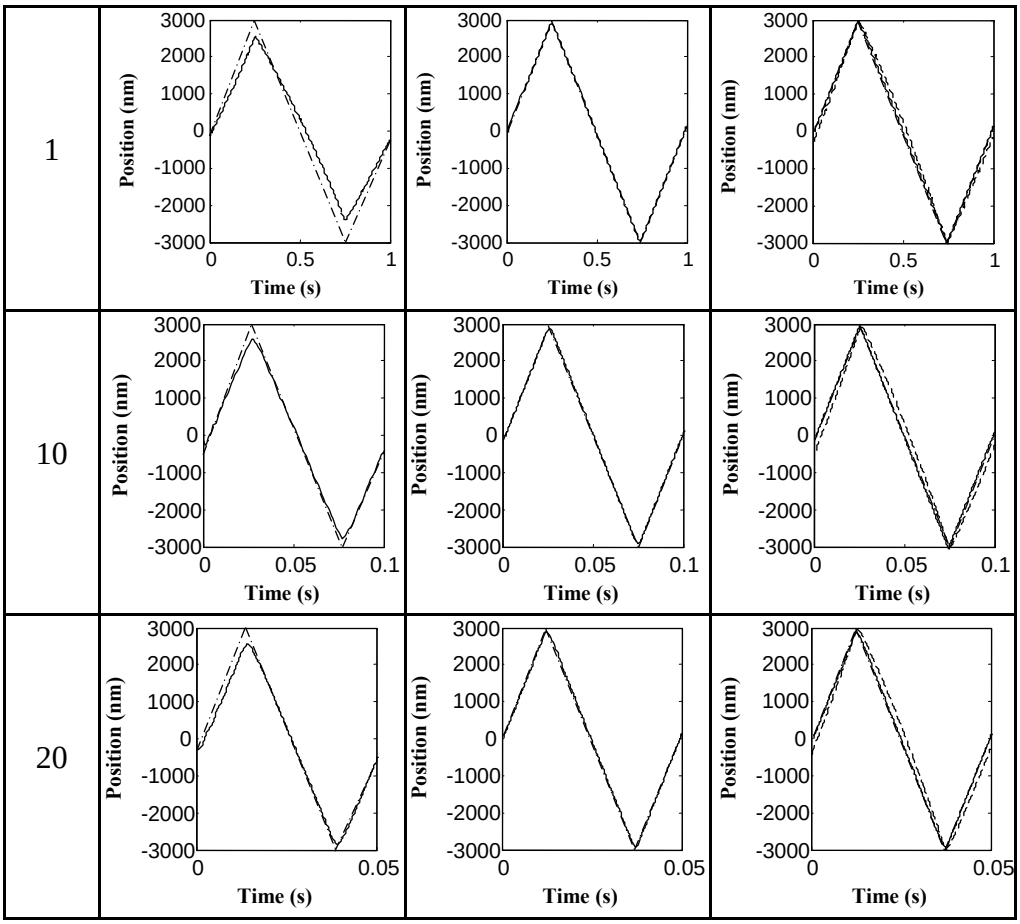

Figure 7: Experimental results for tracking at different frequencies using different displacement estimators. The dot-dashed line (-.-) is desired displacement, the solid line (-) is the actual displacement and the dashed line (--) is the open-loop response

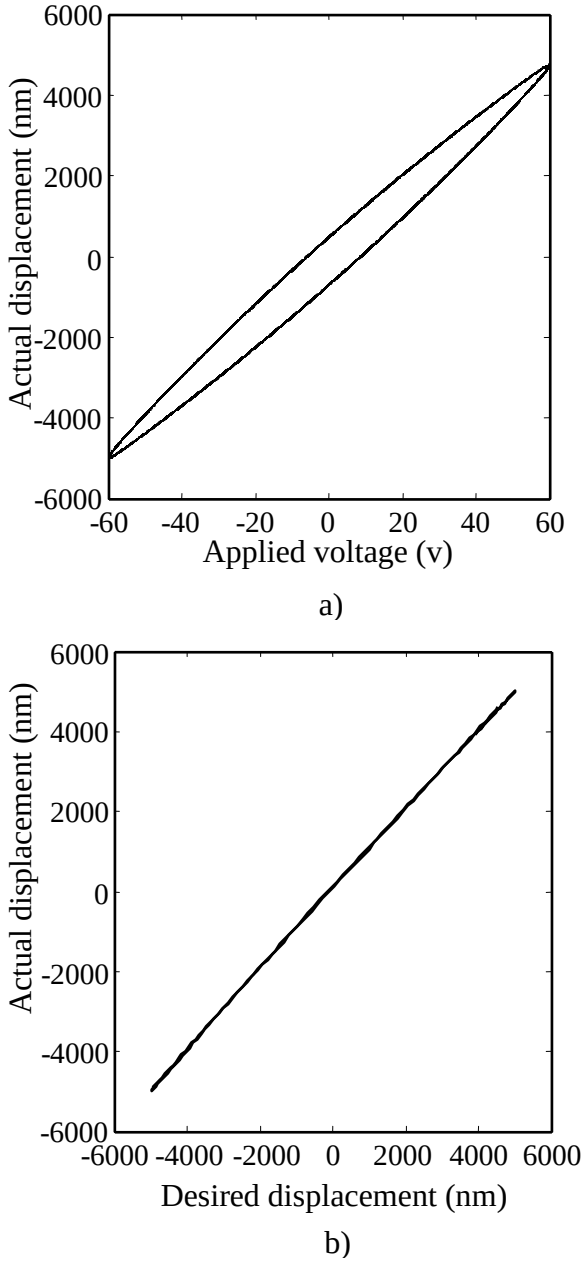

Figure 8: a) Displacement versus open-loop applied voltage at a sinusoidal frequency of 5 Hz. b) Control performance for tracking a sinusoidal reference displacement at 5 Hz

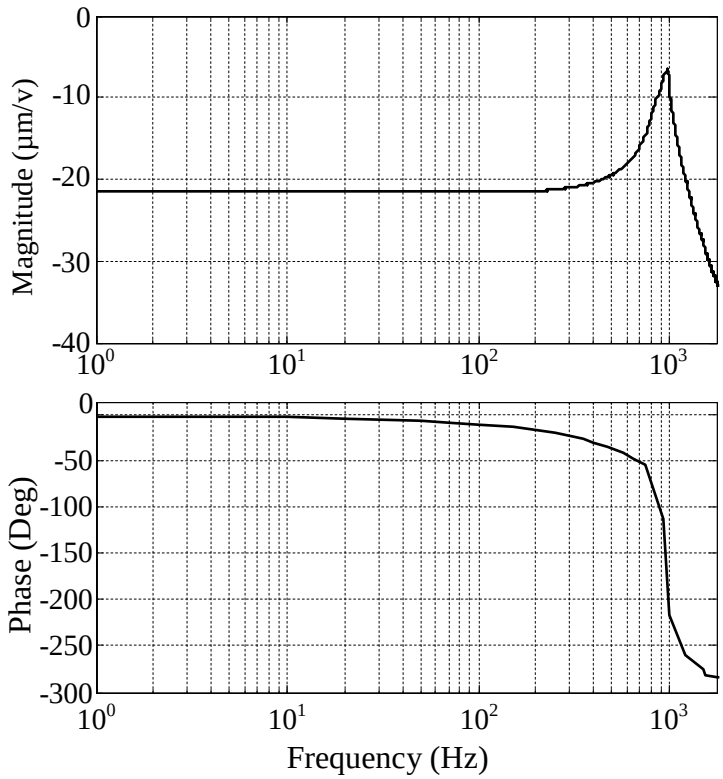

Figure 9: Open-loop frequency response of the piezoelectric tube actuator

7 Conclusion

This research considered the design of a digital sensorless control system for the displacement of piezoelectric tube actuators. As the electrical charge is an accurate estimator of displacement over a wide range of excitation frequencies, the sensing voltage (Figure 1) was employed to estimate charge. A grounded-load digital charge-based displacement estimator was developed to replace displacement sensors on this basis. However, charge-based displacement estimation methods fail to perform satisfactorily at low frequencies. A semi-linear neural network was designed and trained to estimate displacement based on the piezoelectric voltage at low frequencies

(<0.5 Hz) (Figure 1). The ANN and charge-based displacement estimators were used together through a complementary filter to increase the bandwidth of displacement estimation and control. Using a proportional controller, promising experimental results were achieved.

References

Abramovitch, D.Y., Andersson, S.B., Pao, L.Y. and Schitter, G., 2007. A tutorial on the mechanisms, dynamics and control of atomic force microscopes. *In: American Control Conference.* pp. 3488–3502.

Bazghaleh, M., Grainger, S., Cazzolato, B. and Lu, T.-F, 2011. Model-based drift correction of a digital charge amplifier, *In: International Conference on Mechatronics Technology*. Melbourne, Australia.

Bazghaleh, M., Mohammadzaheri, M., Grainger, S., Cazzolato, B. and Lu, T.-F., 2013. A new hybrid method for sensorless control of piezoelectric actuators. *Sensors and Actuators A: Physical* 194, 25–30.

Bhikkaji, B. and Moheimani, S.O.R., 2009. Fast scanning using piezoelectric tube nanopositioners: A negative imaginary approach. *In: IEEE/ASME International Conference on Advanced Intelligent Mechatronics (AIM).* pp. 274–279.

Bhikkaji, B., Ratnam, M. and Moheimani, S.O.R., 2007a. PVPF control of piezoelectric tube scanners. *Sensors and Actuators A: Physical* 135(2), 700–712.

Bhikkaji, B., Ratnam, M., Fleming, A.J. and Moheimani, S.O.R., 2007b. High-performance control of piezoelectric tube scanners. *IEEE Transactions on Control Systems Technology* 15(5), 853–866.

Binnig, G. and Smith, D.P.E., 1986. Single-tube 3-dimensional scanner for scanning tunneling microscopy. *Review of Scientific Instruments* 57(8), 1688–1689.

Chen, C.J., 1992. Electromechanical deflections of piezoelectric tubes with quartered electrodes. *Applied Physics Letters* 60(1), 132–134.

Chen, W.T. and Tsao, S.H., 1977. Ink jet head. *IBM Technical Disclosure Bulletin* 20(2), 504–505.

Comstock, R.H., 1981. Charge control of piezoelectric actuators to reduce hysteresis effects. *U.S. Patent* No. 4,263,527.

Devasia, S., Eleftheriou, E. and Moheimani, S.O.R., 2007. A survey of control issues in nanopositioning. *IEEE Transactions on Control Systems Technology* 15(5), 802–823.

Fleming, A.J. and Leang, K.K., 2008. Evaluation of charge drives for scanning probe microscope positioning stages. *In: American Control Conference*. pp. 2028–2033.

Fleming, A.J. and Moheimani, S.O.R., 2004. Hybrid DC accurate charge amplifier for linear piezoelectric positioning. *In: Proceedings of 3th IFAC Conference on Mechatronic Systems*. pp. 283–288.

Fleming, A.J. and Moheimani, S.O.R., 2005. A grounded-load charge amplifier for reducing hysteresis in piezoelectric tube scanners. *Review of Scientific Instruments* 76(7), 73707.

Ghaffari, A., Mehrabian, A.R. and Mohammad-Zaheri, M., 2007. Identification and control of power plant de-superheater using soft computing techniques. *Engineering in Applied Artificial Intelligence* 20(2), 273–287.

Huang, L., Ma, Y.T., Feng, Z.H. and Kong, F.R., 2010. Switched capacitor charge pump reduces hysteresis of piezoelectric actuators over a large frequency range. *Review of Scientific Instruments* 81(9), 094701.

Hui, Z., Shu-yi, Z. and Li, F., 2010. Simplified formulae to investigate flexural vibration characteristics of piezoelectric tubes in ultrasonic micro-actuators. *Ultrasonics* 50(3), 397–402.

Kaizuka, H. and Siu, B., 1988. A simple way to reduce hysteresis and creep when using piezoelectric actuators. *Japanese Journal of Applied Physics* 27(5), 773–776.

Kuiper, S. and Schitter, G., 2010. Active damping of a piezoelectric tube scanner using self-sensing piezo actuation. *Mechatronics* 20(6), 656–665.

Leang, K.K. and Devasia, S.,2002. Hysteresis, creep and vibration compensation for piezoactuators: Feedback and feedforward control. *In: Proceedings of 2nd IFAC Conference on Mechatronic Systems.* pp. 283–289.

Leung, M., Yue, J., Razak, K.A., Haemmerle, E., Hodgson, M. and Gao, W., 2008. Development of a 1 × 2 piezoelectric optical fiber switch – art.

No. 683603. *Proceedings of the Society of Photo-Optical Instrumentation Engineers* 6836, 83603.

Minase, J., Lu, T.F. and Grainger, S., 2010a. Inverse control of a piezoelectric actuator for precise operation of a micro-motion stage. *In: Australasian Conference on Robotics and Automation (ACRA).* Brisbane, Australia.

Minase, J., Lu, T.F., Cazzolato, B. and Grainger, S.,2010b. A review, supported by experimental results, of voltage, charge and capacitor insertion method for driving piezoelectric actuators. *Precision Engineering: Journal of International Society for Precision Engineering and Nanotechnology* 34(4), 692–700.

Mohammadzaheri, M., Chen, L., Ghaffari, A. and Willison, J., 2009. A combination of linear and nonlinear activation functions in neural networks for modeling a de-superheater. *Simulation Modelling Practice and Theory* 17(2), 398–407.

Mohammadzaheri, M., Grainger, S., Bazghaleh, M. and Yaghmaee, P., 2012a. Intelligent modeling of a piezoelectric tube actuator, *In: International Symposium on Innovations in Intelligent Systems and Applications (INISTA).* Trabzon, Turkey. pp. 1-6.

Mohammadzaheri, M., Grainger, S. and Bazghaleh, M., 2012b. Fuzzy modeling of a piezoelectric actuator. *International Journal of Precision Engineering and Manufacturing* 13(5), 663–670.

Moheimani, S.O.R., 2008. Invited review article: Accurate and fast nanopositioning with piezoelectric tube scanners: Emerging trends and future challenges. *Review of Scientific Instruments* 79(7), 071101.

Nelles, O., 2001. Nonlinear System Identification. *Springer-Verlag*. Berlin, Heidelberg.

Newcomb, C.V. and Flinn, I., 1982. Improving the linearity of piezoelectric ceramic actuators. *Electronics Letters* 18(11), 442–444.

Nguyen, D. and Widrow, B., 1990. Improving the learning speed of 2-layer neural networks by choosing initial values of the adaptive weights. *In: International Joint Conference on Neural Networks (IJCNN)*. pp. 21–26.

Ru, C.H., Chen, L.G., Shao, B., Rong, W.B. and Sun, L.N., 2008. A new amplifier for improving piezoelectric actuator linearity based on current switching in precision positioning. *Measurement Science and Technology* 19(1), 015203.

Schitter, G., Astroem, K.J., DeMartini, B.E., Thurner, P.J., Turner, K.L. and Hansma, P.K., 2007. Design and Modeling of a high-speed AFM-scanner. *IEEE Transactions on Control Systems Technology* 15(5), 906–915.

Yi, K.A. and Veillette, R.J., 2005. A charge controller for linear operation of a piezoelectric stack actuator. *IEEE Transactions on Control Systems Technology* 13(4), 517–526.

7 Conclusions and Recommendations for Future Work

The aim of this research was to investigate the efficacy of a synergistic approach to the creation of hybrid digital algorithms which tackle challenges arising in the control of non-linear devices such as piezoelectric actuators. The following section draws conclusions from the research presented in this thesis, while recommended future work is presented in Section 7.2.

7.1 Conclusions

Piezoelectric actuators are the most commonly used nanopositioning actuators. However, they suffer from performance issues arising from their fundamental non-linearities.

The literature review, conducted as part of this thesis, indicates that charge drive is a method which can significantly reduce the nonlinearities of the piezoelectric actuator. Therefore, in this thesis charge drive is used as a promising starting point.

In the first step, a comprehensive analysis was carried out to establish the performance limitations of the charge drive approach and revealed that the charge methods adopted to date were implemented using analog circuitry and as a result have historically been complicated and expensive to implement due to the complexity of the analog circuitry.

In order to overcome these performance limitations this thesis focused on using digital technologies as a platform. This is central to enabling a synergistic approach that combines multiple conceptual technologies as required (e.g. Artificial Neural Networks (ANNs), fuzzy logic and complementary filters) in an integrative fashion.

A novel digital charge amplifier (DCA) was derived for a piezoelectric actuator that overcomes some inherent limitations found in analog charge amplifiers developed in previous research such as poor low frequency performance and significant voltage drop. While the DCA significantly reduced the hysteresis and improved the linearity of piezoelectric actuators the DCA suffers from its own limitations but the synergistic approach opens up the possibility of integration with other displacement control methods to improve the overall performance of the resulting displacement controller. The computational performance of modern digital devices ensures the viability of this.

To address the issue of drift in the DCA a model-based drift correction technique was proposed. It has been shown how a drift free model can be integrated with the DCA to remove the DCA's inherent drift while the DCA itself tackles the issue of hysteresis. To maximize model accuracy, a novel hybrid method was proposed which incorporates a velocity signal into the model to reduce the effect of error accumulation.

Furthermore to extend the DCA operational bandwidth, a technique is proposed that integrates a non-linear model designed and trained to estimate displacement based on the piezoelectric voltage only at low frequencies. The model and charge-based displacement estimators were effectively utilized together through a complementary filter. In addition, the proposed method is designed to be capable of driving grounded-loads such as piezoelectric tube actuators.

This research has satisfied the aim of investigating the efficacy of a synergistic approach to the creation of solutions that allow new levels of performance to be achieved.

7.2 Recommendations for future work

It is recommended that further research be undertaken in the following areas:

- Electrically, a piezoelectric actuator behaves as a non-linear capacitor which is the main reason for nonlinearities. The piezo current, which can be estimated using the sensing resistor, and piezo voltage may be combined to estimate the real-time value of the non-linear capacitor. This value, along with the piezo voltage, can be used to estimate the piezo charge which could be used to implement a new type of charge drive. Moreover, an estimate of the real-time value of the non-linear capacitor may lead to a more accurate controller which can be tuned in real-time. This technique may take advantage of synergistic approaches for better accuracy (e.g. using modeling and complementary filter).

- A controller should be designed for a multi-axis nanopositioner, e.g., piezoelectric tube actuators. The most significant difficulty is the existence of cross-coupling between the x, y and z axes. Due to the complexity of this cross-coupling, a comprehensive controller that can compensate the effect of cross-coupling has not been carried out. The proposed synergistic approach should be investigated in addressing this issue to obtain improved performance.

- Recently the piezoelectric strain-induced voltage has been used to estimate the tube deflection. There is not any research that uses strain-induced charge rather than strain-induced voltage to estimate the deflection of the tube. In addition, there is a potential of integrating the strain-induced charge with the proposed methods in order to increase the accuracy of the displacement controller.

Appendix A. Experimental Setup

In this thesis two separate setups were used; one for driving a piezoelectric stack actuator and the other for driving a piezoelectric tube actuator both of which are described in the following sections.

A.1 Driving a piezoelectric stack actuator

A.1.1 General description

Figure A.1 shows the schematic of the experimental setup for driving a piezoelectric stack actuator. It is driven by a voltage amplifier through a sensing circuit. The sensing circuit, Figure A.2, consists of a sensing resistor which is in series with the piezo and a protection circuit to protect the dSPACE from high voltage. The sensing circuit provides the sensing voltage to the dSPACE in order to estimate the charge across the piezo, as described in Chapter 3. The displacement of the piezoelectric actuator is provided by a strain gauge, attached to the piezoelectric actuator. The strain gauge is in a full bridge configuration in order to compensate for temperature. The strain gauge is connected to a strain gauge signal conditioner. The dSPACE controller board, installed in a PC, provides the control signal to the voltage amplifier, and samples the output of the sensing circuit and the strain gauge signal conditioner.

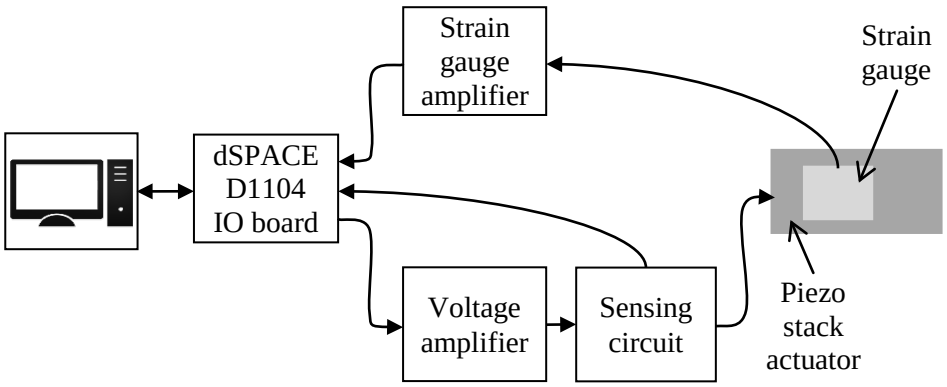

Figure A.1: The schematic of the experimental setup for driving a piezoelectric stack actuator

A.1.2 Sensing circuit

Figure A.2 shows the circuit diagram of the sensing circuit. The sensing resistor, R_{sensing}, is in series with the piezoelectric stack actuator in order to provide the sensing voltage to the dSPACE. The resistor R_{p} and the diodes D_1 and D_2 are used to protect the dSPACE from high voltage.

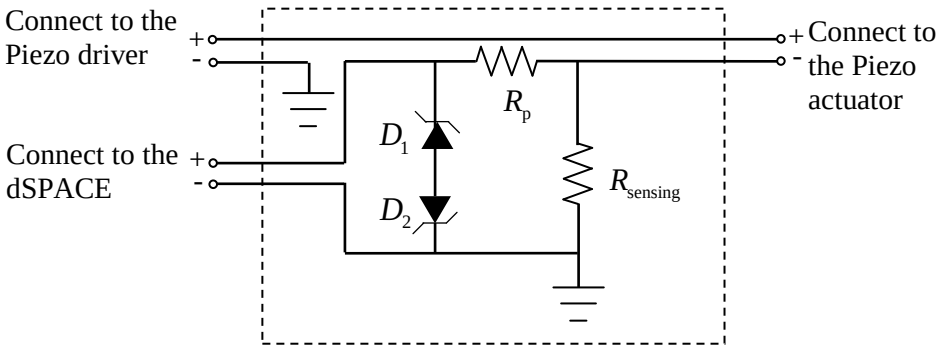

Figure A.2: Circuit diagram of the sensing circuit

A.1.3 The piezoelectric stack actuator

In the first experimental setup a piezoelectric stack actuator, AE0505D44H40, from NEC is used. The specifications are:

Manufacturer:	NEC
Model number:	AE0505D44H40
Dimensions:	5 x 5 x 40 mm
Maximum driving voltage	150 VDC
Recommended driving voltage	100 VDC
Displacement @ Maximum driving voltage	42.0±6.6 µm
Displacement @ Recommended driving voltage	28.0±6.6 µm
Generated force (Compression):	850 N
Resonance frequency	34 kHz
Capacitance	3.4 µm
Insulation resistance	5 MΩ

A.1.4 The strain gauge

The strain gauge EA-06- 125TG-350 from the Vishay Measurement Group, Inc, is used to measure the displacement of the stack actuator. It is glued to the top and bottom of the stack actuator and, in order to compensate for the temperature variation, a full bridge configuration is used. A strain gauge signal conditioner drives the stain gauge sensor and provides the displacement signal to the dSPACE. The specifications are:

Strain gauges:

Manufacturer:	Vishay Micro-Measurements Division, Inc
Model number:	EA-06-125TG-350
Maximum strain:	3% gauge length - 0.1 mm
Resistance@ 24ºC	350.0 Ω ± 0.2%

Strain gauge amplifier:

Manufacturer:	Electronics Workshop, School of Mech. Eng., Univ. of Adelaide
Bridge excitation voltage:	+5 VDC
Bridge type:	Full Wheatstone bridge
Variable gain stage:	5000 V/V
Fixed gain Stage:	100 V/V
Offset voltage:	±12 VDC

A.1.5 Piezo driver

A power amplifier E-865.10 from Physik Instrumente (PI) is used to drive the piezoelectric stack actuator. It provides voltage ranging from -20 V to 120 V, with a maximum power of 30 W and a gain of 10. It has one BNC type input connector and one LEMO type output connector.

Manufacturer:	PI
Model number:	E-865.10 - LVPZ Power Amplifier Module
Output voltage range:	-20 to +120 V
Max. average output current:	0.22 A
Max. output current:	2.0 A
Max. average output power:	30 W
Voltage gain:	10

A.2 Driving the piezoelectric tube actuator

A.2.1 General description

The experimental setup used to drive the piezoelectric tube actuator is shown in Figure A.3. The two opposite electrodes of the tube are each driven by an individual voltage amplifier through a sensing circuit, which

provides the sensing voltages to dSPACE to calculate the charge, described in Chapter 6. The displacement is measured using a capacitive sensor and a signal conditioner which provides the displacement signal to the dSPACE.

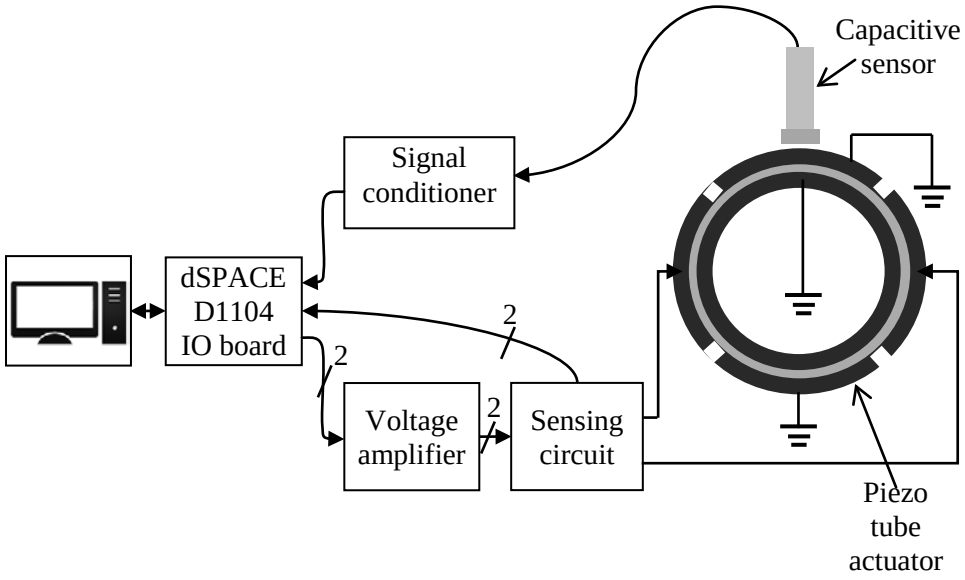

Figure A.3: The schematic of the experimental setup for driving a piezoelectric tube actuator

A.2.2 Test rig of the tube actuator

Figure A.4a shows the test rig for the tube scanner. The tube scanner is mounted into an aluminium base to secure one end of the tube and to hold the tube vertically. The piezoelectric tube scanner deflects the end-effecter in the x, y and z directions. Deflections change the capacitance between the end-effecter and the capacitive sensor that allowing the movement of the end-effecter to be measured.

Figure A.4b shows the cylindrical cover which is mounted on the aluminium cylinder to protect the tube actuator and to keep the capacitive sensors parallel with the end-effecter.

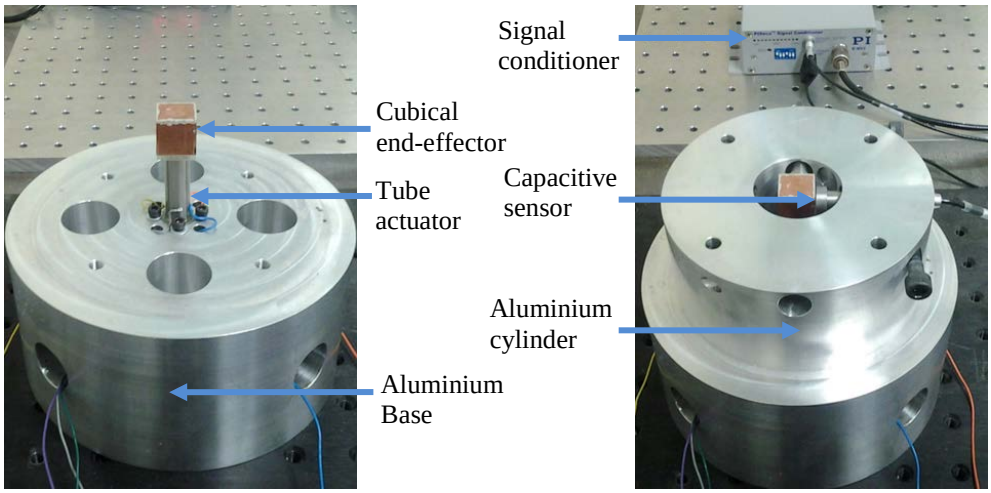

Figure A.4: The piezoelectric tube actuator setup a) with no cover b) covered by the cylinder holding the capacitive displacement sensors

A.2.3 Sensing circuit

Figure A.5 shows the circuit diagram of the sensing circuit for driving the tube actuator. The sensing resistor, $R_{sensing}$, is in series with the piezoelectric tube actuator. The Isolation amplifier is used to provide the sensing voltage to the dSPACE while protecting the dSPACE from high voltage.

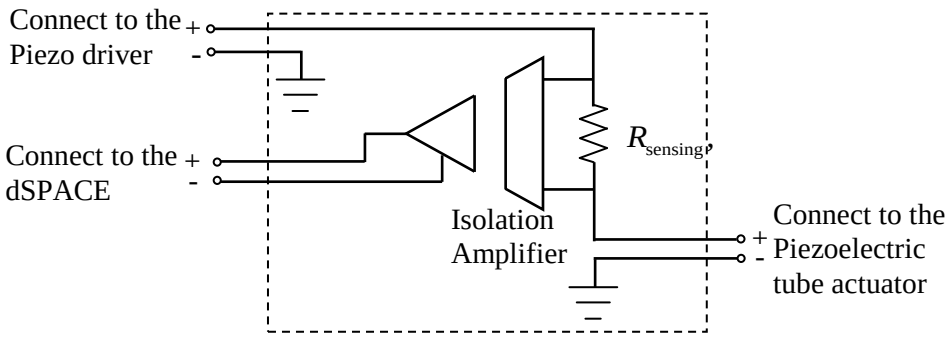

Figure A.5: Circuit diagram of the sensing circuit

A.2.4 The piezoelectric tube actuator

The piezoelectric tube actuator is a PT130.24 from PI. The tube has one inner electrode and four equally distributed outer electrodes (Figure A.6).

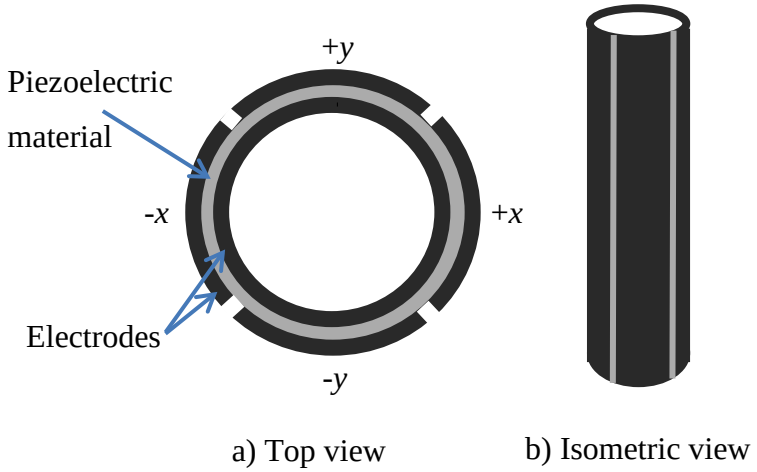

Figure A.6: Schematic of piezoelectric tube scanner PT130.24

The specifications are as follows:

Manufacturer:	PI
Model number:	PT130.24
Dimensions (L x OD x ID*):	30 x 10.0 x 9.0 mm
Number of outer electrodes/ inner electrode	4/1
Maximum operating voltage	200 V
Axial contraction @ Maximum operation voltage	9 µm
Radial contraction @ Maximum operation voltage	3 µm
XY deflection @ Maximum operation voltage	10 µm
Capacitance	4 x 8.5 nF

*L (length), OD (outer diameter), ID (inner diameter)

A.2.5 The capacitive sensor

The capacitive sensor is from PI, model number D-510.050. It allows for non-contact measurement of the end-effecter displacement. The signal conditioner E-852.10 from PI is used to interface the capacitive sensor in order to provide an appropriate displacement signal to dSPACE. The specifications are:

Capacitive sensor:

Manufacturer:	PI
Model number:	D-510.050
Nominal measurement range:	50 µm
Min. gap	25 µm
Max. gap	375 µm
Static resolution	<0.001 % of measurement range
Dynamic resolution	<0.002 % of measurement range
Linearity	<0.1 % of nominal measurement range

Capacitive sensor signal conditioner:

Manufacturer:	PI
Model number:	E-852.10
Number of channel:	1
Bandwidth	0.3 / 3 / 10 kHz
Output voltage	-10 to +10 V / -5 to +5 V / 0 to +10 V

A.2.6 Piezo driver

A power amplifier is used to drive the piezoelectric tube actuator. It provides a voltage range of ±180V with a gain of 50.

Manufacturer:	Elec. Workshop, School of Mech. Eng., Univ. Adelaide
Output voltage range:	-180 to +180V

Bandwidth	DC to 10 kHz
Input voltage range:	-5 to +5V
Voltage gain:	50

A.2.7 dSPACE controller board

dSPACE DS1104 is an Input/output controller board. It is used to deliver the appropriate signal to the piezo driver and record the outputs from the sensing circuits and strain gauge signal conditioner or capacitive sensor signal conditioner.

This board has eight analog/digital converters (ADCs) and eight digital/analog converters (DACs). The voltage range of all ADCs and DACs is ±10 V.

Appendix B. Relevant Conference Papers

B.1 An Innovative digital charge amplifier to reduce hysteresis in piezoelectric actuators

Australasian Conference on Robotics and Automation (ACRA), Brisbane, Australia, 2010.

Bazghaleh, M., Grainger, S., Cazzolato, B. & Lu, T-F (2010) An innovative digital charge amplifier to reduce hysteresis in piezoelectric actuators.
Presented at: Australasian Conference on Robotics and Automation (ACRA), 1-3 December, Brisbane, Australia

B.2 Model-based drift correction of a digital charge amplifier

International Conference on Mechatronics Technology (ICMT), Melbourne, Australia, 2011.

Bazghaleh, M., Grainger, S., Cazzolato, B. & Lu, T-F (2011) Model-based drift correction of a digital charge amplifier.
Presented at: International Conference on Mechatronics Technology (ICMT), 30 November-2 December, Melbourne, Australia

B.3 Using frequency-weighted data fusion to improve the performance of a digital charge amplifier

IEEE International Conference on Robotics and Automation (ICRA), St. Paul, MN, USA, 2012.

Bazghaleh, M., Grainger, S., Cazzolato, B. & Lu, T-F (2012) Using frequency-weighted data fusion to improve the performance of a digital charge amplifier.
Presented at: IEEE International Conference on Robotics and Automation (ICRA), 14-18 May, Saint Paul, Minnesota